Numéro d'ordre : 165-2011 Année 2011

THÈSE

Délivrée par

L'UNIVERSITÉ CLAUDE BERNARD LYON 1
Spécialité : Acoustique

et

L'UNIVERSITA DI FIRENZE
Specialità : Ingegneria dei sistemi Electtonici

DIPLÔME DE DOCTORAT

(arrêté du 7 aout 2006)

ÉCOLE DOCTORALE : MÉCANIQUE, ÉNERGÉTIQUE, GÉNIE CIVIL, ACOUSTIQUE
DOTTORATO DI RICERCA : INGEGNERIA DEI SISTEMI ELETTRONICI

Soutenue publiquement le 5 octobre 2011 par

François VARRAY

Simulation in Nonlinear Ultrasound. Application to Nonlinear Parameter Imaging in Echo Mode Configuration.

Jury

Christian CACHARD	Professeur des Universités, Lyon 1	Co-directeur de thèse
Olivier BASSET	Professeur des Universités, Lyon 1	Co-directeur de thèse
Piero TORTOLI	Professore Ordinario, Florence	Co-directeur de thèse
Christian JUTTEN	Professeur des Universités, Grenoble	Rapporteur, Président
Olivier BOU MATAR	Professeur des Universités, Lille	Rapporteur
Filippo MOLINARI	Ricercatore Confermato, Turin	Rapporteur
Simone BALOCCO	Lecturer Professor, Barcelone	Examinateur
Enrico BONI	Ricercatore, Florence	Examinateur

Abstract

Harmonic imaging is from now on clinical routine because it increases the resolution of ultrasound images. It is based on the nonlinear response of tissues. The novel nonlinear imaging methods, derived from harmonic imaging, currently suffer from a lack of simulation tools. The measure of the nonlinear parameter using ultrasound brings new perspectives in term of imaging and diagnosis. However, no method exists at present to measure this parameter in echo-mode configuration.

This thesis aims to solve the two mentioned limitations by proposing new simulation tools of the ultrasound nonlinear propagation in tissues as well as a new method to measure the nonlinear parameter in echo-mode configuration.

Current simulation tools of ultrasound images do not take into account the nonlinear propagation that is why an angular spectrum method has been proposed to compute the pressure field considering the ultrasound propagation in media with inhomogeneous nonlinear parameter. This pressure field is then used to generate ultrasound images containing the harmonic component, for homogeneous or not nonlinear media. This spectral approach has been implemented on a GPU in order to accelerate the computation and packaged in a free software made available to the scientific community under the name CREANUIS.

In a second time, a comparative method to measure the nonlinear parameter has been proposed. This method has been extended in order to take into account media with inhomogeneous nonlinearity. It is usable in echo-mode configuration by considering a region of the image as a reference. This method assumes that the acoustic pressure is related to the echogenicity of the medium. An extraction step of the mean pressure in echographic images has been realized using alternating sequential filters. Thanks to the developed simulation tools, different configurations have been used to parameterize and to evaluate the proposed method. Some acquisitions have been made on phantoms and animal's livers. Even if the measure presents a relatively weak resolution, the obtained images demonstrate a high potential in the nonlinear parameter imaging of tissues.

Résumé

L'imagerie harmonique est une technique désormais utilisée en routine clinique car elle améliore la résolution des images. Elle est basée sur la réponse non linéaire des tissus. Les nouvelles méthodes d'imagerie non linéaire, dérivé de l'imagerie harmonique, souffre à l'heure actuelle d'un manque d'outils de simulation. La mesure par une technique ultrasonore du paramètre de non linéarité d'un milieu amène de nouvelles perspectives en termes d'imagerie et de diagnostic. Cependant, il n'existe pas actuellement de méthode de mesure de ce paramètre en mode écho classique.

Cette thèse a pour objectifs de répondre aux deux limitations mentionnées ci-dessus en proposant de nouveaux outils de simulation de la propagation non linéaire des ultrasons dans les tissus ainsi qu'une nouvelle méthode de mesure du paramètre de non linéarité en mode écho.

Les outils actuels de simulations d'image échographique ne prennent pas en compte la propagation non linéaire. Il a donc été proposé une méthode de spectre angulaire afin de calculer le champ de pression prenant en compte la propagation ultrasonore non linéaire dans des milieux de non linéarité inhomogène. Ce champ de pression est ensuite utilisé pour générer des images échographiques contenant l'information harmonique, pour des

milieux de non linéarité homogène ou non. Cette méthode spectrale a été portée sur GPU afin d'accélérer le calcul et intégrée dans un logiciel libre mis à disposition de la communauté scientifique sous le nom de CREANUIS.

Dans un deuxième temps, une méthode comparative de mesure du paramètre de non linéarité a été proposée. Cette méthode a été étendue afin de prendre en compte des milieux dont le paramètre de non linéarité n'est pas homogène. Elle est aussi utilisable en mode écho en sélectionnant une zone de l'image choisie comme référence. La méthode implantée fait l'hypothèse que la pression acoustique locale est liée à l'échogénéité du milieu. Une étape d'extraction de la pression moyenne dans les images échographiques a été réalisée grâce à des filtres alternés séquentiels. Grâce aux outils de simulation développés, différentes configurations ont été utilisées pour la mise au point et l'évaluation de la méthode. Des acquisitions ont été réalisées à partir de fantômes et de foies animaux. Même si la méthode de mesure présente une résolution relativement faible, les images obtenues démontrent le potentiel de l'imagerie du paramètre de non linéarité des tissus.

Sommario

L'harmonic imaging è una tecnica già utilizzata nella pratica clinica poiché migliora la risoluzione delle immagini. Si basa sulla risposta non lineare dei tessuti. I nuovi metodi di imaging non lineare, derivati dall'imaging armonico, ad oggi risentono della mancanza di opportuni strumenti di simulazione. La misura del parametro di non linearità di un mezzo, tramite tecniche ad ultrasuoni, apre nuove prospettive in termini di imaging e di diagnostica. Tuttavia, attualmente non esistono dei metodi per la misura di questo parametro nella modalità eco classica.

Questo lavoro di tesi si propone come obiettivo di rispondere alle due limitazioni suddette, proponendo sia dei nuovi strumenti di simulazione della propagazione non lineare degli ultrasuoni nei tessuti che un nuovo metodo per la misura del parametro di non linearità nella modalità eco classica.

Gli attuali strumenti di simulazione per l'imaging ecografico non tengono conto della propagazione non lineare. Al fine di calcolare il campo di pressione considerando la propagazione non lineare degli ultrasuoni in un mezzo con non linearità disomogenea è stato scelto l'Angular Spectrum Method. Il campo di pressione calcolato viene poi utilizzato per generare delle immagini ecografiche contenenti l'informazione armonica, per mezzi con non linearità omogenea o disomogenea. Il metodo proposto è stato poi implementato su GPU così da velocizzare il calcolo ed è stato poi integrato in un software ad accesso libero, messo a disposizione della comunità scientifica con il nome di CREANUIS.

In un secondo tempo, è stato proposto un metodo comparativo per la misura del parametro di non linearità. Questo metodo è stato sviluppato così da tenere conto dei materiali nei quali il parametro di non linearità non è omogeneo. Lo si può anche utilizzare in modalità eco selezionando una zona dell'immagine presa come riferimento. Il metodo realizzato fa l'ipotesi che la pressione acustica locale sia legata all'ecogenità del mezzo. Una tappa consiste nell'estrazione della pressione media nelle immagini ecografiche tramite degli alternating sequential filters. Grazie agli strumenti di simulazione sviluppati è stato possibile utilizzare configurazioni per la messa a punto e la valutazione del metodo. Sono state fatte delle acquisizioni su phantom e su fegati animali. Anche se il metodo di misura presenta una risoluzione relativamente bassa, le immagini ottenute dimostrano il potenziale dell'imaging del parametro di non linearità dei tessuti.

Contents

List of Symbols and abbreviations

Latin letter

B/A	Nonlinear parameter
c	Celerity of the ultrasound wave in the tissue (m.s^{-1})
c_0	Equilibrium celerity of the ultrasound wave in the tissue (m.s^{-1})
f	Frequency (Hz)
$\mathcal{F}$	3D Fourier transform in dimension (x, y, t)
J_n	Bessel function of n-th order
$k = \omega/c$	Waves number (m^{-1})
$p(x, y, z, t)$	Pressure (Pa) of the ultrasound wave at the point (x, y, z) and the time t
p_0	Equilibrium pressure (Pa) amplitude
R, R_{12}	Reflection coefficient (from medium 1 to medium 2)
s	Entropy
T, T_{12}	Transmission coefficient (from medium 1 to medium 2)
$\vec{u}$	Particle velocity (m.s^{-1})
$Z = \rho c$	Acoustic impedance of the medium (kg.m^{-2}.s^{-1})
x	Lateral dimension (m)
y	Elevation dimension (m)
z	Axis distance (m)
z_c	Shock distance (m^{-1})

Greek letter

∇	Nabla operator
α_0	Attenuation constant of the medium (Np.m^{-1}.MHz$^{-\gamma}$)
α_1	Attenuation of the fundamental wave (Np.m^{-1}.MHz$^{-\gamma}$)
α_2	Attenuation of the second harmonic wave (Np.m^{-1}.MHz$^{-\gamma}$)
$\beta = B/2A + 1$	Nonlinear coefficient
γ	Frequency dependent number in attenuation (between 1 and 2 for biological media)
$\lambda = c/f$	Wave length of the pressure wave (m)
ρ	Density of the tissue (kg.m^{-3})
ρ_0	Equilibrium density of the tissue (kg.m^{-3})
$\tau = t - z/c_0$	Delayed time (in s)
$\omega = 2\pi f$	Angular frequency f (Hz)
$\omega_0 = 2\pi f_0$	Fundamental angular frequency f_0 (Hz)

Abbreviations

AM	Amplitude modulation
ASF	Alternating sequential filter
ASM	Angular spectrum method
FWHM	Full width at half maximum
FT	Fourier transform
IFT	Inverse Fourier transform
lpf	Low-pass filter
PI	Pulse inversion
pdf	Probability density function
PSF	Point spread function
RF	Radio frequency
TGC	Time gain compensation
US	Ultrasound
UCT	Ultrasound computed tomography

Thesis Objectives

Objectives

The objectives of this thesis work are based on the nonlinear propagation of an ultrasound wave in biological tissue. Harmonic imaging, with or without injection of contrast agents, has become a clinical routine thanks to the increase in the image resolution [Averkiou *et al.* (1997), van Wijk and Thijssen (2002)]. The nonlinear parameter is, similarly to the speed of sound c_0 or the density ρ_0, one of the parameters characterizing the medium. It impacts the harmonics increase during the nonlinear ultrasound wave propagation. Currently, various techniques exist to measure the increase of the second harmonic response compared to the fundamental one: the amplitude modulation (AM) [Nowicki *et al.* (2007)], the pulse inversion (PI) [Simpson and Burns (1997), Simpson *et al.* (1999)] or phase optimization [Eckersley *et al.* (2005)]. Moreover, in order to increase the detection of the contrast agents, some recent methods have been proposed to reduce either the native nonlinearity of the medium with a broadband reduction of the second harmonic component [Pasovic *et al.* (2010), Pasovic *et al.* (2011)] or the second harmonic component created at the emission by the probe [Novell *et al.* (2009)]. The development of these different strategies would be facilitated by the knowledge of the nonlinear parameter of the tissue. Its measurement from echographic images would be a precious information in nonlinear imaging. The study of this nonlinear parameter is conducted in this thesis for various possible future utilization in medical ultrasound imaging:

- For second harmonic reduction [Novell *et al.* (2009), Pasovic *et al.* (2010)].
- For parametric imaging: combination of the nonlinear parameter information with other measurements.
- For tissue characterization: a difference in the nonlinear parameter between healthy and pathological tissues was largely reported in the literature [Zhang *et al.* (1996), Zhang and Gong (1999), Zhang *et al.* (2001), Gong *et al.* (2004)].

These multiple utilizations of the nonlinear parameter make it an important characteristic to evaluate. From one hand, the local estimation of the nonlinear parameter allows to provide an image of a medium that may be used to detect a lesion and on the other hand, the different values of the map can be used to define the strategies of second harmonic reduction in view to improve the image quality.

Layout of the thesis

In this thesis, I concentrated my efforts on the nonlinear parameter measurement and especially in echo mode configuration which is the classical imaging clinical mode. However, the measurement must take into account the possible variation and inhomogeneity of the nonlinear parameter of the medium and new simulation tools are required. The manuscript is composed of three distinct parts:

- Chapter 1: General introduction. This chapter is devoted to the presentation of the ultrasound, the linear/nonlinear propagation and the different image modalities. No contribution is presented in this chapter.

- Part 1: Presentation of the different simulation tools developed during the thesis. The chapter 2 makes a review of the different simulation tools in the literature for the nonlinear wave propagation and the ultrasound images simulation methods. The advantages and disadvantages of the different techniques are discussed in order to identify the optimal simulator for our purpose, the possible inhomogeneity of the nonlinearity. The chapter 3 presents our original propagation simulator which takes into account the possible inhomogeneity of the nonlinear parameter in the medium. Its evaluation has been made on simulated and experimental data. The chapter 4 presents an original ultrasound image simulator, CREANUIS, based on the previous nonlinear propagation simulator. Thanks to this final tool, the complete echographic image of an inhomogeneous nonlinear medium can now be simulated.

- Part 2: The last part of the thesis is focussed on the nonlinear parameter measurement. The chapter 5 makes a literature review on the nonlinear parameter measurement methods. From the set of described methods, the chapter 6 considers the methods having a potential utilization in echo mode configuration. Moreover, some of them are extended to inhomogeneous nonlinear medium. In this chapter, in addition to the original extensions, the evaluation of these extensions are conducted on simulated data thanks to the previously developed simulation tools. Then, the chapter 7 evaluates one of these extensions on experimental data in order to estimate the accuracy of the proposed method.

To conclude the thesis, a general discussion and conclusion is conducted and highlights the different perspectives of this thesis work. In appendix, different information are given as the different equipments used in the thesis (ultrasound scanner, computer, and graphic card), the user manual of CREANUIS, and different nonlinear parameter value of various media.

Chapter 1

Ultrasound and echography: propagation and beamforming

This chapter presents the background in ultrasound and echography. In a first time, some generalities about the ultrasound are given. Then the nonlinear propagation of the ultrasound is highlighted. Finally, the echographic image beamforming is presented. The different notations and conventions are set in this part.

1.1 Ultrasound generalities

1.1.1 Ultrasound wave

The ultrasound is a compression-dilatation wave which propagates in a medium. The difference between ultrasound and the classical audible sound comes from their frequencies f which are higher in medical ultrasound (1-20 MHz compare to 20 Hz - 20 kHz for the audible sound). More specifically, the pressure wave is successively composed of phases with compression and dilatation which propagate in the medium. In this way, the sound and ultrasound cannot propagate in vacuum. In function of the speed of sound c of the propagation medium, the distance between two compression or dilatation waves, the wavelength λ, is defined as:

$$\lambda = \frac{c}{f} \tag{1.1}$$

In biological medium, the mean value of the speed of sound is 1540 m.s^{-1}. The corresponding wavelengths for ultrasound is usually comprised between 0.08 mm and 1.54 mm

(for frequencies in the range between 1-20 MHz). The wavenumber k, expressed in m^{-1}, is related to the wavelength and is proportional to the number of oscillations. It is expressed with the wavelength or with the angular frequency ω of the wave:

$$k = \frac{2\pi}{\lambda} = \frac{\omega}{c} \tag{1.2}$$

1.1.2 Linear propagation

Mathematical background

The ultrasound wave propagation is based on two major propagation equations in the linear case. Indeed, if the medium is considered homogeneous with a negligeable viscosity and heat effect, the pressure wave p (expressed in Pa), the particule velocity $\vec{u}$ (expressed in $\mathrm{m.s}^{-1}$) and the density ρ (expressed in $\mathrm{kg.m}^{-3}$) evolutions are described by the two linearized Euler's equations [Hamilton and Blackstock (1988)]:

1 - Conservation of the mass

$$\frac{\partial \rho}{\partial t} + \rho \nabla \, . \, \vec{u} = 0 \tag{1.3}$$

2 - Conservation of momentum or motion

$$\rho \frac{\partial \vec{u}}{\partial t} + \nabla p = 0 \tag{1.4}$$

The notation ∇ correspond to the nabla mathematical operator. These two equations characterize the linear behavior of the medium. Indeed, equation (1.3) imposes that no mass is lost or added in the medium during the wave propagation and equation (1.4) related the perturbation of the medium to an external force, here the pressure wave transmitted in the medium. In linear acoustic, the temperature of the medium is considered constant during the wave propagation. With such consideration, the compression is adiabatic and can be described as [Beyer (1960)]:

$$\frac{p}{p_0} = \left(\frac{\rho}{\rho_0}\right)^{\gamma} \tag{1.5}$$

where γ is the ratio of specific heat. The subscript 0 specifies that the variables are taken at their equilibrium. For a constant entropy s, the speed of the propagation wave can be further developed:

$$c^2 = \left(\frac{\partial p}{\partial \rho}\right)_s \tag{1.6}$$

which can be expressed at the equilibrium:

$$c_0^2 = \gamma \frac{p_0}{\rho_0} \tag{1.7}$$

This final expression relates the speed of propagation of an ultrasound wave to the

Medium	Density (kg.m^{-3})	Celerity (m.s^{-1})	Acoustic impedance (MRay)
Air	1.2	344	412e-6
Water	1000	1480	1.48
Blood	1060	1530	1.62
Biological tissue	1000 - 1100	1480 - 1540	1.48 - 1.69

Table 1.1: Presentation of different classical media parameters.

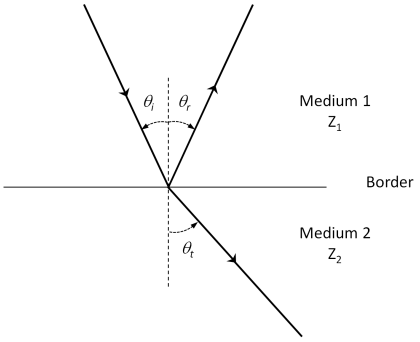

Figure 1.1: Illustration of the incident, reflected and transmitted pressure wave between two different medium.

initial pressure transmitted in the medium and its density.

Transmission and reflection of an ultrasound wave

Each medium can be characterized by its acoustic impedance Z (expressed in kg.m^{-2}.s^{-1} or Rayleigh):

$$Z = \rho c \tag{1.8}$$

Some classical values of density, celerity and acoustic impedance of different media are presented in Table 1.1. The value of the acoustic impedance also depends on the medium's temperature. Indeed, the celerity and the density of the medium slightly change with temperature variation. This evolution is also present on the acoustic impedance.

The acoustic impedance plays a major role when the ultrasound wave go trough different media. Indeed, at the interface between the two media, a part of the ultrasound wave is reflected in the initial medium whereas the rest of the wave is transmitted in the next medium. This phenomenon is highlighted in the Fig. 1.1. The amplitude of the two created waves depends on the incident angle θ_i and the acoustic impedance of the two media. It must be noted that the incident and reflection angles have the same value and the transmitted angle θ_t is defined by the Snell's law. The intensity coefficient of reflection

R and of transmission T are defined as [Ziomek (1995)]:

$$\begin{cases} R &= \dfrac{\left(Z_2\cos(\theta_i) - Z_1\cos(\theta_t)\right)^2}{\left(Z_2\cos(\theta_i) + Z_1\cos(\theta_t)\right)^2} \\ T &= 1 - R = \dfrac{4Z_1Z_2\cos(\theta_i)\cos(\theta_t)}{\left(Z_2\cos(\theta_i) + Z_1\cos(\theta_t)\right)^2} \end{cases} \tag{1.9}$$

In the particular case where the pressure wave arrives perpendicularly to the interface of the two media ($\theta_i = 0°$), the resulting value for the transmitted angle is also equal to 0° and the formulation of R and T are simplified:

$$\begin{cases} R_0 &= \dfrac{(Z_2 - Z_1)^2}{(Z_2 + Z_1)^2} \\ T_0 &= \dfrac{4Z_1Z_2}{(Z_2 + Z_1)^2} \end{cases} \tag{1.10}$$

Two particular cases can be mentioned:

- $Z_1 \gg Z_2$. In this situation, $T_0 \sim 0\%$ and $R_0 \sim 100\%$, meaning that all the pressure wave is reflected in the initial medium.

- $Z_1 \sim Z_2$. In this situation, $T_0 \sim 100\%$ and $R_0 \sim 0\%$, meaning that all the pressure wave is transmitted in the second medium.

The first case corresponds to a situation where the ultrasound wave propagates from a medium to the air. In this situation, all the pressure is sent back to the initial medium. Experimentally, it appends when the ultrasound probe transmits the wave directly in the air. This situation is really dangerous for the transducer because all the energy comes back to the elements and could destroyed them by heating. Using some gel, the acoustic impedance between the probe and the medium is adapted in order to encounter the second case, where the maximum energy is transmitted in the desired medium.

In biological media, such reflections appear in specific cases, for example, when the wave goes from soft tissues to bones. However, in most biological media, the impedance is globally homogenous during the wave propagation and only small limited and small variation can be observed. These inhomogeneities in the medium are seen as scatterers. Two cases can then be summarized with a continuous and a discrete model. With the continuous model, the impedance changes depending on the position and reflection occurs in the medium as described in the Snell's law. With the discrete model, only the scatterers backscatters a signal. Moreover, this backscattering did not follow the previous described law and the scatterers emit a secondary spherical wave with an amplitude related to the incident pressure wave.

1.2 Nonlinear propagation

The linear propagation of an ultrasound wave in a medium is an approximation of the reality. Indeed, the ultrasound propagation is highly nonlinear and the conservation of the momentum (1.4) has to be completed. In the case of the ultrasound nonlinear propagation through non-viscid and lossless medium, the motion equation (1.4) is completed [Hamilton and Blackstock (1988)]:

$$\rho\left(\frac{\partial\vec{u}}{\partial t}+(\vec{u}\ .\ \nabla)\vec{u}\right)=-\nabla p \tag{1.11}$$

In this equation, the convective acceleration term, $(\vec{u}\ .\ \nabla)\vec{u}$, has been introduced in the linear conservation of motion equation. It explains the nonlinear propagation and also complexifies the resolution of equation (1.11).

1.2.1 Nonlinear parameter and nonlinear coefficient definition

Mathematical background

In biological tissues, the relation between the pressure and the density is not driven by equation (1.5) which is only valid for gases. In order to express the evolution of the pressure wave as a function of the density, the pressure is expanded using the Taylor series [Beyer (1960)]:

$$p-p_0=\left(\frac{\partial p}{\partial\rho}\right)_s(\rho-\rho_0)+\frac{1}{2!}\left(\frac{\partial^2 p}{\partial\rho^2}\right)_s(\rho-\rho_0)^2+\frac{1}{3!}\left(\frac{\partial^3 p}{\partial\rho^3}\right)_s(\rho-\rho_0)^3+... \tag{1.12}$$

by using $p^{'}=p-p_0$, $\rho^{'}=\rho-\rho_0$ and the three following parameters A, B and C:

$$\begin{cases} A &= \rho_0\left(\dfrac{\partial p}{\partial\rho}\right)_s\equiv\rho_0 c_0^2 \\ B &= \rho_0^2\left(\dfrac{\partial^2 p}{\partial\rho^2}\right)_s \\ C &= \rho_0^3\left(\dfrac{\partial^3 p}{\partial\rho^3}\right)_s \end{cases} \tag{1.13}$$

the equation (1.12) can be written as:

$$p^{'}=A\left(\frac{\rho^{'}}{\rho_0}\right)+\frac{B}{2!}\left(\frac{\rho^{'}}{\rho_0}\right)^2+\frac{C}{3!}\left(\frac{\rho^{'}}{\rho_0}\right)^3+... \tag{1.14}$$

This development of the Taylor series defines the accuracy of the relationship between the pressure and the density. Indeed, if only the A parameter is kept, the development is equivalent to the linear propagation theory. However, as soon as the B parameter is kept, the relationship between the pressure and the density is nonlinear. The nonlinear parameter is defined as the ratio between the B and A coefficients. Its expression depends

on the celerity, the density and the pressure:

$$\frac{B}{A} = \frac{\rho_0}{c_0^2}\left(\frac{\partial^2 p}{\partial \rho^2}\right)_s \tag{1.15}$$

The nonlinear parameter has a direct impact on the velocity of the pressure wave:

$$c = c_0\left(1 + \frac{B}{2A}\frac{u}{c_0}\right)^{\frac{2A}{B}+1} \tag{1.16}$$

Because the ratio between the particle velocity and the celerity u/c_0 is small, the velocity is usually simplified by:

$$c = c_0 + \left(1 + \frac{B}{2A}\right)u \tag{1.17}$$

From this equation, the nonlinear coefficient β of the medium is defined:

$$\beta = 1 + \frac{B}{2A} \tag{1.18}$$

This nonlinear coefficient is linearly linked to the nonlinear parameter B/A. Finally, the final formulation for the velocity is expressed as:

$$c = c_0 + \beta u \tag{1.19}$$

Visualization of the nonlinear effect

The nonlinear effects are visible on the velocity of the pressure wave expressed in equation (1.19). Using the expression of the particle velocity, the celerity can be further developed as:

$$c = c_0 + \beta\frac{p}{\rho_0 c_0} \tag{1.20}$$

The speed of sound variation Δc can then be expressed as a function of the pressure variation Δp:

$$\Delta c = c - c_0 = \frac{\beta}{\rho_0 c_0}\Delta p \tag{1.21}$$

However, in the particular case of the ultrasound propagation, the mean pressure value is null and the variation is the same of the pressure value ($\Delta p = p$). The maximum and minimum celerity, respectively c^+ and c^-, are then expressed as:

$$c^{\pm} = c_0 \pm \frac{\beta}{\rho_0 c_0}p \tag{1.22}$$

The analysis of equation (1.22) demonstrates that the high pressure part of the wave (compression part) travels faster than the low pressure wave (dilatation part) (Fig. 1.2.a). Because of the cumulative behavior of nonlinear effects, the initial sinusoidal signal (monochromatic signal) turns into a sawtooth signal during the propagation (Fig. 1.2.b). This phe-

nomenon is visible on the Fourier spectrum of the two signals where, initially, just the fundamental component is present (Fig. 1.2.c). After distortion of the initial pressure, the apparition of several harmonics is visible and these harmonics translate the nonlinear behavior of the propagation (Fig. 1.2.d). Higher the nonlinear coefficient, faster the distortion. In theory, the distortion is amplified during the propagation until the pressure wave becomes sawtooth and the high pressure wave overtakes the low pressure one. In medical imaging, such cases are not reach because of the attenuation of the medium and the pressure amplitude transmitted in the medium. The propagation distance to reach this shock wave z_c is expressed as a function of the medium characteristic [Angelsen (2000)a,Ma *et al.* (2005)].

$$z_c = \frac{\rho_0 c_0^3}{\omega \beta p_0} \tag{1.23}$$

In this formulation, it can be seen that the nonlinear process is not only linked to the nonlinear parameter. Indeed, higher the frequency of the initial amplitude, faster the nonlinear components in the signal takes place. The classical characteristics of the medium also impact the shock wave distance and the apparition of the nonlinear components. However, this discontinuity in the pressure wave did not appeared experimentally. A dissipation phenomenon causes the shock progressively looses amplitude and avoids this discontinuity.

1.2.2 Burgers equation

Lossless Burgers equation

For a plane wave in an inviscid (no viscosity) and lossless medium, the propagation of the pressure wave is defined thanks to the lossless Burgers equation [Beyer (1974)]:

$$\frac{\partial p}{\partial z} = \frac{\beta p}{\rho_0 c_0^3} \frac{\partial p}{\partial \tau} \tag{1.24}$$

where z is the propagation direction and τ is the delayed time ($\tau = t - z/c_0$). [Fubini (1935)] proposed a solution of this equation and expressed the pressure wave at z position as:

$$p(z,\tau) = p_0 \sum_{n=1}^{\infty} \frac{2}{n\sigma} J_n(n\sigma) \sin(n\omega_0 \tau) \tag{1.25}$$

where n is the harmonic number, ω_0 is the central angular frequency of the transmitted signal, J_n is the Bessel function of n^{th} order and σ is a dimensionless distance expressed as a function of the medium parameter:

$$\sigma = \frac{\omega_0 \beta p_0}{\rho_0 c_0^3} z = \frac{z}{z_c} \tag{1.26}$$

With such a formulation, valid if $\sigma < 1$, the increase of the harmonics is related to the different probe and medium parameters. In Fig. 1.3, the evolution of the fundamental

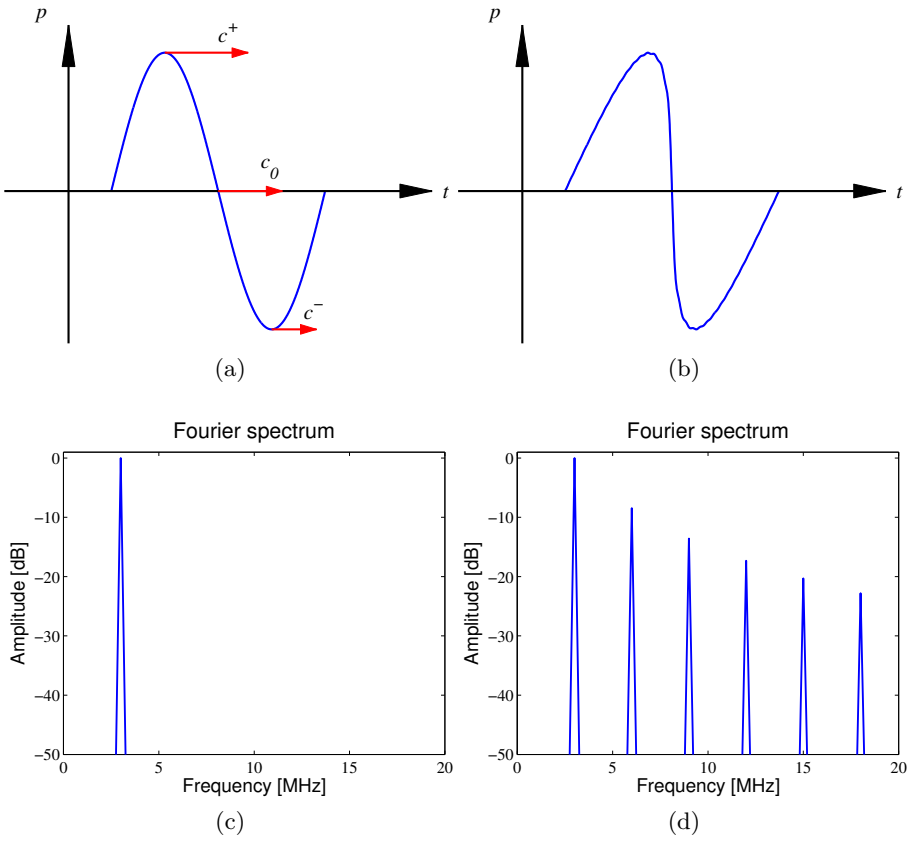

Figure 1.2: Sinusoidal pressure wave transmitted at $z = 0$ (a) and after $z = 500$ mm (b). In the Fourier spectrum, the harmonics, initially absent (c) appear during the propagation (d). The illustration has been obtained for a 3 MHz wave with an initial pressure of 100 kPa after 500 mm of propagation in water ($B/A = 5$). The values and the figure are used for illustration purposes in order to clearly see the sawtooth behavior of the pressure.

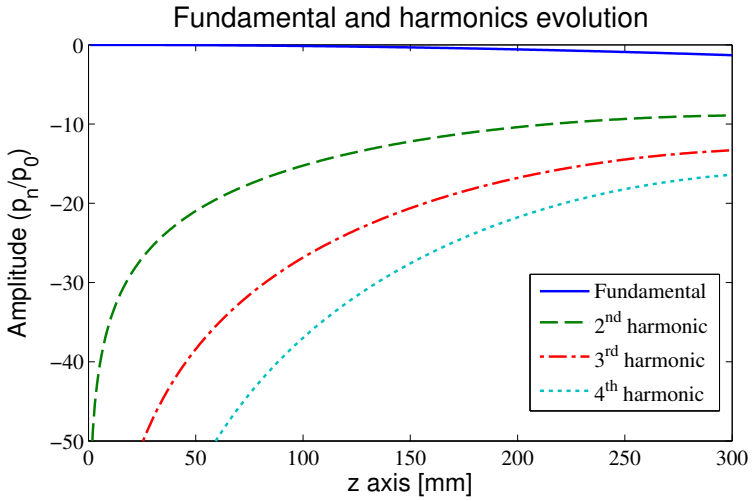

Figure 1.3: Evolution of the fundamental and first three harmonics at different depths for a 2 MHz transmitted wave with an initial pressure p_0 of 300 kPa transmitted in water ($B/A = 5$). The amplitude is normalized by p_0 and then expressed in dB

and the first three harmonics (given in equation 1.25) is displayed at different depths. As shown on the figure, the fundamental component is decreasing whereas the harmonics amplitudes are increasing during the propagation.

Complete Burgers equation

The previous formulation of the propagation is an approximation of the reality. Indeed, without considering the attenuation, the shock wave phenomenon can appear in the medium if the propagation distance is large enough. This configuration is avoided if the attenuation of the medium is considered during the propagation. It simulates the fact that the energy of the propagated wave is dispersed in the medium and transformed in heat due to dissipation. The previous lossless Burgers equation (1.24) is extended to the Burgers equation [Beyer (1974)]:

$$\frac{\partial p}{\partial z} = \frac{\delta}{2c_0^3}\frac{\partial^2 p}{\partial \tau^2} + \frac{\beta p}{\rho_0 c_0^3}\frac{\partial p}{\partial \tau} \tag{1.27}$$

where δ combined the different effect of the thermo-viscious dissipation. According to the medium and the considered approximations, the expression of δ can differ. The previous solution of Fubini is then no more valid.

1.2.3 KZK equation

The previous proposed propagation equation did not take into account the finite size of the transducer transmitting the ultrasound wave into the medium. For finite transmitter sizes, the diffraction of the transducer has to be taken into consideration into the propagation equation. The Burgers equation (1.27) becomes the KZK equation, described

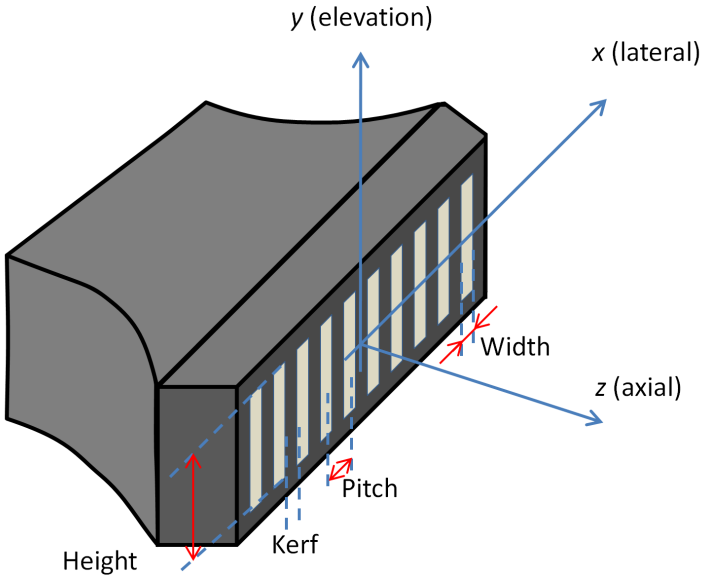

Figure 1.4: Geometrical description of the linear array parameters and of the landmark (x, y, z).

by [Kuznetsov (1970), Zabolotskaya and Khokhlov (1969)]:

$$\frac{\partial p}{\partial z} = \Delta_{\perp} p + \frac{\delta}{2c_0^3}\frac{\partial^2 p}{\partial \tau^2} + \frac{\beta p}{\rho_0 c_0^3}\frac{\partial p}{\partial \tau} \tag{1.28}$$

where $\Delta_{\perp} p$ represents the diffraction's effect of the transmitter. This diffractive term defines the pattern of focalization due to the probe's geometry. Interactions between the different elementary sources focus the energy in the medium for the fundamental and also the harmonics. Generally, two types of transmitter are used. Circular elements of radius r are often used in research applications because of their easiest known modelling, their experimental simplicity and cost. They can also be focalized or not. The second type of transmitters are the medical probes used on commercial scanner. These probes are defined by a set of geometric dimensions that is of major importance for the diffraction. A probe is usually composed of N_{ele} identical elements (elementary transducer) which have a dimension Width and Height in the lateral and elevation direction. The spacing between two consecutive elements is the Kerf. Another dimension, the Pitch correspond to the distance between the center of two consecutive elements (Pitch = Width + Kerf). For a linear array, these geometric parameters are highlighted in Fig. 1.4.

In the KZK equation, the formulation of the diffraction's effect depends on the probe shape: a circular piston source leads to equation (1.29) and a linear array, as shown in Fig. 1.4, to equation (1.30):

$$\Delta_{\perp} p = \int_{-\infty}^{\tau} \left(\frac{\partial^2 p}{\partial r^2} + \frac{1}{r}\frac{\partial p}{\partial r} \right) d\tau' \tag{1.29}$$

$$\Delta_{\perp} p = \int_{-\infty}^{\tau} \left(\frac{\partial^2 p}{\partial x^2} + \frac{\partial^2 p}{\partial y^2} \right) d\tau^{'} \tag{1.30}$$

where $\tau^{'}$ is the integration variable related to the retarded time τ, (x, y) are the lateral and elevation dimension in the probe plane (perpendicular to the propagation axis).

1.3 Echographic image beamforming

1.3.1 Principle of the image formation

In echographic image, the echoes are based on the previously described discrete model. From the initial transmitted ultrasound wave, the different scatterers of the medium backscatter echoes to the ultrasound probe. By using the ultrasound probe in reception mode, meaning that the probe records the pressure that hits its surface and converts it in an electrical signal, an image is created. Indeed, all the scatterers emit a wave that arrives at different time to the probe surface according to their position. The sum of these different echoes gives to the resulting image its noisy aspect, called the speckle.

The ultrasound image is obtained by repeating the same operations. First, a sub-part of the ultrasound probe is selected and only this part of the transducer transmits the ultrasound wave in the medium. From the global pressure wave backscattered by the medium, each selected active transducer of the probe recorded the echo and creates, for each of them, a signal called radio frequency (RF) signal. By juxtaposing these signals together, the elementary or pre-beamformed RF image is obtained. However, in function of the beamforming strategy used in reception (apodization, focalization), the elementary RF image is combined into one signal: the post-beamformed RF line. Then, by changing the sub-part of the used probe, different post-beamformed RF lines are created and correspond to different part of the medium. Using all these lines together, the final post-beamformed RF image is obtained. Conveniently, the term post-beamformed is often suppressed when it deals with RF image. To summarize, from the initial pressure wave transmitted by the sub-probe, the medium backscattered waves which are recorded by the active element and converted into a single RF line. When the different parts of the probe are used, the final RF image is computed.

However, the RF image, even if it contains a lot of information, is difficult to visualize because it presents a lot of oscillations at the transmitted frequency (Fig. 1.5.a). To visualize the image, it is necessary to demodulate the signal around a lower frequency that contains less information compared to the RF signal. This demodulation is conducted thanks to a low pass filter. The absolute value of an Hilbert transform can also be used. The resulting image, called the B-mode image, proposes an interpretable image (Fig. 1.5.b). To reduce the dynamic of the image and to highlight the different regions, a log-compression is used. In the resulting image, expressed in dB, all the structures are finally visible and the user has the possibility to chose the dynamic in the display (Fig. 1.5.c). In this way, the user can chose the number of dB wanted in the image. In the tissue, the

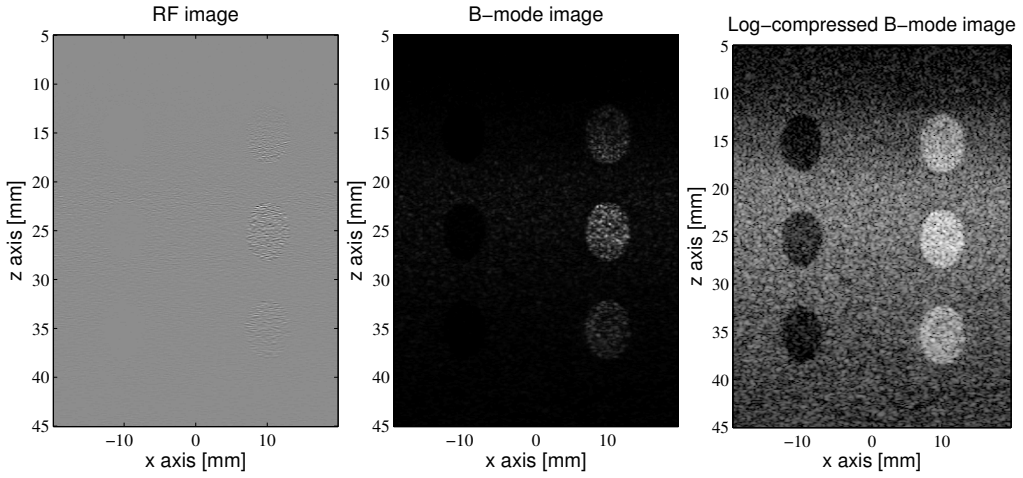

Figure 1.5: Illustration of the different ultrasound image: (a) the RF image, (b) the B-mode image and (c) the log-compressed B-mode image. The final log-compressed B-mode image show clearly the different structures in the medium. A dynamic of 50 dB has been used in the log-compressed image.

ultrasound are attenuated. To compensate this effect, a time gain compensation (TGC) function is used. The TGC increases the dynamic in function of the depth to compensate the loss due to the attenuation, for example a TGC of 1 dB.cm^{-1} increases the dynamic by 1 dB each centimeter. All these denominations (RF, B-mode, log-compressed B-mode image) are used in the manuscript to describe the different ultrasound images.

1.3.2 Resolution in echographic images

The resolution in echographic image characterizes the possibility to distinguish two close scatterers. From one hand, the axial resolution and on the other hand, the lateral and elevation resolutions do not depend on the same parameters. The two last resolutions are usually considered as equal. In the three dimensions, the resolution differs because it strongly depends on the beam shape described by different parameters:

- The transmitted frequency
- The number of cycles in the transmitted signal
- The aperture/geometry of the probe
- The depth of interest
- The beamforming strategies, in transmission and reception

The two first parameters define the length of the transmitted pulse in the medium. The shorter the pulse, the better the axial resolution. Increasing the frequency and decreasing the number of cycles is a way to improve the axial resolution. However, for a higher

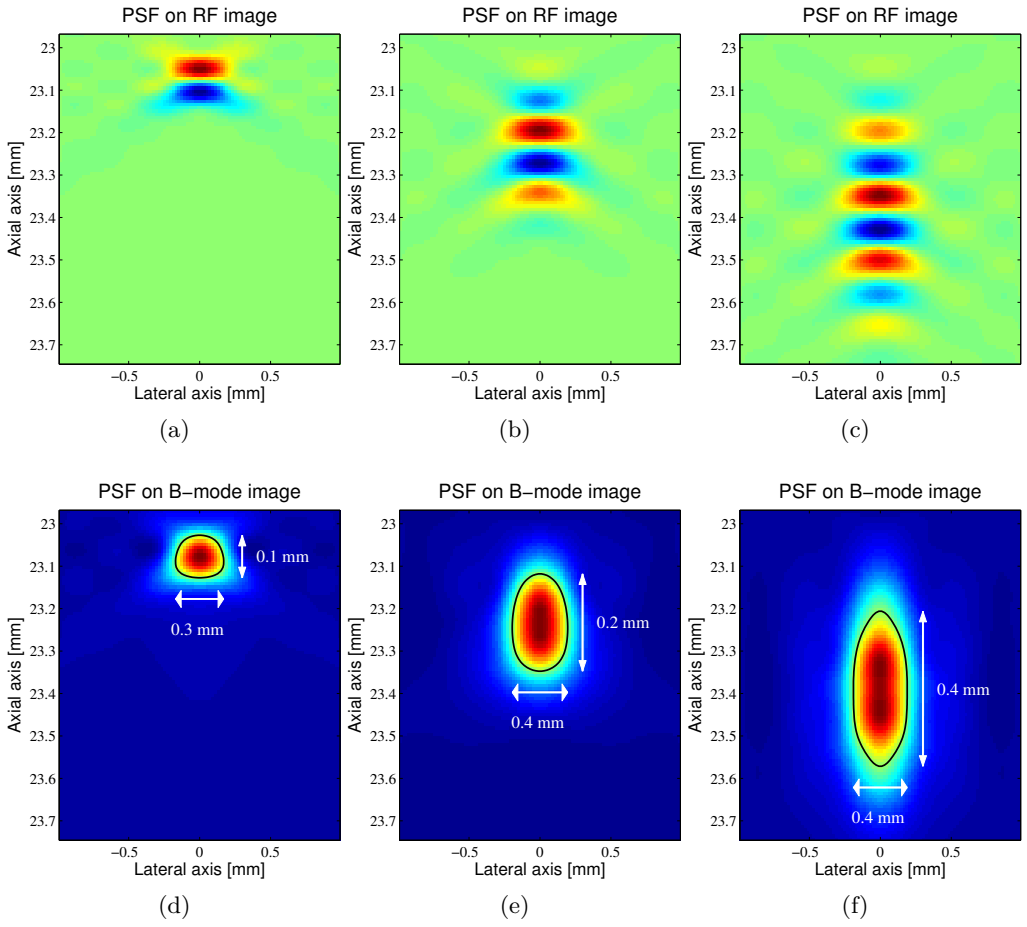

Figure 1.6: PSF on RF and B-mode image for an initial signal composed of 1- (a, d), 3- (b, e), and 5-cycles (c, f) of a 5 MHz sine. The resulting axial and lateral resolutions are measured at half maximum and are highlighted on the B-mode image.

frequency, the propagation depth of the ultrasound wave is decreased. A trade off has to be found between the desired axial resolution and the investigated depth to reach. The other parameters rather impact the shape of the beam and the lateral and elevation resolution.

The resolution can be defined thanks to the point spread function (PSF). The PSF corresponds to the response of a theoretical unique scatterer in the medium. It depends on the parameters listed above. Different PSF, obtained in simulation, can be seen in the Fig. 1.6. In this figure, only the number of cycles of the excitation signal has been changed for the three images. The PSF is displayed as a RF image (Fig. 1.6.a-c) or as a B-mode image (Fig. 1.6.d-f). The resolution for the axial and lateral dimensions can be defined thanks to full width at half maximum (FWHM) amplitude of the PSF in the B-mode image [Angelsen (2000)b, van Wijk and Thijssen (2002)]. These resolutions are highlighted in the corresponding figure.

1.3.3 Broadband, fundamental and second harmonic images

In medical imaging, the RF image contains the backscattered frequencies of the pressure field. Because of the nonlinear propagation, the RF image contains fundamental but also harmonic components in its spectrum. Different images can then be extracted from the same initial RF image:

- **Broadband image**: the entire spectrum is used
- **Fundamental image**: the spectrum is filtered around the fundamental component
- **Second harmonic image** (named harmonic imaging): the spectrum is filtered around the second harmonic component

In medical imaging, the fundamental and the broadband images are quite similar because of the low level of the second harmonic component and the broadband image is usually displayed on commercial scanner. However, the harmonic image is increasingly used because of its higher resolution [van Wijk and Thijssen (2002)] and the used of contrast agents [Bleeker *et al.* (1990), Zhang *et al.* (2000), Eckersley *et al.* (2005), Bouakaz and de Jong (2007)]. Indeed, contrast agents have a strong nonlinear coefficient [Wu and Tong (1998)] and they backscatter a lot of harmonics. This behavior makes the harmonic imaging perfectly adapted to contrast agents. They are usually injected into the blood circulation and allow to highlight the perfused tissues. Another clinical information comes from the possibility to image the progressive washing-out of the contrast agent perfused in some organs with fresh blood. Such considerations have also developed research actions of drug or gene delivery using the contrast agents as a carrier [Scheller *et al.* (2003), Ferrara *et al.* (2007), Escoffre *et al.* (2010)].

1.4 Conclusions

This introductive chapter sets the different notations and the vocabulary used in medical ultrasound. The linear and nonlinear propagation models have been presented as well as the image beamforming [Wells (2006)]. In medical imaging, the scanner usually provides the B-mode image but not the RF data. However, to be able to do research works on harmonic techniques, this image is crucial in order to access to the different frequency components. On some research scanners, this image is available and several methods are currently developed in order to propose new imaging modalities and original results.

The nonlinear parameter is an important characteristic of the medium. Indeed, various authors have shown that it changes for different materials. Moreover, the B/A parameter of contrast agents is higher than the tissue one [Wu and Tong (1998)]. Its evaluation can be very interesting in terms of tissue characterization or parametric imaging. In this way, it will be very promising to be able to simulate media with inhomogeneous nonlinear parameter and to evaluate it. These issues are developed in the next two parts of the thesis.

I Simulation in nonlinear ultrasound

Chapter 2

Review of simulation tools in medical ultrasound

This chapter is a review of the different resources that are described in the literature for ultrasound simulation. Two groups of simulation tools have so far been presented: those devoted to the simulation of the linear or nonlinear ultrasound wave propagation and those implemented for the simulation of ultrasound images.

2.1 Review on pressure field simulator with nonlinear propagations

During the last fifty years, the nonlinear propagation of ultrasound in media has been studied and the first significant results have been presented by [Freedman (1960)], who worked on the acoustic field produced by a rectangular piston, followed by [Ingenito and Williams (1971)] who focalized their work on the second harmonic generated by such sources. Other authors, as [Lucas and Muir (1983)], derived the previous formulation to the case of focusing sources. In the next sections, different propagation simulators based on the nonlinear equations are presented. The solutions used are summarized in three groups:

- Finite difference approaches
- Spectral approaches
- Coupled approaches

2.1.1 Finite difference approaches

To solve the KZK equation presented in equation (1.28), [Lee and Hamilton (1995)] and [Hamilton and Blackstock (1997)] proposed a time domain algorithm as solution. The proposed algorithm takes into account the diffraction of the probe and the nonlinearity of the medium. However, the solution is only valid for circular piston sources. This work has been extended in the same laboratory to take into account the absorption effect [Cleveland *et al.* (1996)]. The resulting software is called the Texas code and can be freely downloaded on the Internet. Several years later, [Yang and Cleveland (2005)] proposed an extension of the previous software. The major improvement comes from the change of the coordinate system (spherical coordinate to Cartesian system). The finite difference scheme has been updated and new probes can be simulated. The experimental results are in good agreement with the simulated one. A similar approach has been developed by [Kaya *et al.* (2006)] to simulate the propagation from a square or a rectangular array.

Another simulator can be used to simulated the nonlinear propagation of an ultrasound pressure wave. Voormolen proposed an algorithm to solve the KZK equation for rectangular array with arbitrary excitation [Voormolen (2007)]. The experimental results are in good accordance with the simulated one. The advantage of this method comes from the possibility to easily simulate clinical array with the desired beamforming strategy in transmission. The impact of the different dimensions of the array (pitch, height and kerf) is taken into account during the solution. In his work, the different effects are solved only with a finite difference scheme. However, in order to decrease the computation time, the steps in the propagation direction are not equal because in the near field, more accuracy is required. Similar schemes have been done to take into account the possible inhomogeneity of the speed of sound, density, and the different reflection effects [Pinton *et al.* (2009), Pinton *et al.* (2011)].

In all the finite difference schemes, the propagation starts with the transmission and then, the pressure evolution is computed step by step in the propagation direction. Doing this, a high order of nonlinear interaction is considered and the evolution of the entire frequency spectrum is simulated.

To summarize, the time domain solution algorithms present the advantage to propose a very accurate solution with a high order of nonlinear interaction. However, the computation time is very long because of the accuracy requirement between the different steps to ensure the convergence of the solution.

2.1.2 Spectral approaches

The spectral approaches can be divided into two groups:

- Use of the Fourier series decomposition of the pressure field to solve the KZK equation
- Solve the propagation equation in the Fourier domain using an angular spectral

method (ASM)

Fourier series decomposition

The use of the Fourier series to solve the KZK equation has been initially proposed by [Aanonsen *et al.* (1984)]. One direct application of this proposition has been implemented in the Bergen code [Berntsen (1990)] which simulates the ultrasound propagation from a piston or a 2D source. The accuracy of the simulation has been tested and improved by [Kamakura *et al.* (1992)], [Sahin and Baker (1994)] and [Baker *et al.* (1995)].

A similar formulation has been used by [Ding (2000)]. He simplified the algorithm to compute only the second order field (second harmonic, sum- and difference-frequency components) by linearizing the solution with a set of complex of Gaussian beams. With this formulation, a mathematical solution can be computed under this approximation. This algorithm has been extended to arbitrary sources [Ding (2004)] and limited diffraction beams [Ding and Huang (2007)].

Angular spectrum method

The angular spectrum method (ASM) solves the propagation equation in the Fourier domain in order to reduce the derivative order on the initial equation. Alais *et al.* used the Fourier transform (FT) to solve different propagation equations [Alais and Hennion (1976), Alais and Hennion (1979)] and [Szabo (1978)] proposed to use it in order to compute the profile of any source. Then, Christopher and Parker have reused this theoretical background in order to compute the linear and nonlinear propagation in a medium [Christopher and Parker (1991)a, Christopher and Parker (1991)b] and the mathematical justification of the conservation of energy and the absorption has been published by [Wójcik (1998)].

After the initial formulation of Szabo, [Schafer *et al.* (1987)] have studied the impact of the propagation through two different media. Then, a similar work has been conducted by [Landsberger and Hamilton (2001)] to study the second harmonic generation of a wave propagating through a solid inserted in a surrounding fluid.

Some years after the work of Christopher, Vecchio *et al.* have compared the predicted pressure obtained in simulation with the experimental pressure received at different depths [Vecchio and Lewin (1994), Vecchio *et al.* (1994)]. A circular source has been used and the correspondence between the different planes showed an error inferior to 1.5 dB. Today, some explicit formulations have been proposed for the second harmonic [Dursun *et al.* (2005), Yan and Hamilton (2006)] but also for the higher ones [Pasovic *et al.* (2009)]. With such formulations, the fundamental and the harmonic components can be simulated. No higher-order interaction (such as sum- and difference-frequencies) can be investigated. To obtain a correct accuracy in the near field, [Zeng and McGough (2008)] have estimated the dimensions of the required matrix and the necessary zero-padding.

The ASM is faster than the previous proposed simulators (time-domain, Fourier series) thanks to the reduction in the nonlinear order resolution. Indeed, only the fundamental

and corresponding harmonic are computed and no nonlinear interaction (as sum- and difference-wave) are computed. Moreover, it allows to compute the second harmonic field in a particular point and not in all the space which also strongly reduces the computation time. An open source software based on the ASM, has been proposed by Anderson [Anderson (2000)]. A 2D rectangular array is designed as transmitter to investigate a volume and the resulting simulation time has been decreased using the ASM. A feasibility study to use ASM coupled with FieldII [Jensen (1996)] has been done by Du *et al.* [Du and Jensen (2008), Du *et al.* (2010)] but with the high sampling of the probe computed with FieldII, the computation time is too high to be envisaged.

2.1.3 Coupled approaches

In the literature, a set of methods did not use just the finite difference approach or the ASM. [Lee and Hamilton (1995)] have shown that the different effects (absorption, diffraction and nonlinearity) can be solved separately. [Christopher and Parker (1991)a] proposed to solve the diffraction and the absorption of the wave using the ASM and, then, to use a classic finite difference method for the nonlinear effects. The same strategy has been used by various authors [Zemp *et al.* (2003), Wójcik *et al.* (2006), Wójcik *et al.* (2008)]. The difference in these methods comes from the different sampling or sub-sampling used to solve the diffraction and absorption effects from one hand and the nonlinear propagation resolution on the other hand. With such considerations, higher-order of nonlinear interaction can now be simulated using some advantages of the ASM approaches.

The team of the Norwegian University of Science and Technology proposed another simulation tool, called Absersim, to simulated the nonlinear ultrasound propagation [Frijlink *et al.* (2008)]. The program is based on this splitting theory. The diffraction is solved with the ASM and the attenuation has been chosen frequency dependent [Varslot and Taraldsen (2005), Varslot and Måsøy (2006)]. The nonlinear effects are considered only in the propagation direction to reduce the complexity, but the introduced error is negligible. The resulting pressure maps obtained are in good agreement with FieldII for the fundamental component [Frijlink *et al.* (2008)]. One drawback of this simulation tool comes from the definition of the kerf of the probe which is not integrated in the Abersim simulator.

A recent novel method, proposed by Verweij *et al.* called Iterative Nonlinear Contrast Source (INCS), defines the nonlinear effect as a contrast source. This contrast source is solved with an iterative scheme [Verweij and Huijssen (2009), Huijssen and Verweij (2010)]. The contrast source is computed in the Fourier domain in order to reduce the number of derivative terms. Recent works allow to linearize the INCS method and the results are in good agreement with other simulators [Demi *et al.* (2010)b]. Proposition to simulate the inhomogeneity in the absorption and the nonlinear coefficient in the propagation direction have also been made [Demi *et al.* (2010)a].

Simulator name	Method used	Source shape	Dimension
Bergen code [Berntsen (1990)]	Fourier series	Piston or 2D sources	1D/2D
KZK Texas [Lee and Hamilton (1995)]	Time domain	Piston	1D
Voormolen [Voormolen (2007)]	Time domain	Phased array transducer	3D
Absersim [Frijlink *et al.* (2008)]	ASM / Time domain	Phased array transducer	3D
INCS [Huijssen and Verweij (2010)]	ASM / Time domain	Phased array transducer	3D

Table 2.1: Main characteristics of nonlinear propagation simulators described in the literature.

2.1.4 Conclusion

The different theoretical and implemented simulation tools have been presented and are summarized in Table 2.1. The principal specifications of each simulator are presented. The time domain solutions propose a higher order in nonlinear interaction but need a long computation time to converge to the solution. The ASM allows to quickly compute the second harmonic component at a specific point in the medium with the use of the Fourier transform. With recent coupled method, the advantage of each method are kept to decrease the computation time. The diffraction is quickly computed in the Fourier domain and a classical finite difference method is used to keep a higher order nonlinear interaction.

The Abersim and the Voormolen simulators are illustrated in Figure 2.1. The field is produced by the linear array LA533 described in Appendix A.2. A five-cycle sine at 5 MHz with a Gaussian window and focalized at 70 mm has been used. No apodization has been used on the different transmitted elements. From the 3D spatial field, the one-way field is extracted from the plane $y = 0$.

In order to quickly simulate the second harmonic field, the ASM background appears to be the more attractive. However, no theoretical background has been developed for inhomogeneous nonlinear medium. Only the Voormolen or the INCS simulators allow to consider a spatial variation of the nonlinear parameter in the propagation direction. Classic medical media have inhomogeneous nonlinear parameter and not only axial variation. No simulation tool exists to quickly simulate the second harmonic field of any 3D inhomogeneous nonlinear medium. We propose a new simulator that answers these issues in the chapter 3.

2.2 Review on medical RF ultrasound image simulation

The simulation of medical RF ultrasound images has been largely developed during the past years and two types of method exist:

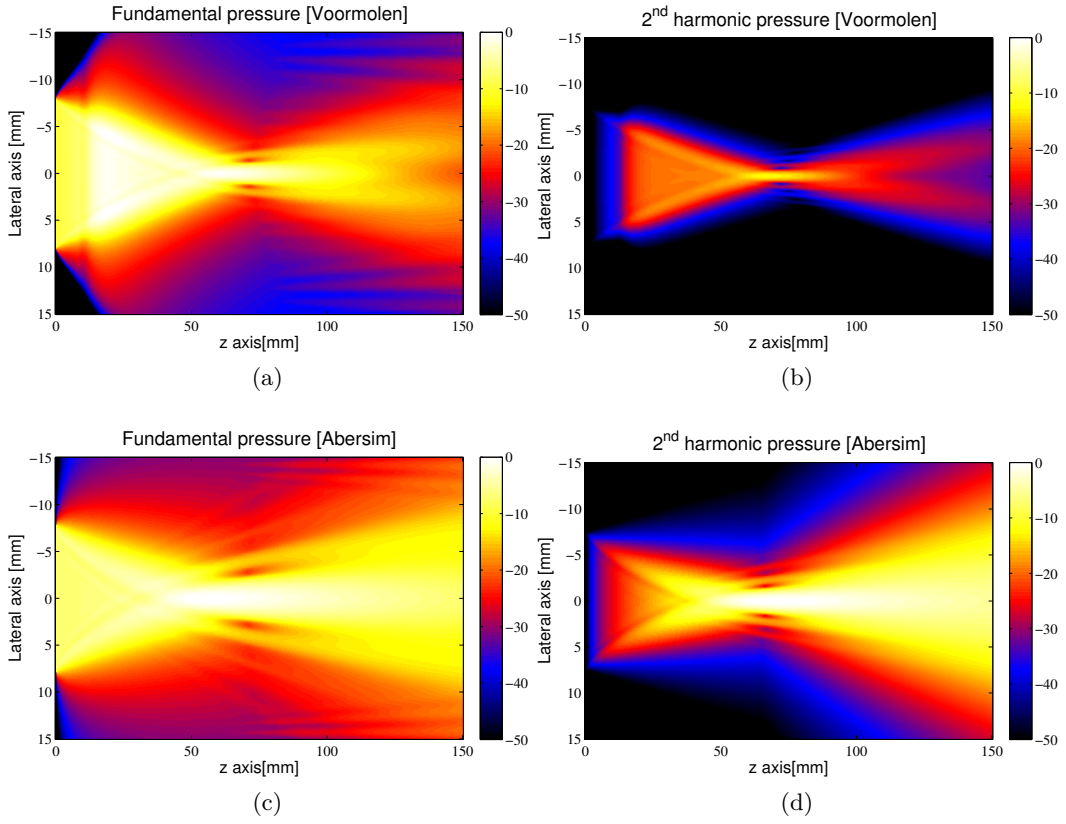

Figure 2.1: One-way field computed with (a-b) Abersim [Frijlink *et al.* (2008)] and (c-d) Voormolen simulator [Voormolen (2007)]. (a, c) show the fundamental component and (b, d) show the second harmonic one. A five-cycle sine at 5 MHz with a Gaussian window and focalized at 70 mm has been used. No apodization has been used on the 64 active elements of the probe.

- Methods based on an acoustic model of the ultrasound field propagation
- Methods based on a linear convolution model

2.2.1 Acoustic model

Models

The acoustic model directly takes into account the different parameters that impact the image construction. The probe and space dimensions (1D, 2D or 3D), such as the beamforming strategies in transmission and reception impact the image formation. The acoustic model is close to the physical phenomena and provides realistic images but need a long time of computation. The most famous tools in the ultrasound community in RF image simulation is FieldII [Jensen and Svendsen (1992), Jensen (1996)] which is based on the approaches developed by [Tupholme (1969)] and [Stepanishen (1971)a, Stepanishen (1971)b]. With this tool, the complete probe and space parameters as well as the beamforming strategies (in transmission and reception) can be controlled. Consequently, very complex and realistic simulations can be conducted. Other tools exist in the literature to simulate images. DREAM (Discrete Representation Array Modeling), also based on the Stepanishen approach, has been proposed by [Piwakowski and Sbai (1999)]. Using the discrete representation of the Rayleigh integral, [Holm (2001)] designed Ultrasim which computes the acoustic field with different approximations in the near and far fields. The advantage of this software is the possibility to simulate data either for medical or sonar applications. For non destructive testing applications, [Calmon *et al.* (2006)] designed the CIVA software.

FieldII

FieldII software is very realistic and is very accurate. Indeed, the PSF calculated with FieldII depends on the depth and on the different acoustic parameters of the probe, medium and beamforming strategies. For each scatterer of the medium, the backscattered signal is recorded by the active elements of the probe and the elementary RF lines are constructed. With the beamforming sets in reception, the elementary lines are combined using appropriate delays to create one RF line of the resulting image. Then the simulation is repeated for the different RF lines in the image. The major drawback of FieldII is the large computation time, but it has been shown that the creation of the different RF lines can be parallelized to reduce the total computation time [Jensen and Nikolov (2000)].

2.2.2 Linear convolution model

The linear convolution model, initiated by [Bamber and Dickinson (1980)], consists to convolve the PSF of the system and the scatterers of the medium. Contrary to the acoustic method, the PSF used in the convolution is constant for a given medium. Meunier and Bertrand [Meunier and Bertrand (1995)a, Meunier and Bertrand (1995)b] used this type

of simulations to quickly simulate RF images. With the convolution model, different authors have worked on the relation between the axial resolution and the signal to noise ratio [Srinivasan *et al.* (2003)].

The main interest of such a simulation technique comes from its fast algorithm based on a 2D or 3D convolution for each image. Large amount of data can then be easily and quickly simulated.

The convolution model is also used for different algorithm validations. [Yu *et al.* (2006)] have estimated the variation in the speckle intensity in function of the movement of tissues and the resulting effect on the movement estimation algorithm. In the movement estimation field, [Jiang and Hall (2007)] have estimated the performance of their approach with simulated images using the linear convolution model. [Gilliam and Acton (2007)] have proposed a myocardial model to estimate the performance of their image segmentation. In elastography, the out-of-plane movement impact has been estimated by [Lee *et al.* (2007)] with a 3D scatterers map which is moved in the simulations. The scatterers movement has also been simulated by Marion *et al.* to estimate the blood flow speed in 2D+t images into the CREASIMUS simulator [Marion and Vray (2009), Marion *et al.* (2009)]. [Franceschini *et al.* (2007)] have used this model in tissue characterization application to estimate the accuracy of their structure size estimation approach.

2.2.3 Comparison between FieldII and CREASIMUS

Two different images obtained with CREASIMUS [Marion and Vray (2009), Marion *et al.* (2009)] and FieldII [Jensen (1996)] are displayed in Figure 2.2. The probe used in the simulation is the LA533 (Appendix A.2). The transmitted pulse is a four-cycle sine at 3.5 MHz with an Hanning windows and focalized at 60 mm. A Hanning apodization has been used in transmission and reception on the different active elements in the FieldII beamforming strategy. The PSF has been first calculated thanks to the FieldII image and then, used in the CREASIMUS in the linear model. The cyst phantom is composed of 100 000 scatterers (3.6 scatterers/mm^3) and defined as in [Jensen and Munk (1997)]. The scatterers are randomly set in the medium but three different area can be highlighted: five punctual scatterers on the left, five hyper-echoic cysts in the middle (with increasing diameters versus depth) and five hypo-echoic cysts on the right (with decreasing diameters versus depth). On the resulting images, the PSF variability is visible. The resolution in the CREASIMUS image (Figure 2.2.b) is constant during the propagation although the resolution in the FieldII (Figure 2.2.a) image is better in the focal region compared to the near field. The punctual scatterers present in the left part are also more visible. However, the computation time to obtain the FieldII image is bigger than CREASIMUS. Indeed, approximately 2 hours are required for the FieldII image whereas the CREASIMUS simulation takes less than 1 second. Approaches based on the linear convolution model are often used to simulate big amount of data although acoustic model are used to simulate very realistic images.

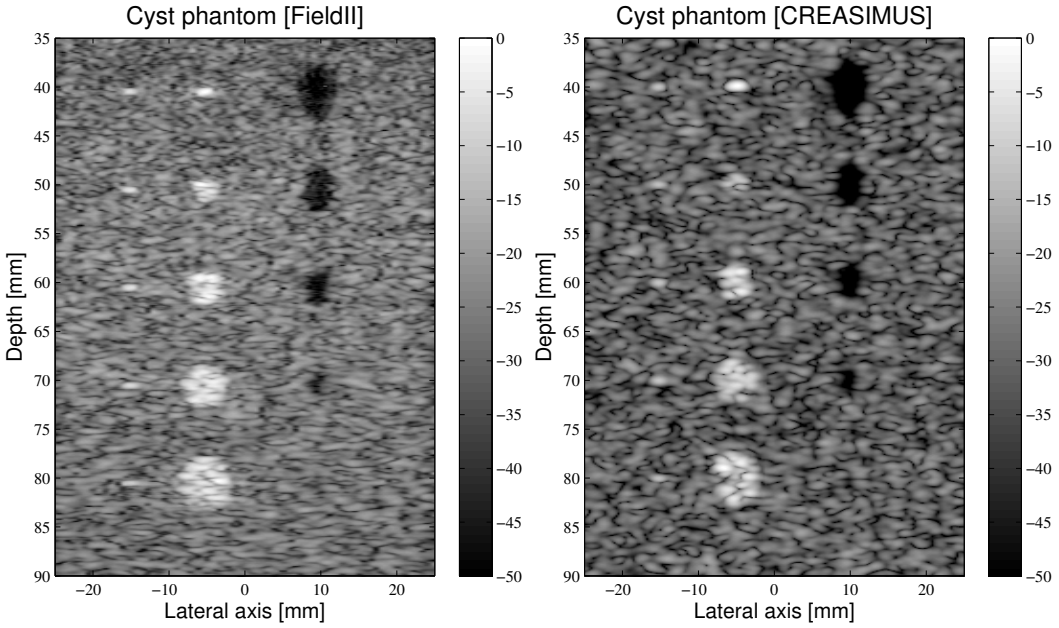

(a) (b)

Figure 2.2: B mode image of the cyst phantom obtained with FieldII (a) and CREASIMUS (b). The resolution in CREASIMUS is constant during the propagation thanks to the linear convolution model, while the one of FieldII is better in the focal region. A four-cycle sine at 3.5 MHz with an Hanning window and focalized at 60 mm has been used. An Hanning apodization has been used in transmission and reception on the 64 active elements of the probe.

2.3 Discussion and conclusion

In this chapter we have introduced the different tools that exist in the literature to simulate the nonlinear propagation and the RF ultrasound image creation. In nonlinear propagation, the time-domain and Fourier solution composed, with their mixed approaches, the two major strategies in nonlinear propagation simulation. However, no very fast tool, allowing heavy simulation, exists in the literature. Some approaches have proposed a nonlinear parameter variation along the propagation axis but none of them proposed a completely free nonlinear parameter distribution in the medium. Concerning the ultrasound image simulation, FieldII software, despite its long computation time, is the most popular and used tool in ultrasound community. However, it did not propose the nonlinear image simulation which appear to be necessary to test every harmonic imaging techniques. We propose in the two next chapters to answer this issue and proposed some new algorithms which allow to simulate nonlinear propagation in tissue.

Chapter 3

Computation of fundamental and second harmonic field in media with inhomogeneous nonlinear coefficient

This chapter is devoted to the presentation of a new nonlinear propagation simulator which takes into account the possible variation of the nonlinear parameter in the medium. This work has been published in IEEE UFFC [Varray *et al.* (2011)f] and accepted in a conference [Varray *et al.* (2011)d].

3.1 Introduction

As detailed in the previous chapter, when an ultrasound wave propagates, distortion of the wave induced by the medium appears, and harmonics of the transmitted frequency are created. The increase in harmonics depends on the medium (density, sound velocity, and nonlinear parameter B/A), the initial pressure, and the propagation distance. The ultrasound propagation in nonlinear medium can be either experimentally tested or studied in simulation. However, specific tools are needed to simulate media with an inhomogeneous nonlinear parameter, for instance, a vessel or an hyper-vascularized tumor with contrast agents surrounded by tissue.

In chapter 2, the different nonlinear propagation methods and simulators have been reviewed. All these techniques did not take into account the possible spatial variation of the nonlinear coefficient β. When complex media are simulated, such as media containing

contrast agents, the evolution of the nonlinear parameter is crucial. The objective of the simulator is to compute fastly the nonlinear propagation and to have the possibility to use arbitrary nonlinear coefficient map. In this sense, a generalization of the angular spectrum method (GASM) based on the mathematical background of [Alais and Hennion (1979)] and [Aanonsen *et al.* (1984)] has been used. This GASM makes it possible to simulate propagation using the Westervelt equation with inhomogeneous nonlinear media.

The chapter is organized as follows. The first part reviews the mathematical solutions for the first and the second-harmonic of the pressure field, using the ASM. Taking into account the spatial variations of the nonlinear parameter of the medium, the generalization is then described. The second part describes the algorithm implementation and the graphic process unit (GPU) solution proposed to decrease the computation time. Indeed, the implementation of the GASM is particularly adapted to the high parallelism computing proposed by the GPU. Then a third section is devoted to the results obtained with this new tool. First, the pressure fields in media with a homogeneous nonlinear parameter are simulated and compared with those obtained with established simulators. Then GASM simulations of media with an inhomogeneous parameter are presented. Experimental measurements are also shown, demonstrating GASM's high level of accuracy. Finally, the conclusions are presented.

3.2 The mathematical background of GASM

3.2.1 The basis of the ASM

The ASM is based on the computation of the FT of the pressure field $p(z, x, y, t)$ at a propagation distance z from the source. Indeed, the evolution of the pressure is not computed in the temporal domain but in the Fourier domain. The principle of ASM is schematized in Fig. 3.1. A 3D hybrid FT must be used, corresponding to the superposition of a transverse 2D FT in the spatial lateral-elevation (x, y) plane and the temporal domain. These Fourier transforms of the function p are defined as:

$$F_{xy}[p] = \iint p(x, y) e^{-i2\pi(f_x x + f_y y)} dx dy \tag{3.1}$$

$$F_t[p] = \int p(t) e^{i2\pi f_t t} dt \tag{3.2}$$

with f_x and f_y the spatial frequencies in the x and y direction and f_t the temporal frequency. Then, the final 3D hybrid FT is obtained with:

$$\mathcal{F}(p) = F_t \left[F_{xy}[p] \right] \tag{3.3}$$

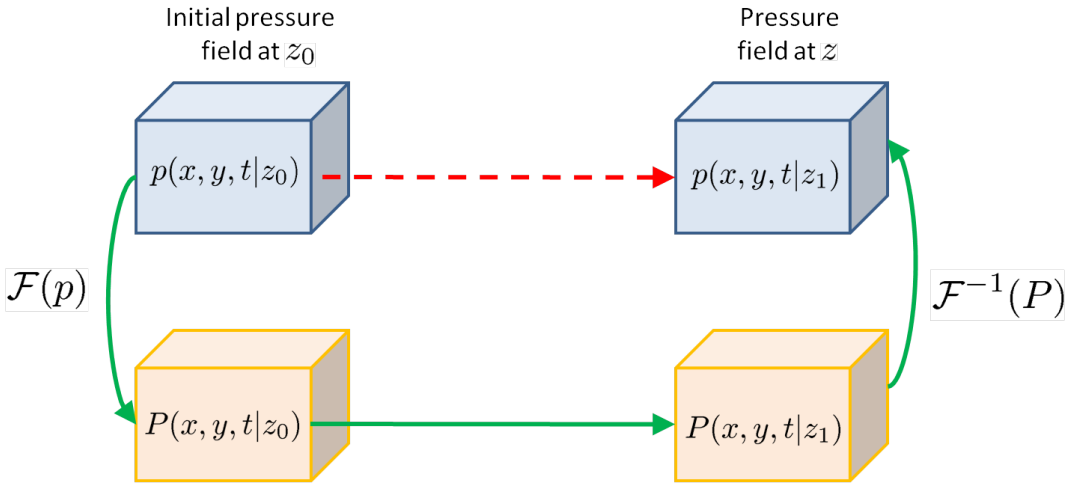

Figure 3.1: Principle of the ASM. The pressure p is not computed in the temporal domain, but in the Fourier domain thanks to the FT and the IFT.

Using the same notations, the FT and the inverse Fourier transform (IFT) of the pressure are respectively expressed as:

$$P(z, f_x, f_y, f_t) = \iiint p(z, x, y, t) e^{-i2\pi(f_x x + f_y y - f_t t)} dx dy dt \tag{3.4}$$

$$p(z, x, y, t) = \iiint P(z, f_x, f_y, f_t) e^{i2\pi(f_x x + f_y y - f_t t)} df_x df_y df_t \tag{3.5}$$

From the definitions in (3.4) and (3.5), the following property of the FT is obtained:

$$\mathcal{F}\left(\frac{\partial^n p}{\partial v^n}\right) = (-2i\pi f_v)^n \mathcal{F}(p) \tag{3.6}$$

$$\mathcal{F}\left(\frac{\partial^n p}{\partial t^n}\right) = (2i\pi f_t)^n \mathcal{F}(p) \tag{3.7}$$

with the variable v corresponding to x or y.

3.2.2 Propagation equation

The lossless Westervelt propagation equation expressed the evolution of the pressure wave $p(z, x, y, t)$ in the medium as [Westervelt (1963), Aanonsen *et al.* (1984)]:

$$\left(\bigtriangledown^2 - \frac{1}{c_0^2}\frac{\partial^2}{\partial t^2}\right) p = -\frac{\beta}{\rho_0 c_0^4}\frac{\partial^2 p^2}{\partial t^2} \tag{3.8}$$

where $\bigtriangledown$ is the Laplacian and is expressed as:

$$\bigtriangledown^2 p = \left(\frac{\partial^2}{\partial x^2} + \frac{\partial^2}{\partial y^2} + \frac{\partial^2}{\partial z^2}\right) p \tag{3.9}$$

The pressure $p(z, x, y, t)$ can be defined as the sum of the harmonics p_i:

$$p = p_1 + p_2 + p_3 + ... + p_n \tag{3.10}$$

The ASM can compute the fundamental p_1 and second harmonic p_2 of the pressure wave at a given position. However, its use is based on the quasi-linear approximation, which state that $p_1 \gg p_2$ and that the higher harmonics are negligible. This approximation reduces the total pressure p to the sum of the fundamental and second-harmonic wave [Du and Breazeale (1985), Dursun *et al.* (2005), Yan and Hamilton (2006)]. Using such hypothesis, p^2 can be expresses as:

$$p = p_1^2 + p_1 p_2 + ... \tag{3.11}$$

Equation (3.8) can then be separated into two equations: the first one corresponds to the fundamental frequency f_0 and the second one to the second harmonic frequency $2f_0$ so that two classic propagation equations are obtained. Indeed, in equation (3.11), the term in p_1^2 correspond to the second harmonic frequency and the term $p_1 p_2$ to the third harmonics. With such considerations, p_1 and p_2 can be expressed as a function of the medium parameters:

$$\left(\bigtriangledown^2 - \frac{1}{c_0^2} \frac{\partial^2}{\partial t^2} \right) p_1 = 0 \tag{3.12}$$

$$\left(\bigtriangledown^2 - \frac{1}{c_0^2} \frac{\partial^2}{\partial t^2} \right) p_2 = - \frac{\beta}{\rho_0 c_0^4} \frac{\partial^2 p_1^2}{\partial t^2} \tag{3.13}$$

The 3D FT of equations (3.12) and (3.13) is computed to obtain the pressure wave P_1 and P_2 in the Fourier domain.

3.2.3 Solution for the fundamental frequency

For the fundamental, the 3D FT of equation (3.12) coupled to the properties (3.6) and (3.7), the equation is changed to:

$$4\pi^2 \left(-f_x^2 - f_y^2 \right) P_1 + \left(\frac{2\pi f_t}{c_0} \right)^2 P_1 + \frac{d^2 P_1}{dz^2} = 0 \tag{3.14}$$

It can be noticed in equation (3.14) that the ratio $2\pi f_t / c_0$ is similar to the standard wave vector $k_t = 2\pi f_0 / c_0$. Moreover, $2\pi f_x$ and $2\pi f_y$ are directly related to the x- and y-axis definition and can be assimilated to the wave vector on these axes. Using $k_t = 2\pi f_t / c_0$, $k_x = 2\pi f_x$, and $k_y = 2\pi f_y$, equation (3.14) can be rewritten as a classical harmonic oscillator differential equation:

$$\frac{d^2 P_1}{dz^2} + K^2 P_1 = 0 \tag{3.15}$$

with K the 3D k-vector that depends on the sampling frequencies in m^{-1}:

$$K(k_x, k_y, k_t) = \sqrt{k_t^2 - k_x^2 - k_y^2} \tag{3.16}$$

Only the part where K is real has been kept (*i.e.*, $k_t^2 > k_x^2 + k_y^2$) because an imaginary K corresponds to evanescent waves, which can be ignored without loss of accuracy if the wave propagates longer than a few wavelengths [Belgroune *et al.* (2002)]. In our case, this condition is considered to be respected.

The solution for the fundamental wave at each point (x, y, z) of the medium can be expressed from equation (3.15) as:

$$p_1(z, x, y, t) = \mathcal{F}^{-1}\left(P_0(z_0, k_x, k_y, k_t)e^{-iK(z-z_0)}\right) \tag{3.17}$$

with P_0 the 3D FT of the source wave p_0 at the original position z_0. The final expression of the fundamental wave corresponds to a simple phase shift in the Fourier domain of the initial waveform. The matrix P_0 depends on the probe definition and the transmission strategy. Specific windows and signals can be used on the transducer because of its discretization. With an array transducer, specific apodization can also be selected on each element.

3.2.4 Solution for the second-harmonic frequency

For the second-harmonic wave, the left part of equation (3.13) is solved in a procedure similar to that of the fundamental. When considering the FT of the right part, if the nonlinear parameter β is considered homogeneous in each direction, it can be removed from the integral in the FT and the resulting expression is similar to the one proposed by Du and Jensen [Du and Jensen (2008)]. Our contribution consists in considering the possible variations in the three spatial directions of the nonlinear parameter of the medium. The expression of the FT of the right part of (3.13) is developed as:

$$\mathcal{F}\left(-\frac{\beta}{\rho_0 c_0^4}\frac{\partial^2 p_1^2}{\partial t^2}\right) = \frac{-1}{\rho_0 c_0^4}\mathcal{F}\left(\beta(x, y, z)\frac{\partial^2 p_1^2}{\partial t^2}\right) \tag{3.18}$$

As the nonlinear parameter does not depend on time, the Fourier term of equation (3.18) can be rewritten as:

$$\mathcal{F}\left(\beta\frac{\partial^2 p_1^2}{\partial t^2}\right) = \mathcal{F}\left(\frac{\partial^2 \beta p_1^2}{\partial t^2}\right) = -4\pi^2 f_t^2 \mathcal{F}\left(\beta p_1^2\right) \tag{3.19}$$

According to (3.19), the FT of equation (3.13) becomes:

$$\frac{d^2 P_2}{dz^2} + K^2 P_2 = \frac{k_t^2}{\rho_0 c_0^2}\mathcal{F}\left(\beta p_1^2\right) \tag{3.20}$$

The solution to equation (3.20) is equivalent to solving, for each (k_x, k_y, k_t), a differential second-order equation in z with the general form:

$$\frac{d^2g(z)}{dz^2} + K^2 g(z) = M(z) \tag{3.21}$$

After variation of the constant (Appendix B) and considering only the forward propagation, the inverse FT of P_2 is computed to obtain the final expression of the pressure wave $p_2(z, x, y, t)$:

$$p_2(z, x, y, t) = \mathcal{F}^{-1}\left(\frac{-i}{2K}\left(\int_{z_0}^{z} M(u, k_x, k_y, k_t) e^{iKu} du\right) e^{-iKz}\right) \tag{3.22}$$

with:

$$M(z, k_x, k_y, k_t) = \frac{k_t^2}{\rho_0 c_0^2} \mathcal{F}\left(\beta(z, x, y) p_1(z, x, y, t)^2\right) \tag{3.23}$$

The formulation proposed in equation (3.22) allows the 3D computation of the second-harmonic temporal wave propagating in media with an inhomogeneous nonlinear parameter in space.

3.2.5 Involvement of the attenuation

The attenuation of acoustic media can be described by various laws [Szabo (1978), Treeby and Cox (2010)]. In classic biological media, the attenuation is frequency-dependent and the K vector can be written [Wójcik (1998), Szabo (1978), Christopher and Parker (1991)b] as:

$$K_a = K - i\alpha(f_t) \tag{3.24}$$

with $\alpha(f_t)$ the frequency-dependent attenuation. It is expressed as:

$$\alpha(f_t) = \alpha_0 \left(\frac{f_t}{1e6}\right)^{\gamma} \tag{3.25}$$

with γ a number between 1 and 2 for biological media that translates the frequency-dependent law and α_0 the attenuation constant of the medium in Np.m^{-1}.MHz$^{-\gamma}$. To take into account the attenuation of the medium using the GASM, the previous expressions of p_1 and p_2 using the K vector have to be updated by replacing K with K_a. If different absorption behaviors have to be used, only this part must be updated to take into account the new law.

3.3 Algorithm implementation

3.3.1 Introduction

Equations (3.17) and (3.22) were implemented on a central processing unit (CPU) and a graphic processor unit (GPU). The implementation of these two equations are particularly

suited to the GPU programming because each product and sum in the 3D pressure image (2D+t) are involved one voxel at a given position in the image. Indeed, in the two proposed equations (3.17) and (3.22), the x, y, and t parameter did not appear. The computation in the z direction did not depend on the other parameter, so the calculus can be parallelize in the x, y, and t direction. This type of calculation is very efficient on a GPU because only the current position is used in the different input and output images and the high level of parallelization of the GPU hardware is fully used. The only complex and time consuming part of the GASM is the FT that is computed several times. This operation is done using an external library. The ASM implementation is conducted on a CPU and a GPU to compare their performance. The reference CPU programming was done in C++ and the GPU programming was done in CUDA (Compute Unified Device Architecture), which is an extension of the standard C language developed by nVIDIA. This is an API (Application Programming Interface) that is used to create the parallel programming tasks, called kernels, which are executed on the GPU. The different kernels and computing strategies are highlighted hereafter.

3.3.2 Computation of the fundamental

The evolution of the fundamental component is only linked to the initial wave source, P_0, and to the propagation distance z. In equation (3.17), the exponential term corresponds to a complex rotation, and a specific kernel needs to be designed. This kernel will be used several times in the GASM implementation. The P_1 spectrum is obtained after the computation of the rotation kernel in the Fourier domain, then the IFT is used to obtain the final solution. It must be noted that the fundamental wave component does not depend on the z-axis sampling used. Indeed, its evolution can be directly computed anywhere in the medium.

3.3.3 Computation of the second harmonic

The second harmonic wave component is solved in five steps. First, from the initial p_1 image, the new term βp_1^2 is computed. Second, the FT of the resulting image is done. Third, the spectrum is rotated. Fourth, the spectrum is integrated. Finally, the integrated Fourier spectrum must be rotated once more. The different rotations are defined with the same rotation kernel. To compute the integration part, the z sampling used is important. The descriptions of the different kernels are highlighted hereafter.

3.3.4 Fourier transform

The FT library used in the CPU implementation is the FFTW library, which is considered the most efficient in the community [Frigo and Johnson (2005)]. Otherwise, for the GPU implementation, nVIDIA proposed a dedicated library, cuFFT, which is an extension of the FFTW library. Defining p_1 and p_2 as 3D real images and P_1 and P_2 as complex

images means that the dimension of the complex images can be halved and consequently the computation time in both the FT and IFT decreased.

3.3.5 Kernel description

The kernels used in the GPU implementation are described below. The different kernels are particularly suited for the GPU because the mathematical operations used in the ASM only involve the voxels at a given position in the 3D images. No access to other specific memory areas is needed to compute the output images, which is very efficient in GPU programming. The proposed kernel's names have been chose in order to explain the realized operations done inside.

Rotation kernel

To compute the fundamental and the second harmonic, a rotation kernel is needed. According to the Euler formula, the complex exponential is considered in its Cartesian form, then a classic multiplication is computed to obtain the new complex number. Only the angle is require in input of the kernel.

Kernel to compute βp_1^2

Because of the possible inhomogeneous nonlinear parameter map, its corresponding 3D (x, y, z) map is saved in the texture memory in order to easily access its values. With this initial setup, the spatial sampling has no more impact on the computation of the product $\beta(x, y, z)p_1^2(x, y, z, t)$. Indeed, the bilinear interpolation, naturally present in the texture memory, is used to extract the correct value of the investigated plane. Concerning multiplication, since p_1 is real, its value is simply multiplied by itself to obtain the square value. This operation is very efficient in GPU programming.

Kernel to compute the integral

The integral computation is the most complex part. In order to compute it, a finite difference scheme was used. Contrary to the fundamental evolution computation, a z sampling is needed and is defined by the finite difference scheme:

$$I(z + dz) = \int_{z_0}^{z+dz} M(u)e^{iKu}du = \int_{z_0}^{z} M(u)e^{iKu}du + \int_{z}^{z+dz} M(u)e^{iKu}du \tag{3.26}$$

The final formulation for the integral is obtained with the trapeze formula:

$$I(z + dz) = I(z) + \frac{M(z)e^{iKz} + M(z + dz)e^{iK(z+dz)}}{2}dz \tag{3.27}$$

To compute the integral at the $z + dz$ position, two previously computed values have to be saved, *i.e.*, the previous value of the integral $I(z)$ and the image $M(z)$, which take

$p_0 \rightarrow P_0$	[FT]
For each z point	
$P_0 \rightarrow P_1$	[rotation kernel]
$P_1 \rightarrow p_1(z)$	[IFT]
Compute βp_1^2	[βp_1^2 kernel]
$\beta p_1^2 \rightarrow \mathcal{F}(\beta p_1^2)$	[FT]
Rotate $\mathcal{F}(\beta p_1^2)$	[rotation kernel]
Compute integral I	[integration kernel]
$I \rightarrow P_2$	[rotation kernel]
$P_2 \rightarrow p_2(z)$	[IFT]

Table 3.1: Illustration of the different steps of the ASM. The different FTs, IFTs, and kernels are represented in square brackets.

into account the value of the fundamental pressure at a distance z. In the kernel, the sums and multiplications have to be computed for the $z+dz$ position and then are saved for the calculation of the next position. The different constants are also summed in this kernel.

3.3.6 Final algorithm

The final algorithm is described in Table 3.1. For each z position, the fundamental and then the second harmonic components are computed.

3.4 Results

3.4.1 Pressure-wave simulation in a medium with a homogeneous nonlinear parameter

The accuracy of the GASM is evaluated in comparison with two simulators used as the reference for a medium with a homogeneous nonlinear parameter. First, the well-known linear FieldII simulator [Jensen and Svendsen (1992), Jensen (1996)] is used for the calculation of the pressure field at the fundamental frequency f. To compare the second-harmonic component, the finite difference Voormolen simulator [Voormolen (2007)] was chosen. This simulator, based on the KZK equation [Zabolotskaya and Khokhlov (1969), Kuznetsov (1970)], can calculate both the fundamental and the second-harmonic in the entire 3D space. The one-way fields obtained with the GASM are compared with those obtained with FieldII and with Voormolen's simulator. From the 4D (3D+t) data computed by the simulators, the maximal pressure is extracted at each 3D points. In particular, the one-way field presented hereafter correspond to the pressure values in the plane $y = 0$.

The probe parameters used for the simulations are summarized in Appendix A.2. A five-cycle 5 MHz sinusoidal tone burst weighted with a Gaussian function was transmitted on each elementary transducer with initial pressure $p_0 = 100$ kPa. The focal point has been set to 70 mm. All the simulations were conducted in a medium considered as water

Parameter	Value
Density	1000 kg.m^{-3}
Speed of sound	1540 m.s^{-1}
Attenuation	0.025 Np.m^{-1}.MHz^{-2}
γ	2

Table 3.2: Water acoustic characteristics.

with a homogeneous nonlinear parameter value of 3.5. The medium parameters used in the simulations are summarized in Table 3.2. The resulting one-way fields are presented in Fig. 3.2 for the fundamental and in Fig. 3.3 for the second harmonic. A first visual estimation on the shape of the fundamental field calculated with the GASM is similar to both reference simulators. For the second harmonic, the GASM field is very close to the field obtained with the Voormolen simulator. In Fig. 3.2.c and Fig. 3.3.b, the one-way pressure fields appear to contain some noise. This noise exhibits a symmetric pattern along the z-axis and is a result of the numerical error in the FT due to the discretization of the space used.

To evaluate the accuracy of the GASM simulation, an error map was computed to compare the resulting one-way field with those obtained with the two reference simulators. At each point, a difference pressure was calculated and then normalized by dividing the values by the pressure at the focal point in the Voormolen simulator. The deviation is expressed as:

$$D_i = \frac{|p_i^{Voormolen} - p_i^{GASM}|}{max(p_i^{Voormolen})} \tag{3.28}$$

with i equal to 1 or 2 when the deviation is evaluated for the fundamental or the second-harmonic one-way field, respectively. The resulting maps are presented in Fig. 3.4. In the focalization area of the field, defined by the -12 dB isoline around the focal point in the GASM and delimited by the dashed line, the maximum deviation, the mean deviation, and the standard deviation are computed for the two nonlinear propagation simulators. For the pressure at the fundamental frequency (Fig. 3.4.a), the difference obtained is $1.9\% \pm 1.3\%$ with a peak of 8.5% inside the delimited surface. For the second harmonic (Fig. 3.4.b), the difference is $1.9\% \pm 1.6\%$ with a peak of 8.8%.

3.4.2 Pressure-wave simulation in a medium with an inhomogeneous nonlinear parameter

The GASM takes into account the variations of the nonlinear parameter by the integrative part of the variable $M(z, k_x, k_y, k_t)$ (equation (3.23)). With Voormolen's simulator [Voormolen (2007)], it is possible to simulate a variation of the nonlinear parameter only along the z-axis. To compare the two simulators, we considered the case of a surrounding medium with a nonlinear parameter $\beta_1 = 3.5$ with an inclusion of a nonlinear parameter $\beta_2 = 7$. A linear slope of the nonlinear parameter's evolution was used at the interface of the two media to avoid a discontinuity (Fig. 3.5.a). The probe parameters are

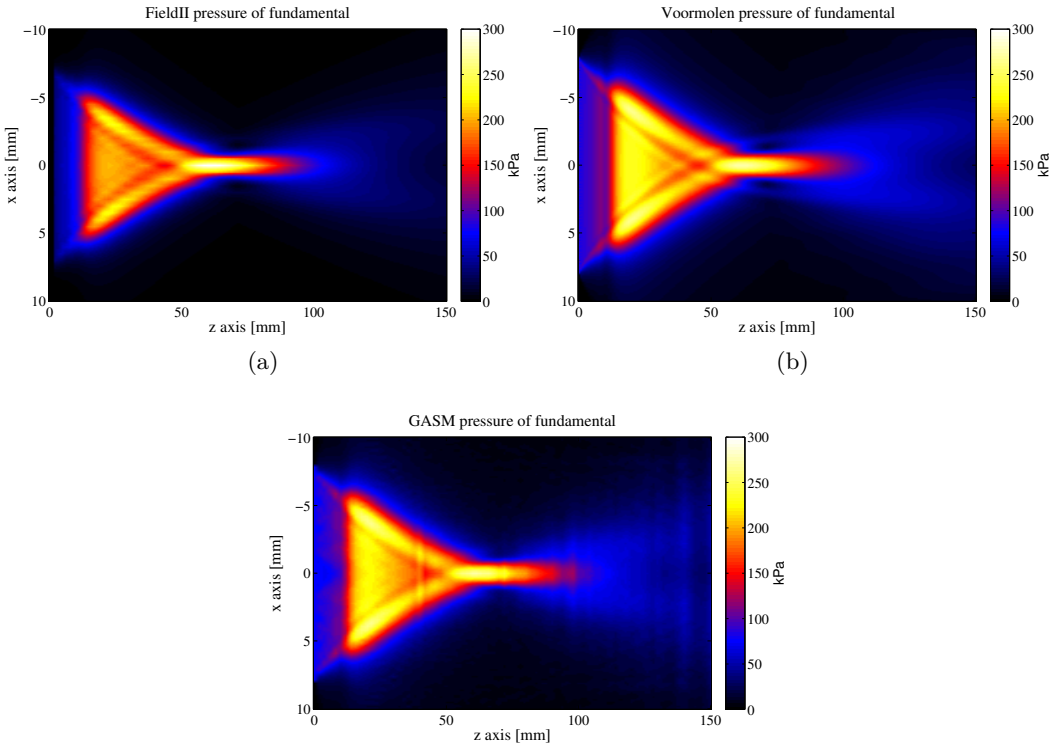

(a) (b)

(c)

Figure 3.2: One-way fundamental amplitude pressure fields obtained through the FieldII simulator (a), the Voormolen simulator (b) and the GASM simulator (c).

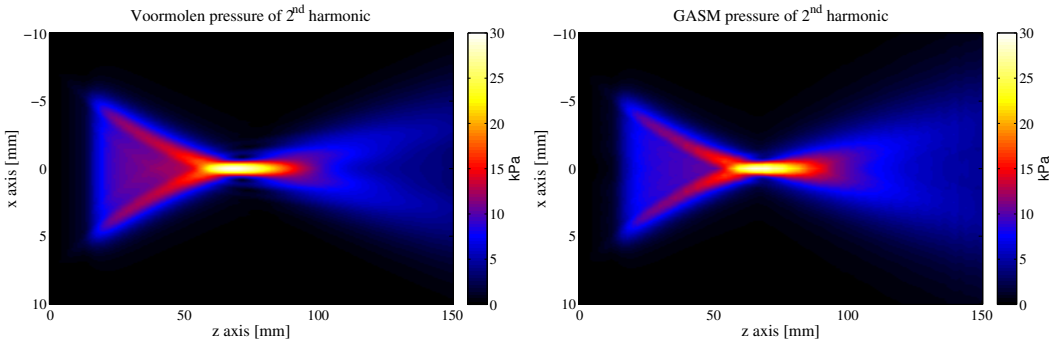

(a) (b)

Figure 3.3: One-way second-harmonic amplitude pressure fields obtained through the Voormolen simulator (a) and the GASM (b). The pressure field obtained with the GASM is very close to the Voormolen pressure field.

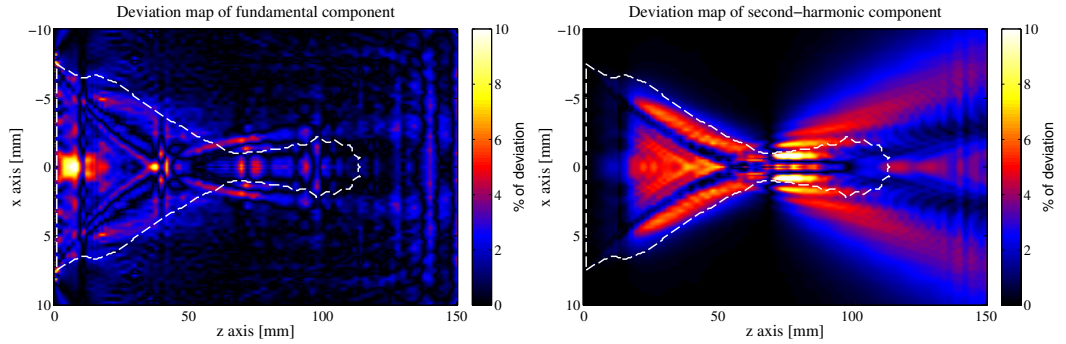

(a) (b)

Figure 3.4: Deviation map of the fundamental component D_1 (a) and of the second-harmonic component D_2 (b) of the GASM in comparison with the Voormolen simulator. The dashed line is the -12 dB isoline and outlines the region where the deviation is considered. The pressure fields are normalized by the pressure obtained in the focal point.

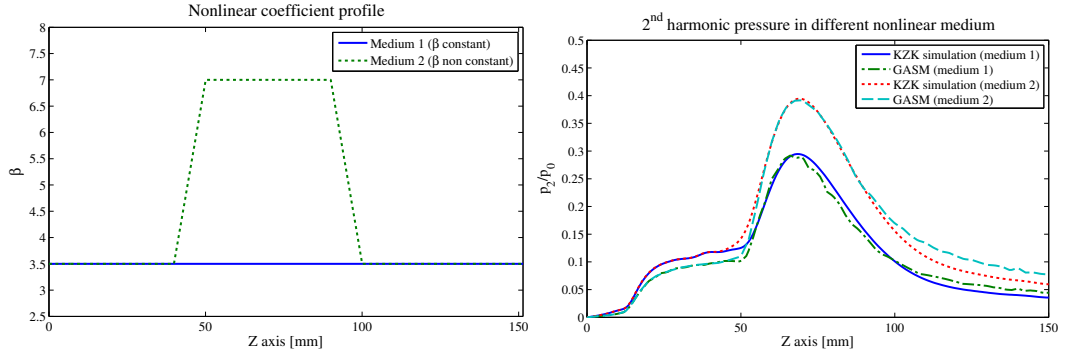

(a) (b)

Figure 3.5: (a) Profiles along the z-axis of the nonlinear parameter set in simulations; it is constant in medium 1 but not in medium 2. (b) Second-harmonic normalized pressure profile computed with the Voormolen and GASM simulators along the beam axis.

the same as the previous ones. The peak of the temporal response was computed along the z-axis of the probe with the two simulators. The resulting pressure profiles are presented in Fig. 3.5.b. Its evolution is very similar to that calculated with the Voormolen simulator. The mean deviation obtained for the second harmonic, when a medium with a homogeneous nonlinear parameter is considered, is $3.7\% \pm 1.9\%$ with a peak deviation of 8.1%. When the inclusion is considered (inhomogeneous β), the mean deviation is $3.4\% \pm 2.2\%$ with a peak deviation of 7.8%.

The GASM simulates complex media, with 3D variations of the nonlinear parameter which cannot be simulated by the previously mentioned simulators. This property of the GASM is illustrated by two simulations. The first one is based on a phantom including two media disposed as follows: the upper region (corresponding to the negative x-axis on Fig. 3.6) has a nonlinear parameter that is ten times higher than in the lower region.

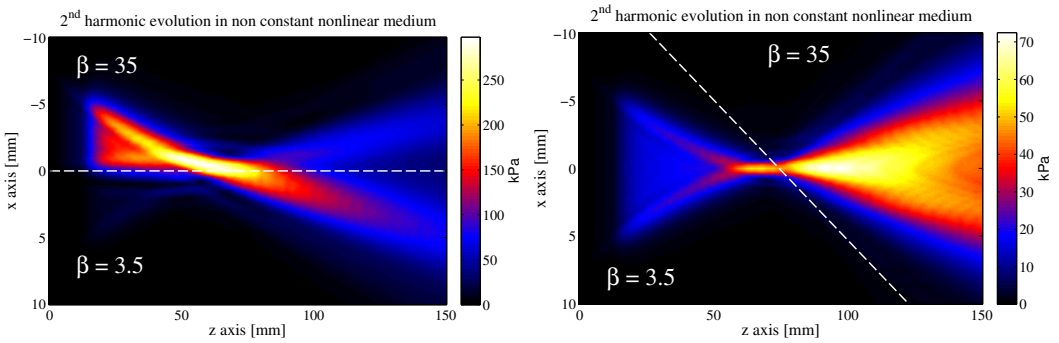

(a) (b)

Figure 3.6: One-way field of the second harmonic when the nonlinear parameter is not homogeneous in different directions of space. The dashed line separates the two different regions defined by the nonlinear parameter. Note that these simulations are not possible with the Voormolen and FieldII simulators.

The resulting second-harmonic field obtained with the GASM is shown in Fig. 3.6.a. The pressure field is significantly different in the two regions. The amplitude of the second-harmonic component is larger in the area with higher nonlinear parameter and the peak is not centered on the probe axis. In the second simulation, the nonlinear parameter varies simultaneously along the x and z directions. The resulting second-harmonic image is shown in Fig. 3.6.b. This variation creates two focal points in the second-harmonic field: one at a position close to the focal point of the fundamental, and another one in the region where the nonlinearity increases sharply.

3.4.3 Experimental measurements

To test the accuracy of the simulator, experimental acquisition of the fundamental and of the second-harmonic pressure fields was performed and compared with the simulation results. The scanner used was the ULA-OP system (see Appendix A.1) developed in the Microelectronics System Design Lab of the University of Florence [Tortoli *et al.* (2009)] coupled with the same probe as previously described (Appendix A.2). We repeated the experiment for two different transmission modalities. First, a conventional beam was considered. A five-cycle sine at 6.5 MHz with a Hanning window focused at 20 mm was transmitted. A Hanning apodization was also used on the active elements. Then a nonstandard transmission was used, requiring the application of specific apodization weights w_i to each element. A Bessel function apodization with respect to the x-axis was chosen [Lu (1997)] :

$$w_i = J_0(\alpha r_i) \tag{3.29}$$

with J_0 the zero-order Bessel function, α the spatial compression factor and r_i the distance between the active element and the center of the probe. To have the maximum intensity transmitted between 10 and 50 mm, an α value of 2100 m^{-1} was used. A five-cycle sine

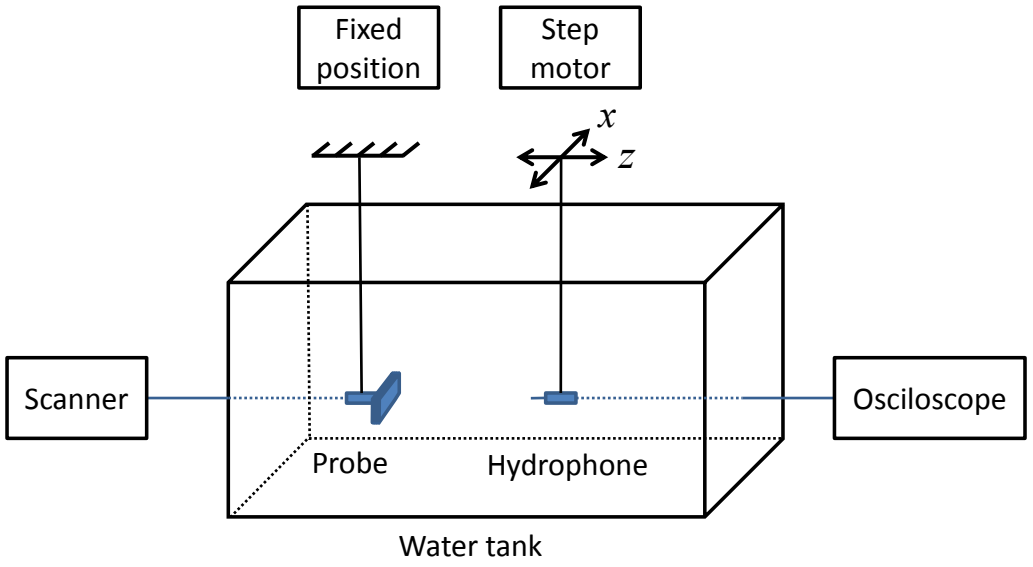

Figure 3.7: Experimental setup.

		Mean deviation	Standard deviation	Peak deviation
Focused beam	p_1	5.4%	2.7%	14.5%
	p_2	6.7%	5.3%	24.8%
Unfocused beam	p_1	6.1%	3.8%	18.2%
	p_2	5.8%	4.6%	30.7%

Table 3.3: deviation between GASM simulations and experimental measure for a focused and unfocused beam.

at 8 MHz with a Hanning window was transmitted. Measurements were made in water, which has a nonlinear parameter of 3.5. A hydrophone (Marconi, Bologna, Italy) recorded the pressure at different positions in the water tank with an accuracy of 0.8 mm in the z-direction and 0.2 mm in the x-direction. An illustration of the experimental setup is presented in Fig. 3.7. The resulting experimental one-way fields are compared with those simulated by GASM in Fig. 3.8 for the focused beam and in Fig. 3.9 for the unfocused beam. The simulated fields show good agreement with the measurement for both the fundamental and second-harmonic components. The deviation maps of the fundamental and second-harmonic one-way fields were calculated as previously described using the -12 dB isoline around the focal point. The deviation value measurement is summarized in Table 3.3. The large deviation peak observed in the second-harmonic field is localized in a very small area that is assumed to be an experimental artifact recorded during the experiment as a slight misalignment between the probe and the hydrophone. Because the signal is filtered around the fundamental and second-harmonic components, higher harmonics did not degrade the quality of the results. Moreover, the third harmonic is merged in the experimental noise recorded by the hydrophone.

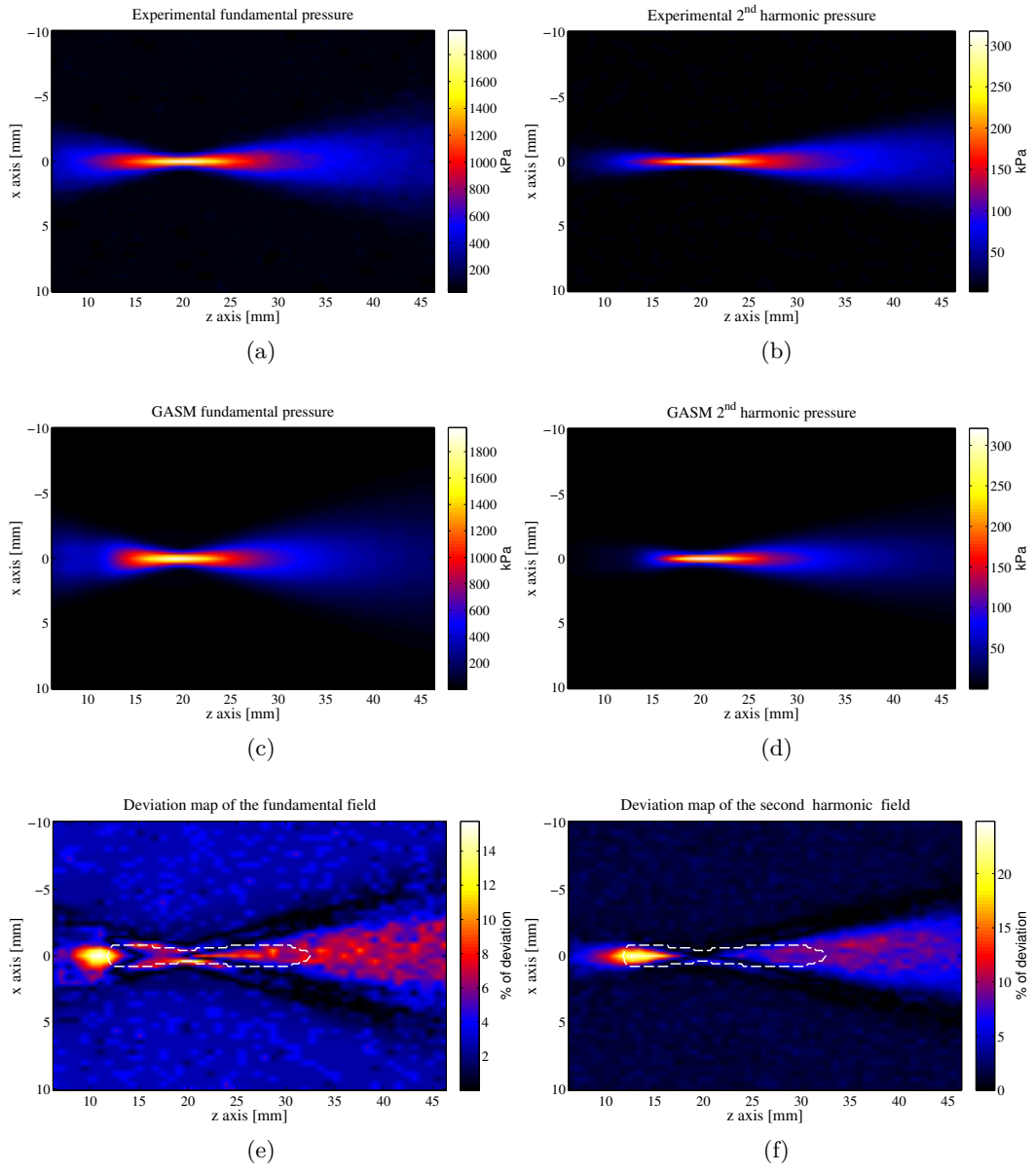

Figure 3.8: Comparison of experimental focused beam (a, b) and GASM simulated (c, d) one-way fields for the fundamental (a, c) and second harmonic (b, d). Error map of the fundamental (e) and the second-harmonic (f) component between the experimental field and GASM simulation. The dashed line is the −12 dB isoline.

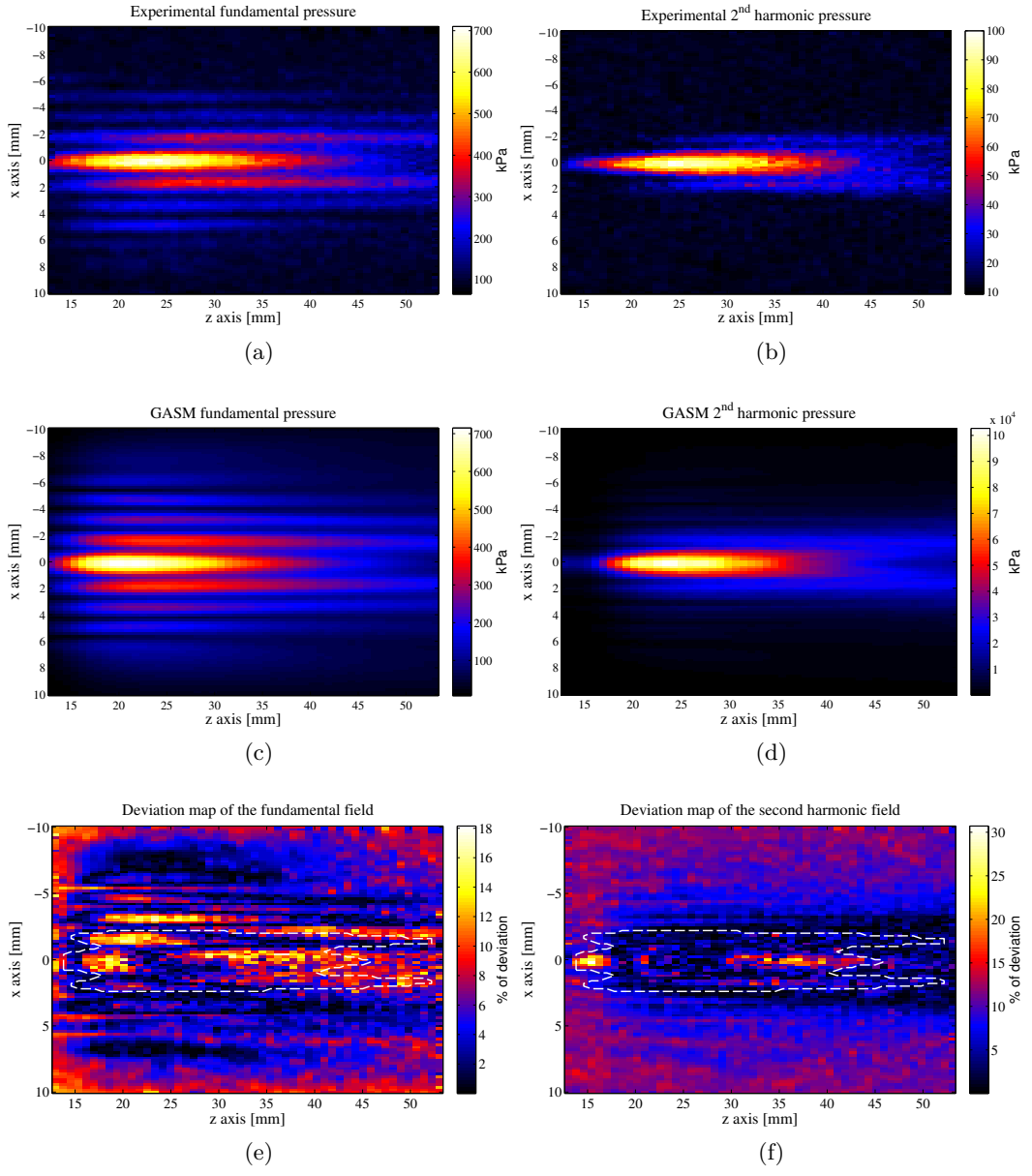

Figure 3.9: Comparison of experimental unfocused beam (a, b) and GASM simulated (c, d) one-way fields for the fundamental (a, c) and second harmonic (b, d). Deviation map of the fundamental (e) and the second-harmonic (f) component between the experimental field and GASM simulation. The dashed line is the −12 dB isoline.

	Voormolen simulator	GASM on CPU	GASM on GPU
Number of points in space (x, y, z, t)	(303, 60, 390, 507)	(128, 64, 51, 512)	(128, 64, 51, 512)
Computation time (Computer 1)	13 min 04 s	58 s	18 s
Computation time (Computer 2)	11 min 11 s	34 s	2.5 s

Table 3.4: Computation time of the Voormolen simulator and the GASM on the two different machines and GPU.

3.4.4 Computation time

The computation time of nonlinear simulations is one of the most problematic points in nonlinear imaging [Zemp *et al.* (2003), Wójcik *et al.* (2006)]. With the GASM, the computation time is strongly reduced by running it in the Fourier domain rather than finite difference approaches. Two different computers have been tested and the characteristic of their CPU and GPU are presented in Table A.1. More detailed information on the GPUs are presented in Appendix A.3. The computation times of the two simulators on both machines are shown in Table 3.4: the GASM is about 13 times faster on the CPU of machine 1 and 19.7 times faster on the CPU of the machine 2. The GPU computation allows to speed-up the calculation by a factor 3.5 on the machine equipped with the Quadro NVS 160M and by a factor 13.6 on the machine equipped with the GTX 285. The total acceleration factor on the GPU compared to the Voormolen simulator is 45.5 on the Quadro NVS 160M and of 268 on the GTX 285.

The difference in computation time comes partially from the number of points required in the two simulators. The finite difference method needs a large spatial sampling to obtain sufficient accuracy, particularly in the near field, for both the fundamental and the second harmonic. With the GASM, the fundamental does not depend on the z sampling. For the second harmonic, even if few points are presented in the discretization, the integration procedure involved in the calculation provides accurate results. Fewer sampling points are necessary for the simulation than for the finite differences method to obtain comparable results.

3.5 Discussion and conclusion

The GASM is a new method to simulate the nonlinear ultrasound propagation that takes into account the diffraction of the probe as well as the nonlinearity and the attenuation of the media. The first step of the GASM is to compute the FT of the probe geometry and the FT of the transmitted signal P_0 (equation (3.17)). The P_0 matrix takes into consideration all the probe parameters (geometry, frequency, probe shape) with the spatial and temporal discretization chosen. This initialization defines all fields obtained with the GASM.

We have shown that, for a homogeneous nonlinear parameter, the GASM's performance is comparable to that of FieldII for the fundamental or to that of the Voormolen finite difference simulator for the second-harmonic. This is illustrated by the deviation maps where no significant differences are observed between the GASM and the other simulators. The major contribution of the GASM is the possibility of simulating complex and arbitrary media in terms of nonlinearity. Indeed, the GASM can simulate any media with spatial variations of the nonlinear parameter *i.e.* related to the spatial reference of the probe along the axial (z), lateral (x), and elevation (y) dimensions. The Voormolen simulator allows to simulate the propagation wave along a stack of layers with different β parameters. These layers remain perpendicular to the propagation direction. As shown in the examples in Fig. 3.6, the GASM can simulate the pressure field that propagates in media with arbitrary nonlinear parameter variations and could be adapted to the simulation of human tissues or of media containing contrast agents having a nonlinear parameter larger than the value in the tissue [Wu and Tong (1998)]. As shown in Fig. 3.8 and Fig. 3.9, the GASM simulated fundamental and second-harmonic fields are close to the experimental fields. The computation time of the GASM is about 13 times faster than standard nonlinear simulators on a CPU and 45.5 on a GPU. On more powerful computer, the speed-up obtained can achieve a factor 19.7 for the CPU and 268 on a GPU. Fast nonlinear simulations of a complete 3D space can be made. Of course, it must be kept in mind that the Voormolen simulator works for higher-order nonlinear interactions, while the GASM is based on first-order perturbation.

The GASM presents certain unavoidable limitations. First, the use of the FT adds noise in the resulting pressure field. This noise slightly degrades the final aspect of the field, although, as shown by the deviation maps, the accuracy of the GASM in the active part of the field is satisfactory. In the proposed approach, a compromise has been made between the accuracy and the speed of computation. An increase of the number of considered points in the different matrix will decrease the aliasing effect but also increase the computation time. For high resolution simulations, tools based on finite difference scheme, computing high order nonlinear effect, have to be preferred. Secondly, no nonlinear interactions between different frequency components are taken into account in the proposed simulator. Indeed, if a wave composed of two frequencies is transmitted in the medium, the simulator processes the wave as two single-frequency waves with no interactions between them. In a real medium, a nonlinear interaction takes place and creates other pressure waves at the difference and sum frequencies. Another limitation of the GASM is the quasi-linear approximation, which limits the simulation in terms of initial amplitude. If the second harmonic is no more small compared to the fundamental, this assumption is no longer valid and the nonlinearity phenomena are too large to be simulated with the GASM. This limit depends on the different probe parameters, on the beamforming in transmission, on the transmitted signal and on the propagation depth to reach. The last approximation made in the proposed method consists in considering only transmitted waves and to not take into account possible reflected waves due to the inhomogeneous nonlinear map. This

effect has to be quantified in future version of the GASM.

The GASM is currently usable for fundamental and second-harmonic computation. However, with the same quasi-linear approximation, a higher order of nonlinearity can be reached. The third or fourth harmonic can be simulated versus an increase in computation time. An optimal implementation has to be found to relate the nonlinear order, the desired accuracy, and the computation time.

The development of this work include the possibility of creating nonlinear RF images combining the GASM field simulation of a 3D nonlinear parameter map with a 3D scatterer map and a strategy in reception to reconstruct the RF image. The development is presented in the next chapter.

Chapter 4

Nonlinear Ultrasound Image Simulation: CREANUIS

This chapter is devoted to the presentation of a new RF image simulator which takes into account the nonlinear propagation. This work has been presented in a conference [Varray *et al.* (2010)a] and a paper is currently submitted in a journal [Varray *et al.* (2011)b]. A software has also been produced under a CeCILL-B licence.

4.1 Introduction

The nonlinear propagation of an ultrasound (US) wave in tissue is currently used since the years 2000 in many clinical applications such as harmonic imaging or tissue harmonic imaging (THI). THI is characterized by a higher spatial resolution compare to classical imaging [Averkiou *et al.* (1997), van Wijk and Thijssen (2002)]. With injection of contrast agent, several techniques have been designed to increase the image of the bubbles response such as pulse inversion (PI) [Simpson *et al.* (1999)], amplitude modulation (AM) [Errabolu *et al.* (1988)], second-harmonic reduction (SHR) [Pasovic *et al.* (2010)] or second-harmonic inversion (SHI) [Pasovic *et al.* (2011)]. In all these techniques, the second-harmonic increase during the propagation is used. However, to test these different nonlinear-imaging methods, no tool exists to simulate realistic radio frequency (RF) images including the nonlinear information.

In this chapter, a novel tool is proposed to simulate RF images containing both the fundamental and the second-harmonic components generated by the ultrasound nonlinear propagation in a medium. A nonlinear ultrasound image simulator (CREANUIS) has been

designed to combine the information of a nonlinear ultrasound field and of a scatterers' distribution. The GASM has been used to quickly compute the 4D (3D+t) evolution of the fundamental and second-harmonic component of any 2D sources and any inhomogeneous nonlinear parameter medium. In a first time, CREANUIS computes the nonlinear ultrasound fields (at fundamental and second-harmonic frequencies) in function of the given probe geometry with the GASM and then, elaborates the nonlinear RF echo-signals using the fundamental and second-harmonic components of the pressure at each scatterers' position [Varray *et al.* (2010)a]. The scatterers' definition and the image reconstruction are conducted in a similar way as in the FieldII implementation. As in every simulation tool, a trade off has to be found between the realization of the simulation and the computation time. The different hypothesis and choice in the GASM and image reconstruction are presented in this chapter.

4.2 CREANUIS method

CREANUIS generates ultrasound images. The RF image is created by repeating the same basic operations for each simulated line. First, the scatterers' distribution (positions and amplitudes) and the nonlinear pressure map of the medium have to be defined. Then, for each RF line, the active part of the probe has to be selected. The 4D pressure is computed with a GASM simulation. The backscattering echoes are then computed in function of the beamforming strategy set in reception and the scatterers' position. A general overview of CREANUIS is proposed in Fig. 4.1.

4.2.1 Nonlinear Propagation simulation

To simulate the nonlinear propagation, different opportunity were available. The nonlinear propagation simulator must provide the pressure evolution in 4D (3D+t) for the different scatterers position in the medium. The Voormolen simulator [Voormolen (2007)] or the GASM can both answer this problematic. Indeed, both can provide the 4D pressure with the desire beamforming strategy in transmission. The transmitted signal can also be specific in both. The difference comes from the high order nonlinear interaction in the Voormolen one and the possibility to simulate inhomogeneous medium with GASM. For CREANUIS, the choice of the GASM has been made because the computation of GASM provides quickly the fundamental and second harmonic component for a given 2D source. The computation time of the nonlinear field is faster with GASM compared to other existing methods. Voormolen simulator required to run a long simulation each time a simple modification is made in the source definition.

4.2.2 Scatterers distribution

In CREANUIS, the scatterers are considered as punctual. They are defined by their 3D coordinates and their response amplitudes. The scatterers' map can be randomly

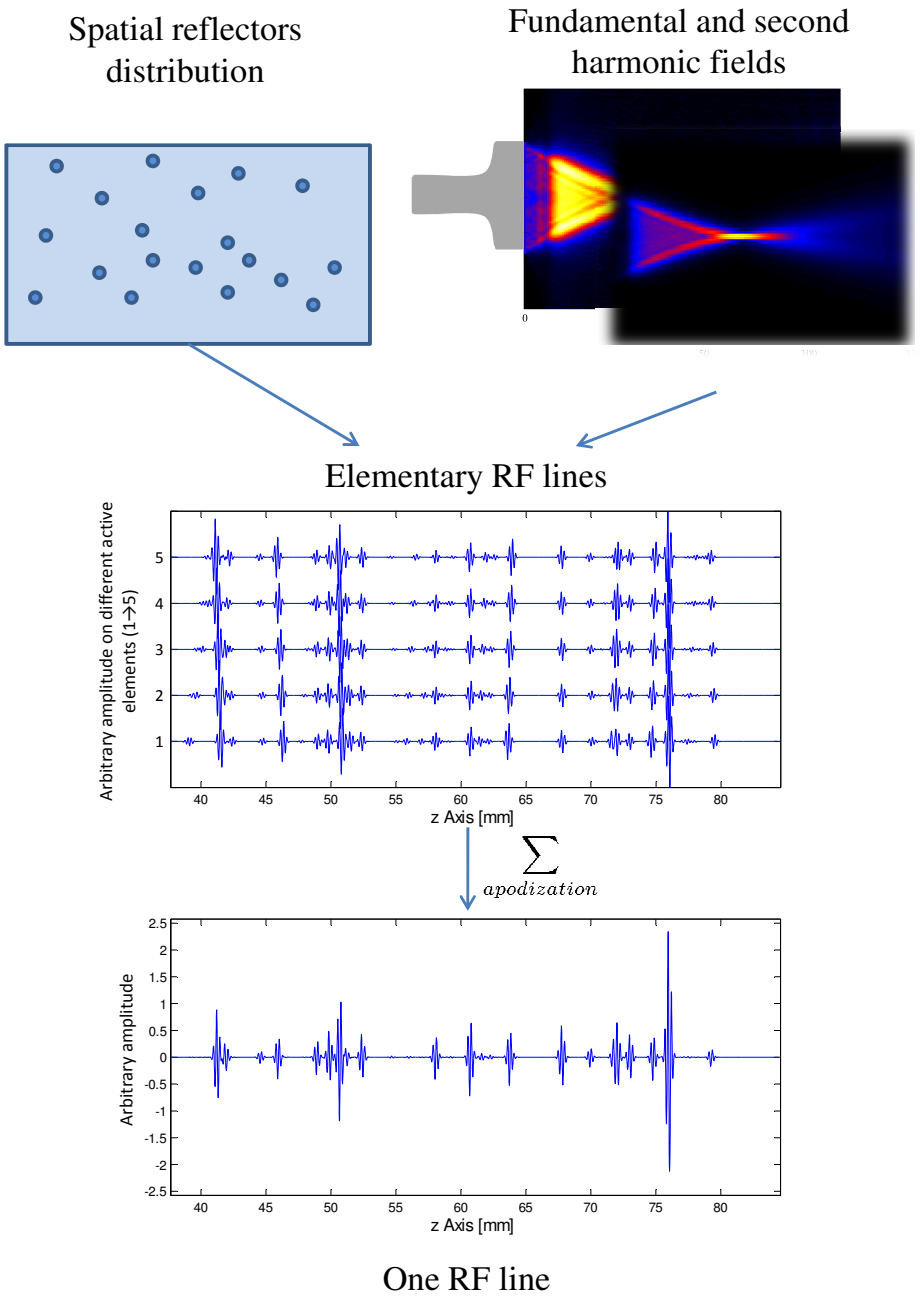

Figure 4.1: Illustration of CREANUIS algorithm steps. The GASM field coupled with the scatterers distribution produce the elementary RF lines. The beamforming strategy sets in reception is used to create one RF line. The same steps are repeated for each RF line of the final image.

chosen, imported from other simulations like, e.g., those based on FieldII [Jensen and Munk (1997)] or defined by the users. Usually, the response amplitude is distributed according to a normal distribution with a standard deviation of 1, but any statistic can be used. When a scatterer is reached by the pressure wave, a secondary spherical wave is created at the scatterer position. Its amplitude is related to the response amplitude of the scatterer.

4.2.3 Elementary RF echoes

The elementary RF signals represent the echoes received by each active element of the transducer after one pulse emission. To simulate these signals, the same operations are repeated for each scatterer. Given the spatial position of a scatterer, the fundamental and second-harmonic contribution is extracted from the field computed previously. This backscattering pressure wave is not directly the one received by the transducer in reception because this echo did not hit the surface of the transducer in a precise instant. Indeed, due to the finite dimension of the transducer piezoelectric surface, the receive pressure depends on the position of the scatterer, the position of the transducer, and the geometry of the transducer. To take into account this interaction, the spatial impulse response of the transducer has to be computed.

The different received signals are then added at the appropriate instant of the elementary RF lines with the correct amplitude depending on the pressure field, the attenuation and the scatterer backscattering amplitude. The same frequency attenuation model, as defined in the GASM in equation (3.25), has been used in backscattering path of the pressure wave.

4.2.4 Final RF line

From the different echoes received by each active element, one RF line of the image can be obtained. Indeed, the elementary RF echoes are combined according to the desired beamforming strategy in reception to produce one line of the image. In CREANUIS, a dynamic focalization has been implemented, but other strategies can be considered and implemented. The apodization in reception is set by the user.

4.2.5 Nonlinear RF image

The previous operations are repeated for each line of the image. The resulting image contains the fundamental and second-harmonic information thanks to the 4D pressure field computed earlier.

4.3 Software implementation and characteristics

4.3.1 Software description

CREANUIS has been implemented in C++. The memory quantity used in the simulation depends on several parameters. In the GASM simulation, the spatial discretization defines the dimension of the 3D matrix used in the Fourier domain. Concerning the RF image reconstruction, the dimension of the resulting image depends on the number of active elements, the number of elements of the probe, the sampling frequency, the speed of sound (constant in the simulation) and the minimal/maximal depth to reach.

For the users, different utilizations are proposed. Indeed, the software allows to specify the different beamforming strategies in transmission and reception. To save simulation time, the GASM simulation can be disabled if the field has previously been simulated. For inhomogeneous nonlinear media, the GASM simulation has to be conducted for each RF line creation with the corresponding nonlinear medium. This increases the total computation time but provides original simulated images. A more technical description of the CREANUIS software is given in Appendix C.

4.3.2 Integration of a scatterer echo on an active transducer

The received signal on the active transducer depends on different factors such as the position of the scatterer, the dimension and the geometry of the active transducer, the amplitude of the backscattering signal. The formulation of this signal has been proposed by [Stepanishen (1971)a, Stepanishen (1971)b] and reused by Jensen in his FieldII software [Jensen and Svendsen (1992)]. It corresponds to the convolution between the initial backscatter signal with the spatial impulse response of the active element. In far-field approximation, when the backscattered signal hits the surface, four different times: t_1, t_2, t_3, and t_4 with $t_1 \leqslant t_2 \leqslant t_3 \leqslant t_4$ can be considered. This four times correspond to the instants where the signal hits the different angles of the active transducer. This is illustrated in Fig. 4.2.a. With the far-field approximation, the 3D spherical wave from the scatterer interacts with the transducer surface along slope thanks to the large distance between the surface and the dimension of the element. The spatial impulse response h of the element has a trapezoidal shape which depends on the different time and of an amplitude A as illustrated in Fig. 4.2.b. The values of the different times and the amplitude are expressed as:

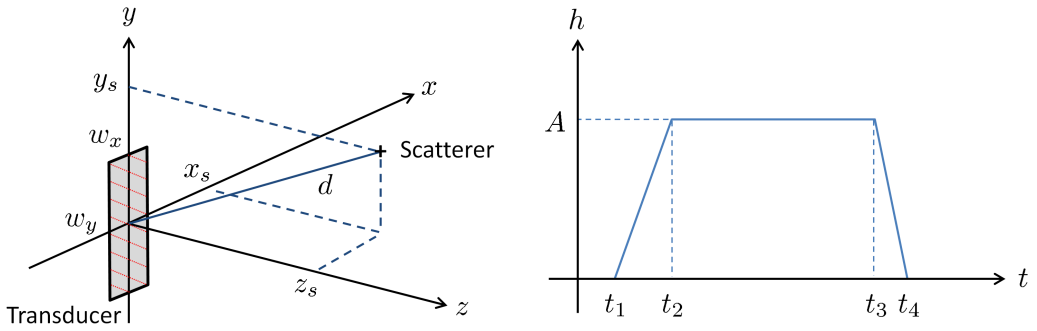

(a) (b)

Figure 4.2: (a) The spatial representation used in the backscatter signal and (b) the characteristic trapezoid shape of the spatial impulse response h. In (a) the red lines of the transducer surface represent, for different times, the intersection between the backscatter signal and the surface. The time t_1 correspond to the upper right corner of the transducer and the time t_4 to the left down one.

$$\begin{cases} t_1 &= \dfrac{d}{c_0} - \dfrac{\Delta t_1 + \Delta t_2}{2} \\ t_2 &= t_1 + \Delta t_1 \\ t_3 &= t_2 + \Delta t_2 \\ t_4 &= t_1 + \Delta t_1 + \Delta t_2 \\ A &= \dfrac{w_x w_y}{2\pi d} \end{cases} \tag{4.1}$$

where d is the distance between the scatterer and the center of the active transducer, w_x and w_y are respectively the half-height and half-width of the active transducer, and Δt_1 and Δt_2 are expressed in function of the scatterer position and the active transducer dimension:

$$\begin{cases} \Delta t_1 &= \min\left(\dfrac{w_y y_s}{d c_0}, \dfrac{w_x x_s}{d c_0}\right) \\ \Delta t_2 &= \max\left(\dfrac{w_y y_s}{d c_0}, \dfrac{w_x x_s}{d c_0}\right) \end{cases} \tag{4.2}$$

where (x_s, y_s, z_s) is the scatterer position in the coordinate system associated to the transducer (cf. Fig. 4.2.a). The final signal is obtained doing the convolution between h and the initial signal.

With CREANUIS, each scatterer creates, in function of its amplitude and position, a specific trapezoid. To speed-up the simulation, all the trapezoid contribution to the RF lines are added in the different RF lines corresponding to each active element. Finally, the convolution is made between the initial signal and each RF line. Then, the different beamforming strategies in reception can be applied to obtain the final beamformed RF

line.

4.3.3 Resolution cell and scatterers' density

In function of the density of scatterers, the statistics of the RF image and of the envelope image change. The probability density function (pdf) has been related to the scatterer's density and more precisely to the number of scatterers per resolution cell. The resolution cell of the simulation system is defined using [van Wijk and Thijssen (2002)]:

$$V_{cell} = FWHMc_0 \times 1.02\lambda\frac{Focus}{L} \times 1.02\lambda\frac{Elevation}{Height} \tag{4.3}$$

with FWHM the full width at half maximum amplitude of the transmitted signal (in second), λ the wavelength of the signal, L and $Height$ the lateral and vertical dimension of the probe respectively, $Focus$ the focal position of the transmitted beam and $Elevation$ the elevation focus of the probe [van Wijk and Thijssen (2002)]. Using this definition of the resolution cell, when the scatterer density reaches ten units per resolution cell, the statistical distribution of the envelope follows the expected Rayleigh distribution. Moreover, when a lower scatterer density is chosen, the envelope distribution follows the K distribution statistical model [Bernard *et al.* (2006), Bernard *et al.* (2007)].

4.4 Results

4.4.1 Comparison with FieldII

Fundamental image

A first simulation, conducted with FieldII and CREANUIS, has been made using a random scatterers' distribution for a total of 600 000 scatterers (30 scatterers/mm^3). A 3-cyle sine at 5.0 MHz with a Hanning window has been transmitted in the medium. A focalization at 40 mm and a Hanning apodization in transmission and reception was also set on the 64 active elements. The resulting normalized B-mode images are presented in Fig. 4.3. Because the RF-image obtains with CREANUIS is composed of the fundamental and second-harmonic component, a fourth-order Butterworth bandpass filter has been used to extract the fundamental B-mode image proposed in Fig. 4.3.b. No noticeable differences between FieldII (Fig. 4.3.a) and fundamental image of CREANUIS (Fig. 4.3.b) are visible. From these two images, a statistical study has been conducted in order to quantify their difference. Different parameters have been computed. First, the mean and the standard deviation in the two images have been computed and the resulting values are 0.208 ± 0.123 and 0.211 ± 0.115, respectively for the FieldII and CREANUIS image. Then, the mean deviation (MD) has been evaluated. It is defined as:

$$\mathsf{MD} = \frac{1}{nm}\sum_{1}^{n}\sum_{1}^{m}|I_{i,j}^{FieldII} - I_{i,j}^{CREANUIS}| \tag{4.4}$$

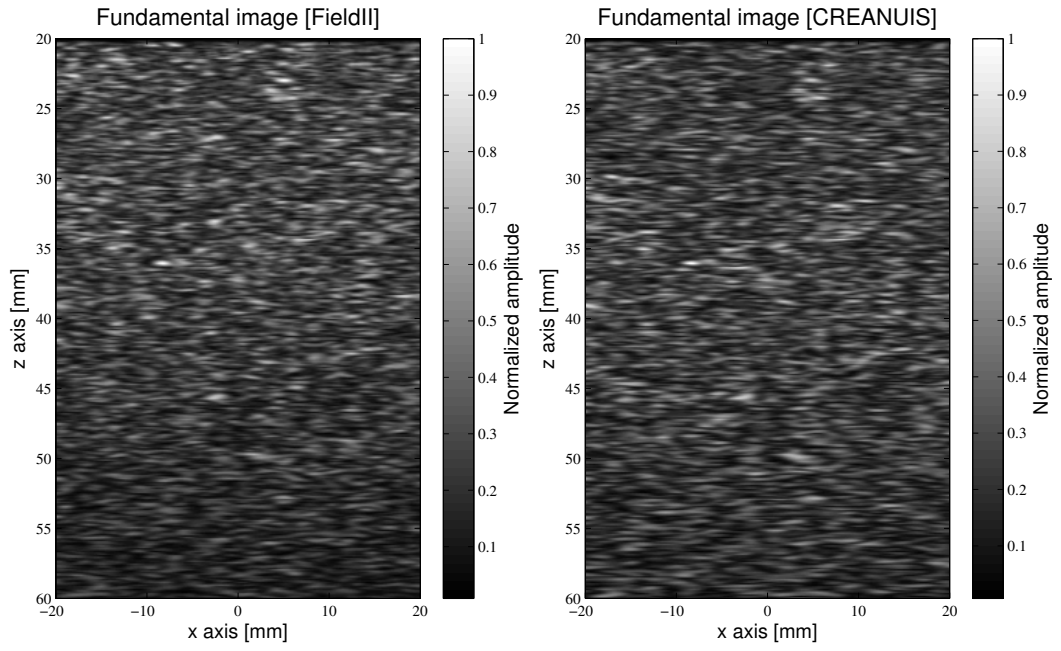

Figure 4.3: Comparison of fundamental B-mode image obtained with (a) FieldII and (b) CREANUIS. These two images are very similar.

with $I^X_{i,j}$ the (i,j) pixel intensity in the X image of dimension (n,m). On the proposed images, a MD of 8.1% is obtained. This value appears to be very satisfying. Indeed, in the GASM simulations, the error between the fundamental component and FieldII has been evaluated of $1.9 \pm 1.3\%$ with a peak error of 8.5%. This initial error has been propagated in the CREANUIS simulation and could explain a part of the total MD observed. However, the resulting images obtained with FieldII and CREANUIS are very close and validate our approach compared to the classical FieldII.

Speckle distribution

Several studies have defined the relationship between the intensity distribution in the RF or B-mode images and the nature of the scatterers [Bernard *et al.* (2006)]. With a large number of scatterers, the produced B-mode images exhibit a fully-developed speckle that follows a Rayleigh distribution. In order to estimate the accuracy of the FieldII and CREANUIS simulation, the theoretical distributions of the previously simulated images have been computed. For each image, the root mean square error (RMSE) between the distribution and the image has been computed. The RMSE is defined as:

$$\mathsf{RMSE} = \sqrt{\frac{1}{N}\sum_{i}^{N}\left(R_i - I_i^X\right)^2} \tag{4.5}$$

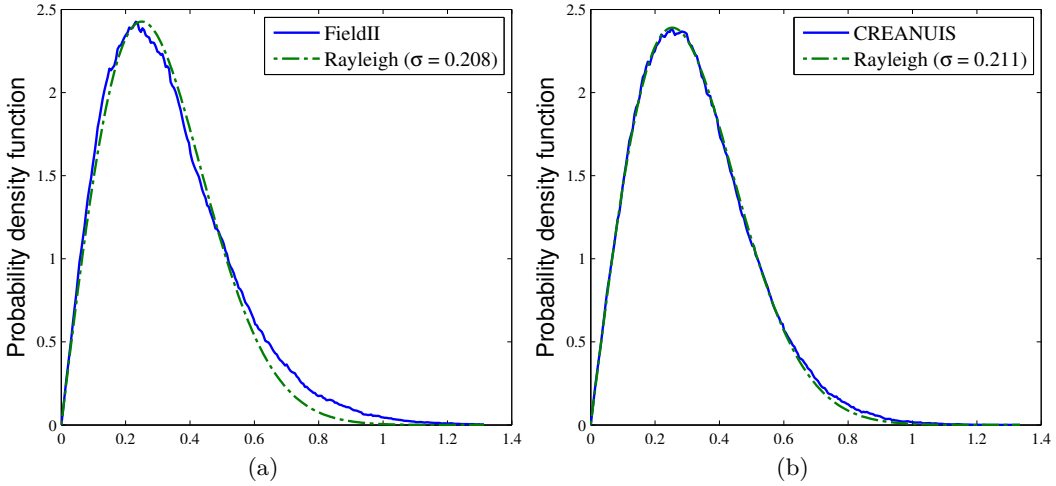

Figure 4.4: Comparison of theoretical Rayleigh probability density function obtained with (a) FieldII and (b) CREANUIS. These two distributions are very similar. The RMSE obtained with CREANUIS is 2.1%, and is smaller than the one obtained with FieldII, 7.7%.

where R_i is the Rayleigh distribution, I_i^X is the distribution of the simulated X image in N bins. The resulting estimations of the Rayleigh distributions with the proposed images are highlighted in Fig. 4.4. The RMSE obtained are respectively of 7.7% and 2.1% for the FieldII and CREANUIS images. The CREANUIS proposed an image which is closer to the theoretical Rayleigh distribution.

4.4.2 Classical image examples

Beamforming strategies

With CREANUIS, the fundamental but also the second-harmonic image is simulated. Different classical medium are then simulated to illustrated the interest of CREANUIS. A 3-cyle sine at 3.5 MHz with a Hanning window has been transmitted in the medium. A focalization at 60 mm and a Hanning apodization in transmission and reception were set.

Punctual scatterers distribution

A first simulation has been made using punctual reflectors having constant amplitude. The resulting images are presented in Fig. 4.5. No noticeable differences between FieldII (Fig. 4.5.a) and fundamental image of CREANUIS (Fig. 4.5.b) are visible. However, CREANUIS proposes a new image corresponding to the second harmonic component (Fig. 4.5.c). As expected, this image presents a resolution which is higher compared to the fundamental image. Note that the colorbar of Fig. 4.5.c are different because of the lower pressure field at second harmonic frequency.

Cyst phantom

The cyst phantom, proposed in [Jensen and Munk (1997)] has been simulated with FieldII and CREANUIS. The cyst phantom consists in two series of five circular areas of variable echogenicity and size. Five punctual reflectors of high echogenicity are also present in the medium. A total of 100 000 scatterers (4.5 scatterers/mm^3) have been used in the simulations in the entire medium. The response amplitude of each scatterer depends on its spatial position and if it belongs to a high or low echogeneous area. The resulting images are proposed in Fig. 4.6. As for the previous results, the difference between FieldII (Fig. 4.6.a) and fundamental image of CREANUIS (Fig. 4.6.b) is visually slight. The resolution of the obtained image are computed thanks to the cross-correlation as proposed by Wagner *et al.* [Wagner *et al.* (1983)]. In the fundamental image, the resolution in the axial and lateral direction is [0.32 mm; 1.91 mm] and is reduced to [0.28 mm; 1.55 mm] in the second harmonic image.

4.4.3 Inhomogeneous nonlinear medium simulation

The use of the GASM to compute the nonlinear propagation field allows to simulate inhomogeneous nonlinear medium. The only constraint is to provide to CREANUIS the nonlinear coefficient map of the medium. Then, the GASM simulation is conducted for the creation of each RF line using the appropriate area of the nonlinear parameter map in front of the active elements. Then, the previously described reconstruction scheme is used to create the RF line. Finally, one GASM simulation is required for each RF line to take into account the correct nonlinear parameter and to obtain an image related to the inhomogeneity of the nonlinear parameter.

Two examples to illustrate the obtained image are presented. First, a medium composed for one half with a nonlinear coefficient $\beta = 3.5$ and another half with $\beta = 7$ (Fig. 4.7.a). Secondly a medium of nonlinear coefficient $\beta = 3.5$ surrounding an egg-shape inclusion of a nonlinear parameter $\beta = 35$ is simulated (Fig. 4.8.a). For the two CREANUIS simulations, a random scatterers distribution has been used. The resulting images are respectively presented in Fig. 4.7 and Fig. 4.8.

In the first medium, the fundamental image on Fig. 4.7.b is completely homogeneous. Indeed, the nonlinear coefficient variation is not visible because in the GASM model, the fundamental did not depend of the nonlinearity. However, on the second harmonic image (Fig. 4.7.c), the amplitude in the image is different in the left and right part. This amplitude is related to the variation of the nonlinear coefficient. In the second simulated medium, the fundamental evolution (Fig. 4.8.b) is again not related to the nonlinear coefficient. However, the second harmonic evolution (Fig. 4.8.c) is impacted by the nonlinear coefficient evolution. The inclusion does not appear as an egg-shaped, because the nonlinearity created during the propagation in the inclusion continue to propagate farther along.

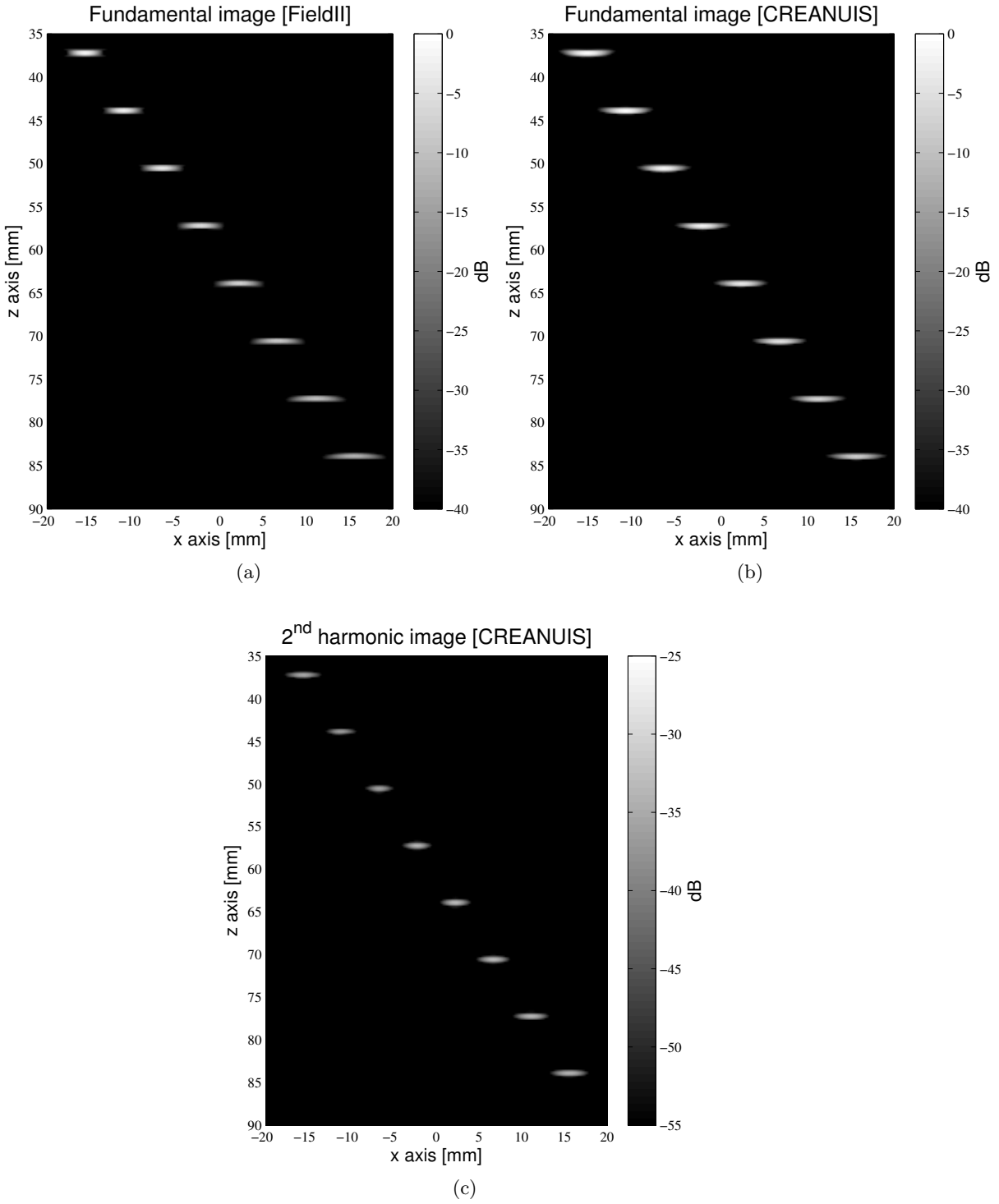

Figure 4.5: Resulting log-compressed images (in dB) of a phantom including identical punctual reflectors at different depth. Image (a) is produced with FieldII, image (b) is the fundamental image produced with CREANUIS and image (c) is the second-harmonic image produced with CREANUIS.

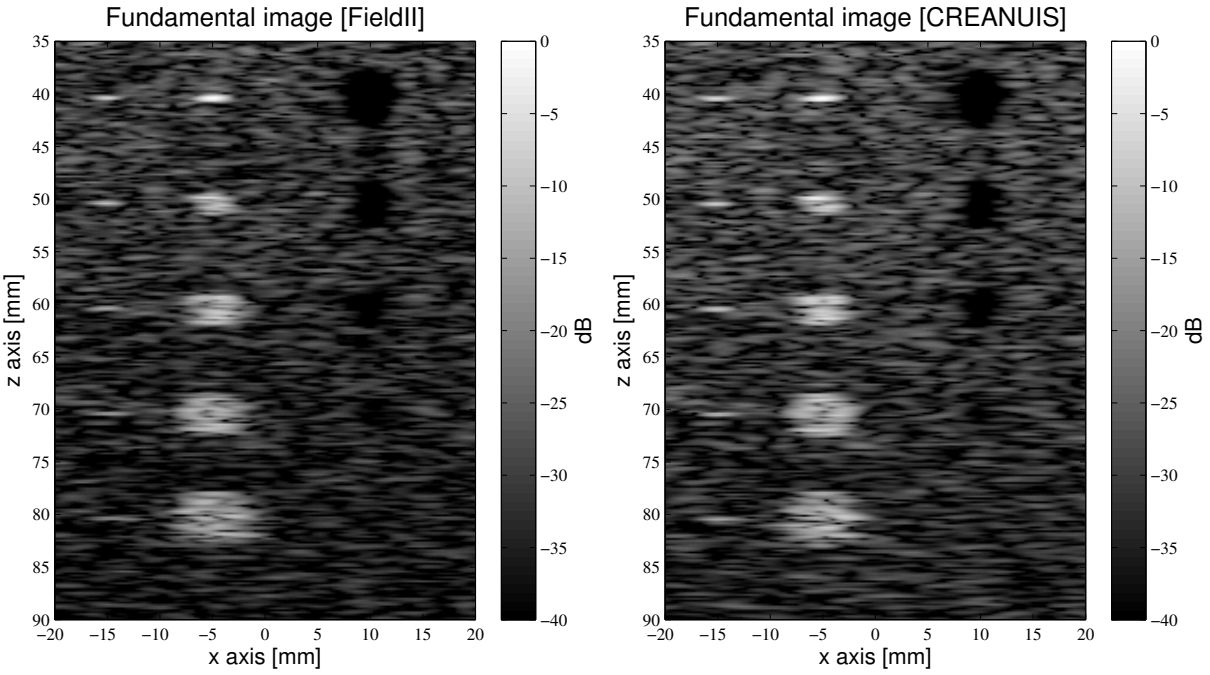

(a) (b)

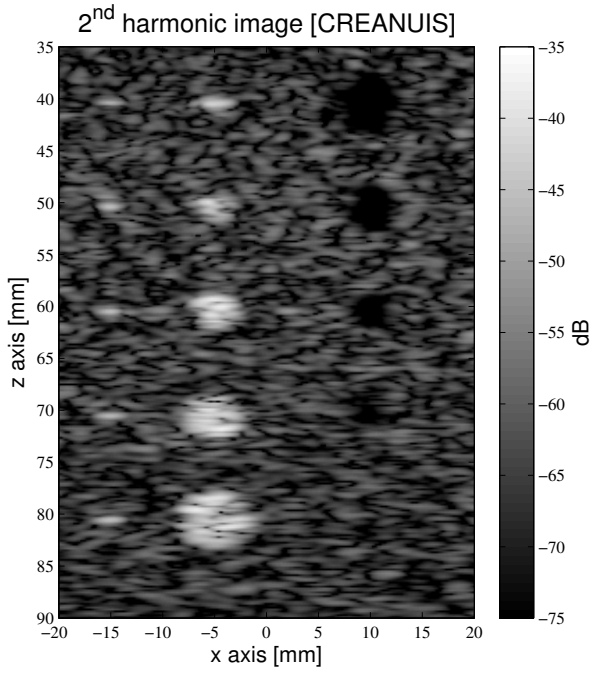

(c)

Figure 4.6: Resulting log-compressed images (in dB) of the cyst phantom. Image (a) is produced with FieldII, image (b) is the fundamental image produced with CREANUIS and image (c) is the second-harmonic image produced with CREANUIS.

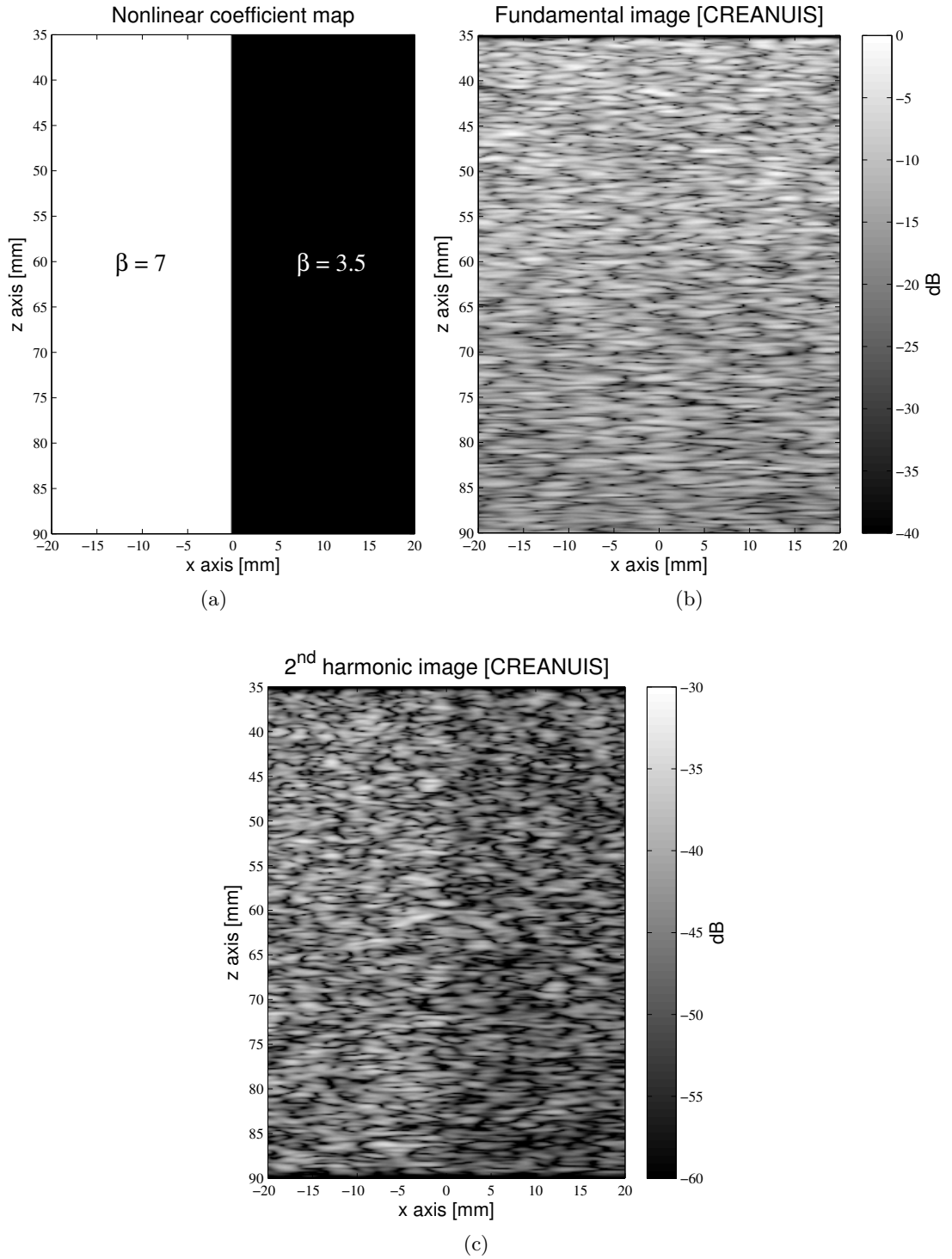

Figure 4.7: CREANUIS resulting B-mode image of an inhomogeneous nonlinear medium. (a) is the nonlinear map use in GASM, (b) is the fundamental image and (c) is the second harmonic one.

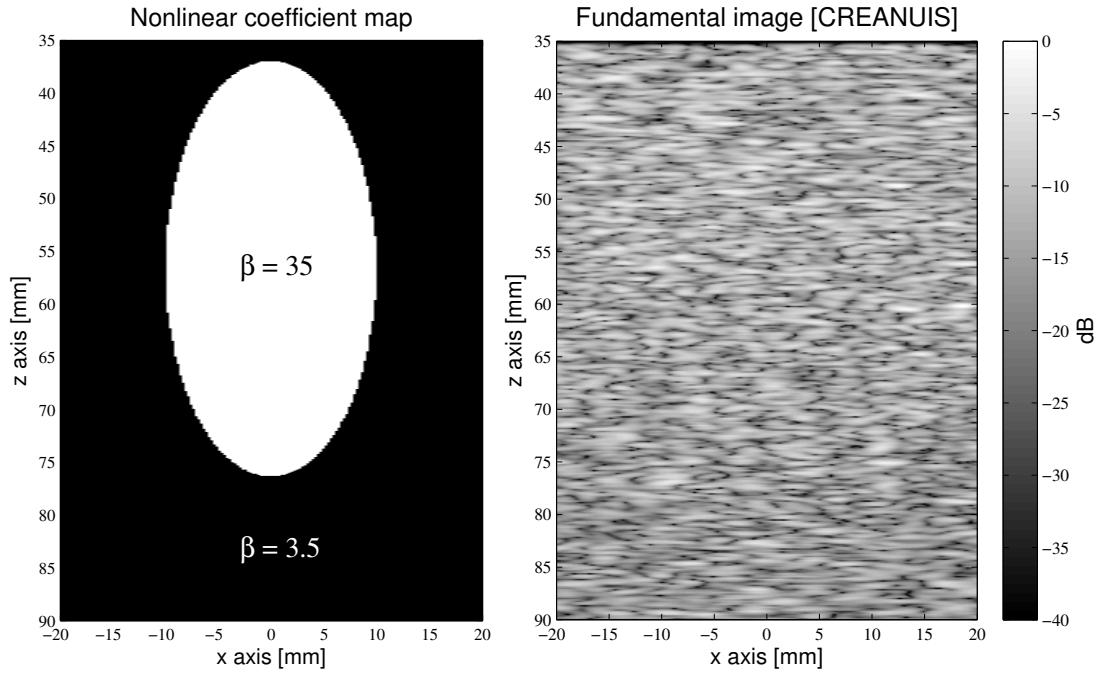

Figure 4.8: CREANUIS resulting B-mode image of an inhomogeneous nonlinear medium. (a) is the nonlinear map use in GASM, (b) is the fundamental image and (c) is the second harmonic one.

4.4.4 Pulse inversion simulation

With CREANUIS, it is now possible to simulate different harmonic imaging techniques such as amplitude modulation, phase optimization... An example is proposed with the PI technique [Simpson *et al.* (1999), Ma *et al.* (2005)]. In the acoustic field simulated with the GASM, the phase of the transmitted signal can be defined. To get a PI image, a first simulation is conducted with an initial transmitted phase of 0°. Then a second simulation with a 180° phase was done for the same scatterers' position. The PI image is obtained by adding the two simulated RF images. In this simulation, the same cyst phantom and corresponding transmission as in Fig. 3 have been reused. The resulting images are presented in Fig. 4.9. The PI image (Fig. 4.9.c) and its spectrum (Fig. 4.9.d) are only contained the second-harmonic frequency. On the Fourier spectrum of the three different images (Fig. 4.9.d), the two initial images (Fig. 4.9.a and Fig. 4.9.b) have the same fundamental component which is suppressed in the PI image. The second-harmonic amplitude of the PI image is increase by a factor 2 with is equivalent to the 6 dB improvement observed in the second-harmonic component in Fig. 4.9.d. A strong advantage of the PI imaging stays in the fact that no filtering is required to obtain the second-harmonic image contrary to the image presented in Fig. 3.c. Moreover, the linear second-harmonic component transmitted by the probe is naturally cancelled. The drawback is the need to acquire two images.

4.4.5 Computation time

To evaluate the computation time, the different simulations have been conducted on the same laptop computer (Intel Core2 Duo T9400 at 2.53GHz, 3.48 GB of memory). The figure given here are valid for the cyst phantoms simulated previously. With FieldII, 60 s are required for each line although only 12 s are needed with CREANUIS. However, this duration does not include the computation of the field which has to be done before. The resulting time to compute the nonlinear field is between 1 and 5 minutes on a CPU and between 5 and 20 s on a GPU. These variations are due to the CPU/GPU used and the discretization in the 4D (3D+t) space. Because the medium has here a constant nonlinear parameter, only one GASM simulation is required for the complete CREANUIS simulation. Finally, to compute the 163 lines of the proposed image, the total time for the FieldII simulation is around 160 minutes although it is only 33 minutes for CREANUIS. An improvement of a factor 4.4 has been obtained with CREANUIS. With inhomogeneous nonlinear medium, the GASM simulation has to be computed for each RF line. The total simulation time is comprised between 47 and 87 minutes. The resulting speed-up factor is then comprised between 1.8 and 3.4. A summary of the computation time are proposed in Table 4.1.

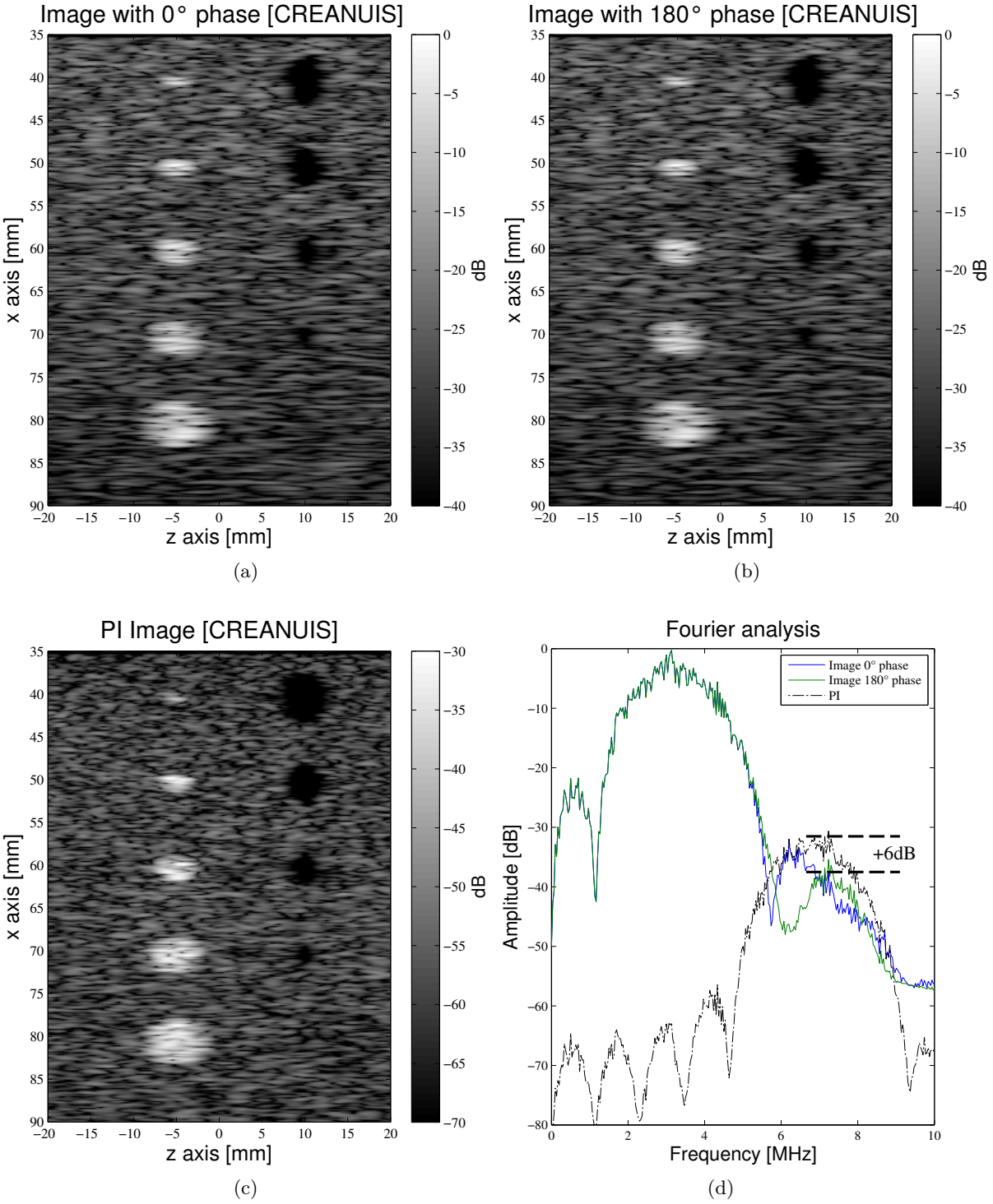

Figure 4.9: Simulations applied to the PI method. (a) and (b) are the initial B-mode images obtained respectively with a 0°phase and a 180°phase, (c) is the PI image after summation of the two first image and (d) is the Fourier spectrum of the presented images, where the 6 dB improvement in the PI image is highlighted.

Simulator	Time	Speed-up factor
FieldII	160 minutes	
CREANUIS (GASM on CPU, homogeneous nonlinear medium)	[33; 38] minutes	[4.2; 4.8]
CREANUIS (GASM on GPU, homogeneous nonlinear medium)	[32; 33] minutes	[4.8; 5.0]
CREANUIS (GASM on GPU, inhomogeneous nonlinear medium)	[47; 87] minutes	[1.8; 3.4]

Table 4.1: Comparison of the computation time obtained with FieldII and CREANUIS.

4.5 Discussion and conclusion

CREANUIS provides realistic nonlinear ultrasound echo-signals images that can be helpful for the development of techniques based on the nonlinearity of media. Indeed, to our knowledge, no tool has so far combined a nonlinear propagation software and a reconstruction algorithm to create nonlinear RF images. With the proposed solution, the user can implement its own beamforming strategy in its simulations. This beamforming facility, which is also provided by some advanced ultrasound equipment [Tortoli *et al.* (2009)], offers the possibility to simulate several nonlinear ultrasound techniques. Such simulations can be useful in the design and the optimization of methods based on the nonlinear propagation.

Currently, only the fundamental and the second-harmonic components have been presented and implemented in CREANUIS. However, by changing the nonlinear propagation simulator, similar developments can be added to take into account higher harmonics in the RF data and to simulate more realistic data and new nonlinear methods such as the super harmonic imaging [Bouakaz *et al.* (2002)]. The use of the GASM in CREANUIS allows to make fast simulation and to take into account the inhomogeneity of the nonlinear coefficient in the medium. Applications such as amplitude modulation, pulse inversion or other nonlinear imaging modalities can now be simulated using or not contrast agent, which has a higher nonlinear coefficient compared to the surrounding medium [Wu and Tong (1998)].

The current limitations of CREANUIS depend on different hypothesis or approximation. First, the probe geometry is limited. Currently, only 2D planar sources can be simulated with GASM, and so, CREANUIS. The GASM mathematical background has to be improved to simulate the nonlinear propagation of arbitrary array, but the current version of CREANUIS allows to consider the majority of nonlinear ultrasound methods. The second limitation concerns the backscattered signal. Indeed, only the attenuation has been taken into account and not the nonlinear propagation on the return path. This approximation was done because only a small amount of the initial pressure amplitude is propagating back to the probe and this back-propagation has been considered as linear. Finally, no filtering function has been defined on the transducer. Indeed, in transmission, the bandwidth is selected thanks to the signal transmitted in the medium. In reception,

an infinite bandwidth has been used in order to be able to work on the second-harmonic component in the RF signal. If a more realistic transducer effect is required in reception, the final RF image has to be filtered with the desired band-pass filter.

The computation time of CREANUIS strongly depends on the number of scatterers used in the simulation and a large variation of the requested time is observed. Moreover, if an inhomogeneous nonlinear parameter medium is considered, the nonlinear propagation simulation has to be computed for each RF line and increase substantially the total simulation time. For homogeneous nonlinear medium, only one nonlinear field simulation is needed. In order to save time, the simulated field can be saved to be reuse. Finally, the computation time has been decreased compare to FieldII simulations of a factor 1.8 to 4.8 depending on the nonlinear parameter homogeneity or not.

The CREANUIS software can be downloaded at the web address: http://www.creatis.insa-lyon.fr/site/en/CREANUIS

II Measure of the nonlinear parameter of media

Chapter 5

State of art in nonlinear parameter measurement

This chapter makes a review on the different methods that exist in the literature to measure the nonlinear parameter in a medium through an ultrasound investigation. In the literature, two major families are described: the thermodynamic methods and the finite amplitude methods [Sato *et al.* (1986), Bjørnø (2002)]. The former ones, even if they are more accurate that the finite amplitude one [Law *et al.* (1983)], need a specific and complex experimental setup which made them difficult to use in clinical applications. This review is an extension of the work presented in two symposia [Varray *et al.* (2009), Varray *et al.* (2010)b] and in a journal paper [Varray *et al.* (2011)a].

5.1 Thermodynamic methods

5.1.1 Basis equation

As presented in chapter 1, the B/A parameter is defined from the Taylor series expansion and is related to the celerity variation in function of the pressure for an adiabatic transformation. [Beyer (1960)] expressed the nonlinear parameter with:

$$\frac{B}{A} = 2\rho_0 c_0 \left(\frac{\partial c}{\partial p}\right)_{\rho_0,s} \tag{5.1}$$

This expression can be further developed with thermodynamic considerations [Coppens

et al. (1965)]:

$$\frac{B}{A} = 2\rho_0 c_0 \left(\frac{\partial c}{\partial p}\right)_{\rho_0,T} + \frac{2c_0 T\eta}{\rho_0 c_p}\left(\frac{\partial c}{\partial T}\right)_{\rho_0,p} \tag{5.2}$$

where $\eta = (1/V)(\partial V/\partial T)_p$ is the volume coefficient of thermal expansion and c_p the specific heat at constant pressure. Then, the B/A parameter has been described by two constants:

$$\frac{B}{A} = \left(\frac{B}{A}\right)' + \left(\frac{B}{A}\right)'' \tag{5.3}$$

with

$$\begin{cases} \left(\dfrac{B}{A}\right)' &= 2\rho_0 c_0 \left(\dfrac{\partial c}{\partial p}\right)_{\rho_0,T} \\ \left(\dfrac{B}{A}\right)'' &= \dfrac{2c_0 T\eta}{\rho_0 c_p}\left(\dfrac{\partial c}{\partial T}\right)_{\rho_0,p} \end{cases} \tag{5.4}$$

In these formulations, the term $(B/A)'$ corresponds to the isothermal nonlinear parameter related to the celerity variation of the pressure at a constant temperature. The second one, $(B/A)''$, is the isobar nonlinear parameter related to the celerity variation in function of the temperature at a constant pressure. In experimental measurements, it has been shown that the isobar nonlinear parameter is smaller than the isothermal one. The measure of the nonlinear parameter has been approximated by several authors to the measure of the isothermal nonlinear parameter [Law *et al.* (1983)].

5.1.2 Experimental methods

To easily compute the nonlinear parameter, [Zhu *et al.* (1983)] proposed to consider two transducers separated by a fixed distance L. The wave travels from one to the other in a time duration τ. The change in the celerity in function of the pressure variation can be expressed as:

$$\frac{\partial c}{\partial p} = \frac{-L}{\tau^2}\frac{\partial \tau}{\partial p} \tag{5.5}$$

The final formulation for the nonlinear parameter is then approximated to:

$$\frac{B}{A} = \frac{-2\rho_0 c_0^2}{\tau}\left(\frac{\Delta\tau}{\Delta p}\right)_S \tag{5.6}$$

This formulation has been reused by various authors but the formulation has been simplified using directly the phase difference [Sehgal *et al.* (1984), Sehgal *et al.* (1985), Sehgal *et al.* (1986), Errabolu *et al.* (1988)]:

$$\begin{cases} \dfrac{B}{A} &= \dfrac{-2\rho_0 c_0^3}{L\omega}\dfrac{\Delta\Phi_S}{\Delta p} \\ \left(\dfrac{B}{A}\right)' &= \dfrac{-2\rho_0 c_0^3}{L\omega}\dfrac{\Delta\Phi_T}{\Delta p} \end{cases} \tag{5.7}$$

where $\Delta\Phi_S$ and $\Delta\Phi_T$ are respectively the two phase-changes when the medium cannot

or can exchange its energy with the surrounding medium. Practically, the measure of the phase $\Delta\Phi_T$ is done half an hour after the measure of $\Delta\Phi_S$.

With the thermodynamic background, different media such as liquid, mixing liquid or biological media have been studied. For immiscible liquid, [Apfel (1983)] linked the nonlinear parameter to the variation of the volume in function of the pressure. He also presented another methodology of prediction of the composition of media using different linear but also nonlinear parameter measurements [Apfel (1986)]. For media composed predominantly of water, [Yoshizumi *et al.* (1987)] proposed a formulation of the nonlinear parameter taking into account the quantity of bounded and free water in the medium. In recent works, [Plantier *et al.* (2002)] have measured the nonlinear parameter of various liquids for different pressures and temperatures. A specific study on the glycerol has been conducted by [Khelladi *et al.* (2009)]. Some measures of the nonlinear parameter in biological materials have been conducted by [Law *et al.* (1985)]. He also compared the thermodynamic and finite amplitude methods [Law *et al.* (1983)].

Some years later, [Everbach and Apfel (1995)] proposed to measure the celerity change in function of the pressure with an ultrasonic interferometer. Under this consideration, the initial formulation (5.1) is extended as:

$$\frac{B}{A} = 2\rho_0 c_0 \frac{\Delta c}{\Delta p} = 2\rho_0 c_0^2 \frac{\Delta f}{f_0 \Delta p} \tag{5.8}$$

In the interferometer, the measure of the slope of $\Delta f/\Delta p$ gives access to the nonlinear parameter. In their works, [Everbach and Apfel (1995)] obtained very reproductive results with a standard deviation less than 1% of the measure. Five years later, [Davies *et al.* (2000)] used the same formulation to compute the nonlinear parameter but replaced the interferometer by a more simple experimental system: a phase technique with continuous wave system. It consists to represent the time of flight between the transmitter and the receiver as a continuous function of the phase and the frequency. With such system, the same experiment is less user dependant and more repeatable. The obtained results have a standard deviation inferior to 0.4% of the B/A parameter and present an error inferior to 5% compared to previous published values.

5.2 Finite amplitude methods

The finite amplitude methods have been largely studied because of their experimental simplicity and the possibility to simulate the nonlinear ultrasound wave propagation. Three different approaches can be highlighted for B/A estimation and the corresponding signals are summarized in Fig 5.1. All these methods are based on the initial transmission of the pressure wave in the z direction. The first method simply consists in transmitting a wave at a given center frequency (Fig 5.1.a) and measuring, in the received signal, the decrease of the fundamental and/or the increase of the second harmonic during the propagation, which is related to the nonlinear property. The second method is character-

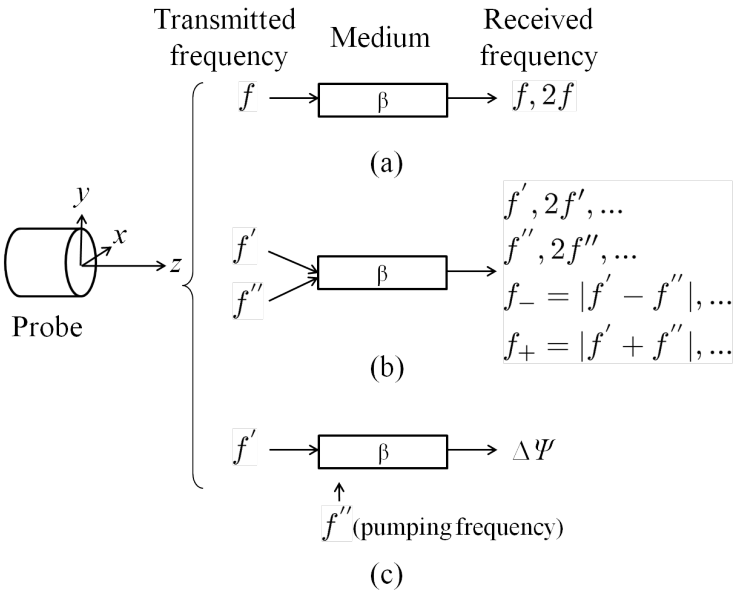

Figure 5.1: Schematic summary of the different approaches to determine the β coefficient of the propagation medium. These methods are differentiated by the transmitted frequencies: (a) methods with transmission of a single frequency, based on the measurement of the fundamental and/or the second harmonic component, (b) methods with composite signal transmission, based on the measurement of the interaction frequencies, (c) methods using pumping waves based on the measurement of the modulation $\Delta\psi$ of the initial transmitted signal.

ized by the emission of several signals at different frequencies (Fig 5.1.b). The received signal contains the contribution of each frequency but also of their interaction and the complementary waves created at the sum- and difference-frequencies. This interaction is related to the nonlinear behavior of the medium. The third approach involves a pumping wave perpendicular to the transmitted wave (Fig 5.1.c) to measure the nonlinear parameter. The interaction between the two waves creates a phase shift that is related to the nonlinear parameter. All these methods are further studied in this section.

5.2.1 Single frequency transmission

Extra attenuation method

During the nonlinear propagation of a pressure wave, the nonlinear distortion converts a part of the fundamental wave into harmonics. This effect, call extra attenuation have been presented by [Blackstock (1964)]. Its name means that the fundamental is not just attenuated by the medium but also by the nonlinear effects. The estimation of this converted quantity of fundamental is related to the nonlinear parameter of the medium (Fig 5.2). [Kashkooli *et al.* (1987)] developed this theory to measure the nonlinear parameter of four liquids. In this situation, the evolution of the fundamental pressure used by

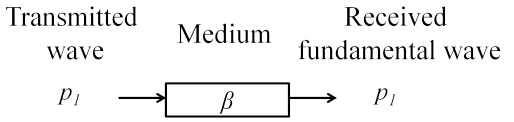

Figure 5.2: Extra attenuation method: the fundamental is attenuated by the medium but also by the nonlinear propagation and the transfer of energy to the second harmonic wave.

Kashkooli *et al.* is:

$$\frac{dp_1}{dz} = -\alpha_1 p_1 - \frac{k\beta}{2p_0 c_0^2} p_1^2 \tag{5.9}$$

where α_1 is the attenuation of the fundamental component. The solution of this equation, proposed by Kashkooli *et al.* is:

$$\frac{p_0}{p_1(z)} = e^{\alpha_1 z} + \frac{k\beta}{2\alpha_1 \rho_0 c_0^2}(e^{\alpha_1 z} - 1)p_0 \tag{5.10}$$

To estimate the nonlinear coefficient β, the measure of the fundamental component p_1 at a distance z is made for different initial pressure p_0. Then, the graph of $p_0/p_1(z)$ versus p_0 exhibits a slope S, related to the nonlinear coefficient:

$$S = \frac{k\beta}{2\alpha_1 \rho_0 c_0^2}(e^{\alpha_1 z} - 1) \tag{5.11}$$

Then, a simple formulation of the nonlinear coefficient for extra attenuation case is obtained:

$$\beta = S\frac{2\alpha_1 \rho_0 c_0^2}{k(e^{\alpha_1 z} - 1)} \tag{5.12}$$

The estimation of the nonlinear parameter of water with this method has conducted to an error of 20%. It must be noticed that this method is valid for plane waves, meaning that the diffraction effect is neglected. The initial energy of the transmitted pressure must also be large enough to be able to differentiate the extra attenuation from the classical attenuation of the medium.

For focussed sources, the diffraction of the transducer has to be taken into account and the received pressure has to be integrated on the surface of the receiver. In the simplified case of a gaussian source, [Liu and Nikoonahad (1989)] extended the previous extra attenuation mathematical background and linked the input voltage V_{in} on the transducer and the output one V_{out} on the receiver with the nonlinear coefficient:

$$\frac{V_{out}}{V_{out}^{max}} = \frac{V_{in}}{V_{in}^{max}} \cosh(Q\beta) \sinh(Q\beta \frac{V_{in}}{V_{in}^{max}}) \tag{5.13}$$

where Q, V_{in}^{max}, and V_{out}^{max} are constants that depend on the system, the attenuation and the distance between the transmitter and the receiver. Experimentally, the method is difficult to implement. First, the two constants V_{in}^{max} and V_{out}^{max} have to be determined in function of the experimental setup. Then, a known nonlinear medium is used and different

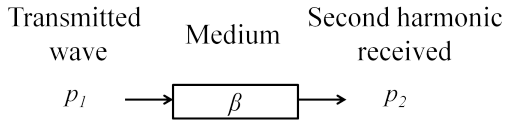

Figure 5.3: Direct method: the second harmonic increase is related to the nonlinear coefficient of the medium.

measurements of the $(V_{in}/V_{in}^{max}, V_{out}/V_{out}^{max})$ are made. A least square resolution is made to fit the experimental points to the model in order to determine the value of Q. Now the system is ready to be used with an unknown nonlinear medium [Nikoonahad and Liu (1990)]. [Liu and Nikoonahad (1989)] measured the nonlinear parameter of ethyl alcohol and the obtained error was around 5%. One advantage of this method is its application in pulse echo mode. However, as for plane wave, the initial pressure must be large enough to measure the extra attenuation effect.

Direct method (DM)

The simplest approach for the nonlinear coefficient measurement consists in transmitting a wave p_1 at a single frequency and selecting the second harmonic component after the propagation in the nonlinear medium (Fig 5.3). According to the theoretical background developed by various authors [Adler and Hiedemann (1962), Dunn *et al.* (1981), Law *et al.* (1981), Law *et al.* (1985)], and followed by Bjørnø [Bjørnø (1986)], the following expression of the nonlinear coefficient β, involving both the pressure amplitude of the fundamental at the source p_0 and the pressure amplitude of the second harmonic components $p_2(z)$ along the propagation axis, can be derived:

$$\beta = \frac{2\rho_0 c_0^3}{\omega} \frac{p_2(z)}{z p_0^2} \tag{5.14}$$

Equation (5.14) is valid when a plane wave is propagating in the medium. If a focused wave is considered, the previous equation can be used for very short distances, to limit the effect of the diffraction pattern. Moreover, to compensate for attenuation, the following formulation was proposed [Law *et al.* (1985)] in which $z \to 0$ indicates the limited range of validity and the necessity to be close to the transducer:

$$\beta = \left(\frac{2\rho_0 c_0^3}{\omega} \frac{p_2(z)}{z p_0^2} e^{-(\alpha_1 + \alpha_2/2)z} \right)_{z \to 0} \tag{5.15}$$

with α_1 and α_2 the attenuation of the fundamental and second harmonic components, respectively. To take into account the diffraction loss in the medium for a piston source, [Law *et al.* (1985)] corrected the second harmonic expression with a diffraction correction term, $F(z)$ defined by [Ingenito and Williams (1971)] for an ideal piston source. The new

expression of the nonlinear coefficient is now:

$$\beta = \left(\frac{2\rho_0 c_0^3}{\omega} \frac{p_2(z)}{z p_0^2} e^{-(\alpha_1+\alpha_2/2)z} \frac{1}{F(z)} \right)_{z\to 0} \tag{5.16}$$

The nonlinear coefficient is related to the second harmonic increase and this component needs to be experimentally measured. [Adler and Hiedemann (1962)] used an optical system to measure the different acoustic components and to evaluate the nonlinear parameter. For acoustic measure, a transmitter and an hydrophone are used to quantify the second harmonic component. The hydrophone recorded p_1 and p_2 after a propagation distance z [Dunn *et al.* (1981), Law *et al.* (1985), Chavrier *et al.* (2006), Wallace *et al.* (2007)]. The error in the β evaluation was approximately 5% [Wallace *et al.* (2007)]. Experimental errors can be created when the receptor is too close to the transmitter. Indeed, some stationary wave can be present and decrease the accuracy of the measure. A second type of experiment have been conducted using the same transmitter in transmission and reception and the second harmonic evolution is recorded after a reflection on a metallic plate. [Gong *et al.* (2004)] considered that the reflection on the plate was not perfect and introduced a reflection coefficient R. In this experimental situation, the second harmonic evolution has been expressed for a constant attenuation in the medium as:

$$p_2(z) = \frac{\beta\omega}{2\rho_0 c_0^3} p_0^2 R(1+R) \int_0^z e^{-2\alpha_1 u - \alpha_2(2z-u)} du \tag{5.17}$$

After calculating the integral of the attenuation, the nonlinear coefficient is then identified:

$$\beta = \frac{2\rho_0 c_0^3}{\omega} \frac{p_2(z)}{R(1+R)p_0^2} \frac{\alpha_2 - 2\alpha_1}{e^{-(2\alpha_1+\alpha_2)z} - e^{-2\alpha_2 z}} \tag{5.18}$$

This second type of measurements shows errors smaller than 5% for the majority of tissues [Gong *et al.* (2004), Vander Meulen and Haumesser (2008)]. However, the different medium parameters as α_1, α_2, c_0, ρ_0, R must be known before the experiments.

Insertion-substitution method

The insertion-substitution method, usable in both transmission and transmission-reception modes, consists in assessing the second harmonic changes as propagating in two different media. One medium is considered as a reference (subscript 0), while the second is unknown (subscript i). The reference medium has a length L and a nonlinear coefficient β_0, whereas the unknown medium is inserted in the ultrasound field and is substituted to the reference medium over a length d. Two consecutive measurements of the second harmonic pressure amplitude are taken, one without the unknown medium to determine p_{20} and the second with the unknown medium to measure p_{2i} (Fig. 5.4).

Gong *et al.* showed that the nonlinear coefficient β_i can be expressed as [Gong *et al.*

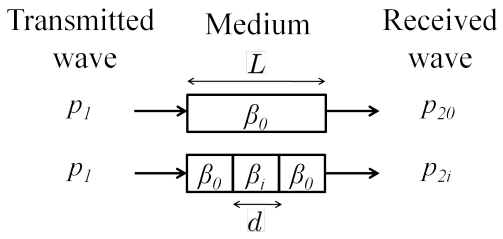

Figure 5.4: Illustration of the insertion-substitution method. A medium of unknown β_i coefficient is inserted within the reference medium of known β_0 coefficient.

(1984)]:

$$\frac{\beta_i}{\beta_0} = \left(\frac{p_{2i}}{p_{20}}\frac{1}{D'D''}\frac{L}{d} - \frac{L}{d} + 1\right)\frac{(\rho c^3)_i}{(\rho c^3)_0}\frac{1}{D''} \tag{5.19}$$

where D' and D'' are dimensionless parameters.

$$\begin{cases} D' &= 2(\rho c)_0/[(\rho c)_0 + (\rho c)_i] \\ \\ D'' &= 2(\rho c)_i/[(\rho c)_0 + (\rho c)_i] \end{cases} \tag{5.20}$$

When the attenuation is considered, equation (5.19) becomes:

$$\frac{\beta_i}{\beta_0} = \left[\frac{p_{2i}}{p_{20}}\frac{L}{d}\frac{1}{I_1 I_2} - \left(\frac{L}{d} - 1\right)\frac{I_2}{I_1}D'D''\right]\frac{(\rho c^3)_i}{(\rho c^3)_0}\frac{1}{D'D''^2} \tag{5.21}$$

where I_1 and I_2 correspond to the attenuation terms:

$$\begin{cases} I_1 &= e^{-\alpha_1 d} \\ \\ I_2 &= e^{-\alpha_2 d/2} \end{cases} \tag{5.22}$$

Some years later, [Gong *et al.* (1989)] extended the previous formulation by considering the diffraction of the piston source. A correction of the diffraction $F(k, z_0, z)$ for a piston of radius a is added with:

$$F(k, z_0, z) = 1 - \frac{2}{z - z_0}\int_{z_0}^{z}\frac{1 - \xi(z - \mu/2)/2k^2a^2}{\sqrt{\pi\xi(z - \mu/2)}}d\mu \tag{5.23}$$

with

$$\xi(z) = k\frac{\sqrt{z^2 + 4a^2} - z}{2} \tag{5.24}$$

The final expression of the insertion substitution method, which takes into account the diffraction, the attenuation and the nonlinearity is expressed as:

$$\frac{\beta_i}{\beta_0} = \left[\frac{p_{2i}}{p_{20}}\frac{L}{d}\frac{1}{I_1 I_2} - \left(\frac{L}{d} - 1\right)\frac{I_2}{I_1}D'D''\frac{F(k_0, d, L)}{F(k_0, 0, L)}\right]\frac{(\rho c^3)_i}{(\rho c^3)_0}\frac{1}{D'D''^2}\frac{F(k_0, 0, L)}{F(k_i, 0, d)} \tag{5.25}$$

Equation (5.21) and (5.25) have been described by different authors in many experiments in transmission mode [Gong *et al.* (1989), Zhang *et al.* (1996), Zhang and Gong (1999), Dong *et al.* (1999), Williams *et al.* (2006), Harris *et al.* (2007)] to measure the nonlinear coefficient of the medium included in water. With this method, the B/A parameter has been studied in different biological medium with an error inferior to 10% [Zhang and Dunn (1987), Zhang *et al.* (1991)]. With the apparition of the contrast agent and their highly nonlinear behavior, different authors have tried to measure their nonlinear parameter for different concentration. [Wu and Tong (1998)] worked on Albunex® and Levovist® and [Zhang *et al.* (2000)] on the SDA® (sonicated dextrose albumin). The results showed that the nonlinear parameter of contrast agent is much higher than the biological tissues with the different concentrations used ($B/A > 300$).

For focussed sources, these formulations are no more correct. In his work, Saito improve the mathematical background of the insertion substitution method for focussed gaussian sources [Saito (1993)]. For plane wave with weak attenuation, a variable R is defined as:

$$R(z) = \frac{p_{2i}(z)}{p_{20}(z)} \left(\frac{p_{10}(z)}{p_{1i}(z)} \right)^{\alpha_2/2\alpha_1+1} = \frac{\beta_i \rho_i c_i^3}{\beta_0 \rho_0 c_0^3} \frac{T_{0i}}{(T_{0i} T_{i0})^{\alpha_2/\alpha_1 - 1}} \tag{5.26}$$

where T_{0i} and T_{i0} are the transmission coefficients of the sound pressure at the reference-studied medium and studied-reference medium, respectively. For a focussed source, the phase parameter φ of the source is defined in function of the phase of the fundamental φ_1 and of the second harmonic φ_2

$$\varphi = \varphi_2 - 2\varphi_1 \tag{5.27}$$

For such focussed sources, Saito defined a new quantity R_F which is derived from R and the phase parameter of the reference medium φ_i and the unknown one φ_0:

$$R_F = R \frac{\sin \varphi_i}{\sin \varphi_0} \tag{5.28}$$

The solution of the right part of equation (5.26) is proposed in the paper by [Saito (1993)]. The final formulation is still related to the nonlinear coefficient β_i of the unknown medium. The experimental setup design by Saito is composed of a gaussian focussed source and an hydrophone. The sample has to be placed exactly at the focal point in order to have accurate results. The presented results exhibit a maximal error of 5% on different liquids and of 12% on some biological media even if some measurements are comprised in the standard deviation of the selected reference value. [Labat *et al.* (2000)] considered the superposition of a Gaussian beam to solve the KZK equation and to access to another formulation of the ratio R, still related to the two different second harmonic components. The error on the estimated nonlinear coefficients is under 6%.

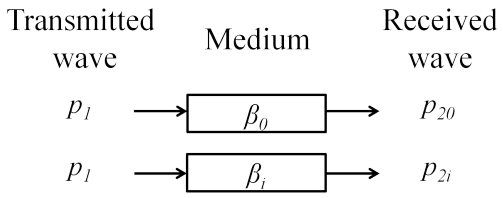

Figure 5.5: Comparative method: the nonlinear coefficient is extracted by comparison between two similar transmissions in the two different media.

Comparative method (CM)

The comparative method (CM) is a particular case of the insertion-substitution one (Fig 5.5). When the inserted medium has the same length as the reference medium, the equation (5.21) can be simplified as:

$$\beta_i = \beta_0 \frac{p_{2i}}{p_{20}} \frac{1}{I_1 I_2} \frac{(\rho c^3)_i}{(\rho c^3)_0} \frac{1}{D' D''^2} \tag{5.29}$$

As for the DM, the CM can be used in simple transmission experiments but also after a reflection on a metallic plate. In such a case, [Kourtiche *et al.* (2001)] updated the comparative formulation with the two reflection coefficients: the first one, R_{r0}, between the water and the reflector and the second one, R_{ri}, between the studied medium and the reflector:

$$\beta_i = \beta_0 \frac{p_{2i}}{p_{20}} \frac{R_{ri}}{R_{r0}} F_\eta F_{diff} F_{att} \frac{\rho_i c_i^3}{\rho_0 c_0^3} \tag{5.30}$$

with F_η the sensitivity function of the transducer, F_{diff} the correction function of the diffraction effect and F_{att} the attenuation correction. [Saito *et al.* (2006)] used the same formulation to create an experimental system that can measure the celerity, the density and the attenuation of the inserted sample. Then, the comparative method is used to measure the nonlinear parameter. The presented results exhibit a maximal error of 6% but is usually less than 3%. [Gong *et al.* (2004)] developed similar applications. In such a case, the second harmonic component has the same expression as (5.17). With such consideration, the ratio of the two second harmonic components between the two media of constant attenuation has been expressed as:

$$\frac{p_{2i}(z)}{p_{20}(z)} = \frac{\beta_i}{\beta_0} \frac{\rho_i c_i^3}{\rho_0 c_0^3} \frac{R_{ri}(1+R_{ri})}{R_{r0}(1+R_{r0})} \frac{\int_0^z e^{-2\alpha_{1i}u - \alpha_{2i}(2z-u)} du}{\int_0^z e^{-2\alpha_{10}u - \alpha_{20}(2z-u)} du} \tag{5.31}$$

where α_{10}, α_{20}, α_{1i}, and α_{2i} are respectively the fundamental and second harmonic attenuation of the reference and unknown medium. The nonlinear coefficient can then be extracted:

$$\beta_i = \beta_0 \frac{p_{2i}(z)}{p_{20}(z)} \frac{\rho_0 c_0^3}{\rho_i c_i^3} \frac{R_{r0}(1+R_{r0})}{R_{ri}(1+R_{ri})} \frac{\int_0^z e^{-2\alpha_{10}u - \alpha_{20}(2z-u)} du}{\int_0^z e^{-2\alpha_{1i}u - \alpha_{2i}(2z-u)} du} \tag{5.32}$$

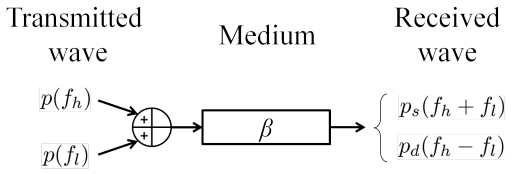

Figure 5.6: Composite transmission: The nonlinear interaction between the two transmitted wave create two new waves at the sum- and difference-frequency. The amplitude of these waves are related to the nonlinear coefficient.

5.2.2 Composite frequency transmission

When two waves at different frequencies are transmitted in a medium, a nonlinear interaction between the two waves takes place and creates, in addition to the harmonics of each pulse, components at the sum- and difference-frequencies. This interaction is related to the B/A parameter and several authors have attempted to determine the nonlinear parameter through this composite emission. The general theory has been presented by [Thuras *et al.* (1935), Westervelt (1963), Fenlon (1972)]. In this section, different approaches of composite emission to determine the nonlinear coefficient are presented.

Composite signal with two different frequencies

When a high and a low frequency signals are transmitted in the medium, nonlinear interaction appears in the medium. At the source, the wave transmitted at the low frequency f_l with an initial amplitude p_0^l is coupled with the wave at the high frequency f_h with an initial amplitude p_0^h (Fig. 5.6). The total pressure wave is expressed as:

$$p(t, z = 0) = p_0^h \sin(2\pi f_h t) + p_0^l \sin(2\pi f_l t) \tag{5.33}$$

with

$$\begin{cases} p_0^l & \gg & p_0^h \\ \\ f_h & > & f_l \end{cases} \tag{5.34}$$

In the paper of [Thuras *et al.* (1935)], a simple formulation for the sum (p_s) and difference (p_d) amplitude has been proposed for gases:

$$p_{s/d}(z) = \frac{\gamma + 1}{2\sqrt{2}\gamma} p_0^l p_0^h \frac{\omega_h \pm \omega_l}{c_0} z \tag{5.35}$$

[Fenlon (1972)] described in the lossless Burgers' equation the evolution of the maximal pressure of the wave created at the sum- and difference-frequencies:

$$p_{s/d}(z) = \frac{2}{(\sigma_h \pm \sigma_l)u_0} J_1((\sigma_h \pm \sigma_l)u_h) J_1((\sigma_h \pm \sigma_l)u_l) \tag{5.36}$$

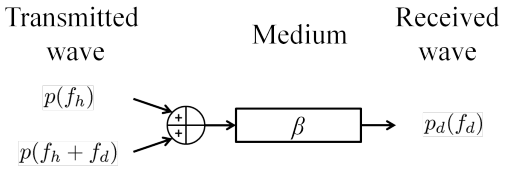

Figure 5.7: Composite transmission with two close frequencies: only the difference wave at frequency f_d is considered with a specific mathematical background developed in this situation.

with:

$$\sigma_i = \frac{\beta \omega_i z}{c_0^2} \tag{5.37}$$

where the subscript i is equal to h or l, J_1 is the first order Bessel function, u_0, u_h and u_l are the particle velocities at the source for respectively the total, the high and the low frequency waves. With this formulation, [Zhang *et al.* (2001)] computed the nonlinear parameter in the case of a piston transducer without diffraction.

[Pasovic *et al.* (2007)] proposed to study the evolution of this sum- and difference-waves when nonlinearity, absorption and diffraction are considered. Simulation and experimental results point out the relation between the ratio of the sum p_s and difference p_d pressure waves and the nonlinear parameter by recording the distorted pressure wave at the focal point. A relation has been shown between the evolution of the ratio p_s/p_d as a function of the initial pressure transmitted in the medium and according to different nonlinear medium. Even if no theoretical relation is explicitly given, the method shows interesting results to determine the nonlinear parameter. A similar approach has been used in metallic materials to detect cracks [Goursolle *et al.* (2008)].

Composite signal with two close frequencies

When the initial composite signal contains two close frequencies, the difference wave p_d created is at a very low frequency (Fig. 5.7). Nakagawa *et al.* proposed to derived $p_d(z)$ to access to the nonlinear parameter [Nakagawa *et al.* (1984), Nakagawa *et al.* (1986)]:

$$\frac{dp_d(z)}{dz} = \frac{\beta(z)\omega_d}{2\rho_0 c_0^3} p_1(z) p_2(z) - \alpha_d p_d(z) \tag{5.38}$$

with α_d the attenuation of the difference wave. The nonlinear parameter can easily be isolated from (5.38):

$$\beta(z) = \frac{2\rho_0 c_0^3}{\omega_d p_1(z) p_2(z)} \left(\frac{dp_d(z)}{dz} + \alpha_d p_d(z) \right) \tag{5.39}$$

[Cai *et al.* (1992)] adapted further the equation (5.38) to compute the B/A parameter for weakly, moderately and strongly scattering medium. Their results, obtained in simulations, are in good agreement with the geometry simulated in their works. In this

description, the nonlinear parameter can be inhomogeneous along the propagation direction.

The drawback of this type of methods comes from the length of the signal used. Indeed, the number of cycles of the two primary waves has to be long enough to allow the creation of the difference wave. For an emission of sinus signals at frequencies 5 MHz and 6 MHz with Gaussian envelope, the number of cycles for the primary wave must be at least 20 to obtain 5 modulated cycles at 1 MHz. Consequently, spatial resolution is decreased compared to the resolution at the high frequency used in the transmitted signal.

Second-order ultrasound field technique

The Second-order UltRasound Field (SURF) technique was initially proposed by [Ueno *et al.* (1990)]. It combines two excitation signals in a specific way: a high-frequency (f_h) pulse is localized during either the increasing part or the decreasing part of a low-frequency (f_l) wave (Fig. 5.8). The high-frequency is typically ten times higher than the low frequency, while the amplitude of the high-frequency pulse is around one-quarter that of the low-frequency pulse. In Fig. 5.8, two different transmitted signals, p_0' and p_0'' (Fig. 5.8.a and Fig. 5.8.d), and the corresponding pressures obtained after 15 cm propagation (Fig. 5.8.b and Fig. 5.8.e) are presented. When the high-frequency pulse is coincident with the increasing part of the low-frequency pressure (waveform p_0' in Fig. 5.8.a), its frequency is reduced during the propagation (Fig. 5.8.c). Inversely, when the high-frequency pulse is coincident with the decreasing portion of the low-frequency pulse (waveform p_0'' in Fig. 5.8.d), its frequency is increased (Fig. 5.8.f).

[Fukukita *et al.* (1996)] further developed the theoretical background to compute the nonlinear coefficient. As summarised in Fig. 5.9, for a given depth z, the two waves $p'(z)$ and $p''(z)$ are first transformed into the frequency domain to produce $P'(f)$ and $P''(f)$, respectively. Then the spectrum ratio $R(z,f)$ is computed over a bandwidth $\pm df$ around the high frequency f_h. This ratio corresponds to the spectral variation of the compression and the dilation of the high-frequency pulse on the two different low-frequency waves:

$$R(z,f) = \frac{P'[f_h - df; f_h + df]}{P''[f_h - df; f_h + df]} \tag{5.40}$$

From, (5.40) the crossover frequency f_x is obtained when:

$$\log[R(z,f)] = 0 \tag{5.41}$$

The slope of the spectral ratio S_x at f_x is also needed to obtain the final value of the nonlinear coefficient:

$$S_x(z) = \left(\frac{\partial \log[R(z,f)]}{\partial f}\right)_{f=f_x} \tag{5.42}$$

$$\beta(z) = \frac{\rho_0 c_0^3 B_0^2}{2\omega_l p_0} \frac{S_x(z)}{z f_x(z)} \tag{5.43}$$

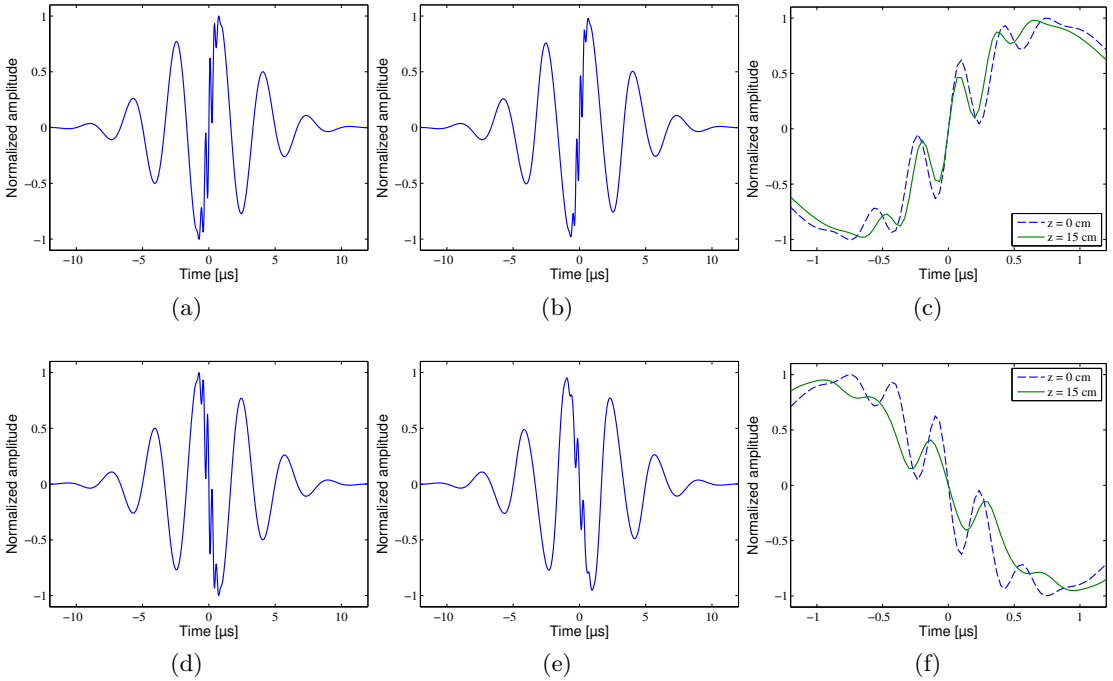

Figure 5.8: SURF method: transmitted signals p_0' (a) and p_0'' (d) at $z = 0$ cm and corresponding signals after a propagation of 15 cm (b, e). The last column (c, f) is a zoom of the signal portion containing the high- and the low-frequency components (the initial signal is represented by a dashed line and the final signal a solid line).

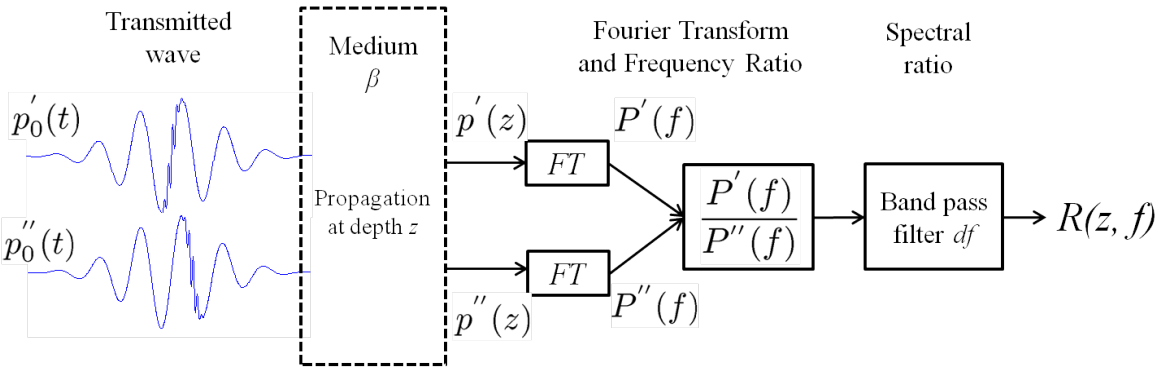

Figure 5.9: SURF method: transmission of two consecutive waves with the different high-frequency pulse localisations. The nonlinear coefficient is computed from the pair of recorded pulses.

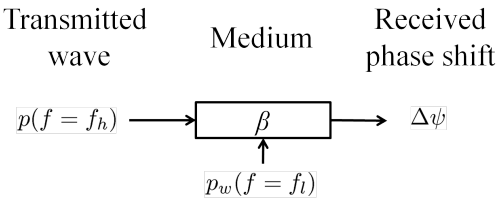

Figure 5.10: Pump wave method: the probe pulse is modified in function of the pump wave and the nonlinear coefficient of the medium.

with B_0^2 the frequency variance of the spectrum as defined by [Fukukita *et al.* (1996)]. Moreover, Fukukita *et al.* pointed out that the influence of diffractive effects of the probe in this method is limited because the calculation is based on the ratio of Fourier transforms. The error in the B/A estimation was estimated at less than 5% with a circular piston probe.

5.2.3 Pump wave method

During the nonlinear propagation, we have seen that interaction between different frequencies create some new wave components. The pump wave methods are based on a composite emission but the measure of the nonlinear parameter is made on the phase information and not on the nonlinear wave components. Indeed, when a low frequency pump wave (p_w) is perpendicularly transmitted in the medium at the same time that the probe pulse p, a phase modulation is present on the probe pulse and is related to the nonlinear parameter (Fig. 5.10). This method was introduced by [Ichida *et al.* (1984)] and they expressed the nonlinear parameter in function of the phase modulation $\Delta\psi$ along a short distance Δz:

$$\frac{B}{A} = -\frac{2\rho_0 c_0^3}{\omega p_w}\frac{\Delta\psi}{\Delta z} \tag{5.44}$$

This formulation is valid for plane wave and circular transducer. [Kim *et al.* (1990)] extended this formulation to take into account the possible variation of the nonlinear parameter along the studied direction. The new formulation of the phase shift is expressed as:

$$\Delta\psi\left(\frac{1}{\lambda_w}, y\right) = \frac{\omega}{2\rho_0 c_0^3} p_w \int_0^z \frac{B}{A}(x, y)\cos\left(\frac{2\pi x}{\lambda_w}\right) dx \tag{5.45}$$

with λ_w the pump wavelength. This formulation can be identified as a part of the Fourier transform of the B/A parameter with the spatial frequency $1/\lambda_w$. With different estimation of the phase shift at different position, an inverse Fourier transform allows to extract the nonlinear parameter map. Some experimental profile and image of the nonlinear parameter of phantoms are presented in the paper but the accuracy of the measure is not discussed. A similar approach was presented by [Cain *et al.* (1986)] which transmitted the two waves on the same transducer. Because the amplitude of the pump wave is larger than the pulse one, the measure nonlinear parameter is simplified and the experimental measures are conducted for different pump wave pressure. The display of the phase shift

versus the pump wave amplitude allow to extract the nonlinear parameter.

Cain also works on a different experimental situations. Indeed, he transmitted the pump and the pulse wave in opposite direction in order to have a specific phase modulation along the propagation axis. To do so, the transducer is placed at a distance L of a plane reflector. Then, the probe wave is emitted. This initial signal is long enough to make the incident and reflected paths. The length of the signal is $2L/c_0$. Then the pump pulse is emitted and the reflected signal is acquired. During the incident propagation of the pump wave, this latter interacts with the probe wave. The acquisition is made during $2L/c_0$. The total time for the transmission and the reception of the signals is $4L/c_0$. The phase modulation corresponds to the difference between the phase of the signal without the pump wave and the one with the pump waves which takes into account the nonlinear parameter. The phase shift depends on the received time τ which is in the range of $[0; 2L/c_0]$. The formulation proposed by Cain is expressed as the convolution between the pump waveform $p(x,t)$ and the spatial distribution of the nonlinear parameter [Cain (1985), Cain (1986)]:

$$\Delta\psi(\tau) = -\frac{\omega}{2\rho_0 c_0^3}\int_0^{c_0\tau/2} p\left(\frac{c_0\tau}{2} - u\right)\frac{B}{A}(u)du \tag{5.46}$$

This formulation has been tested with different pump waves: sinusoidal [Cain (1986)] and chirp [Houshmand *et al.* (1988), Cain and Houshmand (1989)]. The results obtained present good agreement with the nonlinear parameter variation, but no discussion has been conducted on the accuracy of such formulation. This mathematical background is valid for plane wave when the diffraction of the piston source is not taken into account. To solve this problem, [Barrière and Royer (2001)] have used a diffraction model based on plane wave expansions to take into account the diffraction effects. The extension has been validated on water and ethanol with an estimated error of 2%. The method has also been used on solid material with an error of 10% [Jacob *et al.* (2003)]. Another research group has worked on fused silica and phenolic resin with an accuracy in the range of 3% and 25% in function of the reference used [Bou Matar *et al.* (2002), Vila *et al.* (2004), Vander Meulen *et al.* (2004)]

5.3 Experimental approaches

Several authors have experimentally estimated the nonlinear coefficient of a medium using techniques developed for transmission measurement. This section presents these experimental approaches developed for B/A imaging in echo mode.

5.3.1 Radio frequency echo measurement

The first group of methods, which is a direct use of the second harmonic increases during the propagation and presented in [Akiyama (2000)] and [Fujii *et al.* (2004)], uses a mathematical formulation inspired by the equation (5.14). The recorded signal is related to

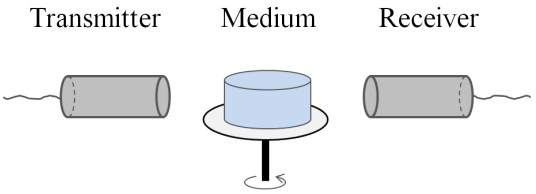

Figure 5.11: Ultrasound computed tomography: to reconstruct the image, different acquisitions are made by rotating the medium or the transmitter/receiver system.

the distorted pressure of the initial wave and the density and echogenicity of the scatterers of the medium. The β coefficient is not directly accessible on the signal. To limit the effect of the scatterers, two distinct transmissions are used to measure the nonlinear coefficient. The first one, at frequency f, and a second one at $2f$, record the changes in the second harmonic caused by nonlinear properties. The authors assume that the scatterer's response to the second harmonic due to the propagation is the same as the response to a wave transmitted at double frequency. The ratio between the two echoes would suppress the scatterer's impact. The authors concluded that the nonlinear coefficient is expressed as:

$$\beta(z) = \frac{\rho_0 c_0^3}{\pi f} \frac{p_0^{\Pi}}{p_0^2} \frac{d}{dz} \left(\frac{p_2(z)}{p_{\Pi}(z)} \right) \tag{5.47}$$

with $p_2(z)$ the second harmonic component amplitude of the backscattering echo of the first transmission at f, $p_{\Pi}(z)$ the fundamental amplitude of the backscattering echo of the second transmission at $2f$, p_0 and p_0^{Π} respectively the initial pressure of the two transmitted waves.

With the knowledge of the initial pressures transmitted in the medium, the authors measured the β value of a homogeneous medium from the experimental signal. Although this approach is relatively easy to implement, it has several limitations. The error between theoretical and experimental values of the nonlinear coefficient is larger than 20%. The authors consider that the ratio between the two waves amplitude results in a normalization of the diffraction effect. However, the ratio computed in (5.47) is directly related to the scatterer's characteristics, which must be the same during the two acquisitions. Consequently, any movements of the medium between the two acquisitions must be avoided.

5.3.2 Ultrasound computed tomography

The first experimental images of the β coefficient were obtained with ultrasound computed tomography (UCT) [Nakagawa *et al.* (1984)]. Using UCT, the theoretical background developed in transmission is valid and can be directly applied. By rotating the transmission-reception setup around the medium, different acquisitions were made and a reconstruction algorithm provided an image of the nonlinear coefficient (Fig. 5.11).

[Nakagawa *et al.* (1986)] and [Cai *et al.* (1992)] created first parametric images of a phantom with regions characterized by different nonlinear parameters. The UCT can

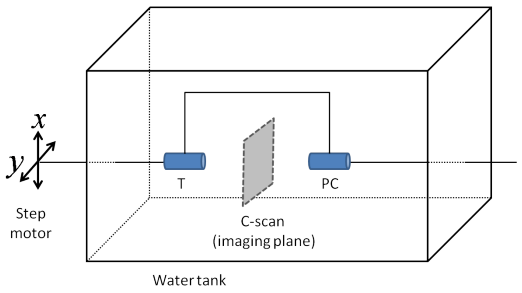

Figure 5.12: Wave phase conjugate acquisition system. The transmitter T and PC (phase conjugate) are used to transmit the initial wave and the reversed it.

use different nonlinear parameter estimation methods in the reconstruction process: the measurement of the second harmonic increase from a monochromatic wave, the insertion substitution technique and the measurement of the difference frequency wave increase when composite emission is used. The resulting images show a good agreement with the phantoms used, but the resolution is not discussed. [Zhang *et al.* (2001)] used the DM and the UCT to estimate the nonlinear parameter of biological media. The error of the measurements was under 10%. The insertion substitution method has also been largely used. Indeed, the comparison between the two media allows to decrease the experimental errors. [Zhang *et al.* (1996), Zhang and Gong (1999), Zhang and Gong (2006)] used the UCT to obtain the nonlinear parameter in egg or biological media. The B/A resulting images show the different region of interest and the global error, measured by the authors between the theoretical B/A value of media and the resulting image, was 6%. [Gong *et al.* (2004)] proposed to use a reflective plate in the UCT. The three methods (second harmonic increase, insertion-substitution method, increase of the wave at the difference frequency) have been tested with phantoms. The images have a good quality and the global errors of the different methods are less than 5%. Similar approaches were presented in [Burov *et al.* (1994), Bereza *et al.* (2008)].

The results obtained with UCT are very accurate and used the simple mathematical background of the finite amplitude methods. However, the UCT setup is not suitable for *in vivo* exams but only in the characterization of different medium sample.

5.3.3 Nonlinear ultrasonic phase-conjugate imaging

The wave phase conjugation is a nonlinear imaging technique based on a phase conjugate wave [Brysev *et al.* (2004)] and is presented in Fig. 5.12. The transducer T transmits in the medium the initial pressure wave. The transducer PC recorded it and reversed the received signal. This time reversed signal is sent back in the medium and its second-harmonic component is extracted at the transducer T. This component creates one point of the C-scan image. After moving the two transducers, another measurement is conducted in a different direction of the medium. The time reversal step can be conducted on the fundamental wave or the second harmonic component received at the PC transducer after

one propagation in the medium. An adjustment is then necessary in the different frequencies used in order to stay in the bandwidth of the transducers. This method is not directly able to extract the nonlinear parameter of the medium but provide an image with a contrast link to the nonlinear parameter inhomogeneity. The provide C-scan show a contrast evolution in function of the nonlinear parameter value [Krutyansky *et al.* (2007), Preobrazhensky *et al.* (2008)]. The mathematical background has also been improved to take into account moving media [Preobrazhensky *et al.* (2009)]

5.3.4 Other nonlinear measurements

Fatemi and Greenleaf have studied the nonlinear parameter in echo mode imaging by working on an effect they called "nonlinear shadowing" [Fatemi and Greenleaf (1996), Fatemi and Greenleaf (1998)]. The idea of the method is to compensate for the nonlinear effect during the propagation as it is done with the time gain compensation for attenuation to emphasize the high nonlinear region in the image. The correction is computed with a single point response for different amplitude excitations. If the excitation is weak, the propagation can be considered as linear and the experimental setup is calibrated. The resulting image are not of good quality in the paper and it is quite difficult to comment the results of the method.

The nonlinear parameter takes into account the second order propagation in tissue. However, the propagation is not reduced to the second harmonic component. If higher components are considered, the third order nonlinear parameter C/A can be considered. The C/A parameter is also computed from the Taylor development of the pressure. It is expressed as:

$$\frac{C}{A} = \frac{\rho_0^2}{c_0^2} \left(\frac{\partial^3 p}{\partial \rho^3} \right)_s \tag{5.48}$$

An insertion substitution method has been proposed to measure the C/A parameter in gases [Xu *et al.* (2003)] and in biological media [Liu *et al.* (2007)]. The estimation error of the C/A parameter was inferior to 5% in biological media.

5.4 Discussion and conclusion

Different techniques to measure the nonlinear parameter have been discussed. The thermodynamic methods are more accurate than the finite amplitude one [Law *et al.* (1983), Kashkooli *et al.* (1987)] but cannot be easily used for *in vivo* exams. The various finite amplitude methods are very interesting. The possible strategies of measuring the fundamental decrease, the second harmonic increase, the comparison between two transmissions, the nonlinear interaction of composite waves or the pump wave transmission are very promising for B/A imaging. In the Table 5.1, the nonlinear parameter of different biological media (healthy or not) are presented. A more extended version can be found in Appendix D.

Medium	Temperature	B/A	Reference
Beef liver		6.88	[Law *et al.* (1983)]
	25°C	7.0	[Law *et al.* (1985)]
	25°C	6.8	[Law *et al.* (1985)]
Pig fat	25°C	10.9	[Law *et al.* (1985)]
	25°C	11.3	[Law *et al.* (1985)]
	25°C	10.8	[Gong *et al.* (1989)]
Cat liver		6.7 ± 0.2	[Zhang and Dunn (1987)]
Porcine liver	26°C	7.1	[Gong *et al.* (1989)]
	27°C	6.9	[Zhang *et al.* (2002)]
		6.9	[Gong *et al.* (2004)]
Breast fat	22°C	9.206	
	30°C	9.909	[Sehgal *et al.* (1984)]
	37°C	9.633	
Multiple myeloma	22°C	5.603	
	30°C	5.796	[Sehgal *et al.* (1984)]
	37°C	6.178	
Human liver	30°C	6.54	[Sehgal *et al.* (1985)]
	Normal 30°C	7.6 ± 0.8	[Bjørnø (1986)]
	Congested 30°C	7.2 ± 0.7	[Bjørnø (1986)]

Table 5.1: B/A nonlinear parameters of media as reported in the literature.

In the set of presented methods, just a few of them take into account the possible variation of the nonlinear parameter in tissue. The possibility to discriminate the different tissues is a major importance in B/A imaging. The extensions to inhomogeneous nonlinear parameter are presented in the next chapter.

Chapter 6

Nonlinear parameter measurement techniques: extensions in echo mode configuration and simulations

6.1 Introduction

In the previous chapter, the review of the existing techniques that measure the nonlinear parameter of media, has been conducted. They are based on thermodynamic or finite amplitude approaches. Among all the methods described in the literature, only the one directly designed for the echo mode and usable in clinical applications or extended to this situation are considered herein. That is why the thermodynamics methods, although they are more accurate than the finite amplitude methods, are not effective for our purposes: they require special equipments and an experimental setups that may not be usable in clinical applications. Moreover, the finite amplitude methods are also preferred because of their experimental simplicity and the possibility of simulating the ultrasound pressure wave propagation with previously presented tools (chapter 2). From the set of finite difference simulators presented in previous chapter, the methods using pumping waves or the UCT are not considered here. Indeed, although they present good agreement with theoretical values, they are not suitable in the context of standard ultrasound medical exams.

The objective of this chapter is to propose a method to image the variation of the nonlinear parameter in the medium and usable in ultrasound medical exam. Extensions of

potential methods of B/A measurement are proposed and evaluated in simulation. This work has been presented in conferences [Varray *et al.* (2009), Varray *et al.* (2010)b] and published in a journal paper [Varray *et al.* (2011)a].

6.2 Extensions of the technique for an inhomogeneous nonlinear parameter

6.2.1 Introduction

The finite amplitude methods are mainly based on the increase of the second-harmonic wave in the medium during the propagation. This evolution of the spectrum has been presented for a plane wave by [Zhang and Gong (1999)]. The related formulation allows to take into account an inhomogeneous nonlinear and attenuating behavior of the medium in the propagation direction:

$$p_2(z) = \frac{\omega p_0^2}{2\rho_0 c_0^3} \int_0^z \beta(u) e^{\int_0^u -2\alpha_1(v)dv - \int_u^z \alpha_2(v)dv} du \tag{6.1}$$

This formulation can also be rearranged:

$$p_2(z) = \frac{\omega p_0^2}{2\rho_0 c_0^3} e^{-\int_0^z \alpha_2(v)dv} \int_0^z \beta(u) e^{\int_0^u (\alpha_2(v)-2\alpha_1(v))dv} du \tag{6.2}$$

6.2.2 Extended direct method (EDM)

The extension of the direct method (EDM) is based on the evolution of the second-harmonic wave in an inhomogeneous nonlinear medium. Rearranging equation (6.2), the nonlinear parameter can be expressed as:

$$\int_0^z \beta(u) e^{\int_0^u (\alpha_2(v)-2\alpha_1(v))dv} du = \frac{2\rho_0 c_0^3}{\omega p_0^2} p_2(z) e^{\int_0^z \alpha_2(v)dv} \tag{6.3}$$

By taking the derivative of the previous equation, the nonlinear parameter can be extracted in function of the other medium parameter:

$$\beta(z) e^{\int_0^z (\alpha_2(v)-2\alpha_1(v))dv} = \frac{2\rho_0 c_0^3}{\omega p_0^2} e^{\int_0^z \alpha_2(v)dv} \left[\frac{dp_2(z)}{dz} + \alpha_2(z) p_2(z) \right] \tag{6.4}$$

$$\beta(z) = \frac{2\rho_0 c_0^3}{\omega p_0^2} \left[\frac{dp_2(z)}{dz} + \alpha_2(z) p_2(z) \right] e^{\int_0^z 2\alpha_1(v)dv} \tag{6.5}$$

The final formulation (6.5) takes into account the possible variation of the nonlinear parameter during the propagation but also of the attenuation in the medium. This evaluation is based on the derivative of the second-harmonic pressure.

6.2.3 Extended comparative method (ECM)

A possible extension of the comparative method (ECM) is based on the expression of the second-harmonic pressure. Using the equation (6.1), the second-harmonic pressure for the reference medium, considered with an homogeneous nonlinear parameter and attenuation, is expressed as:

$$p_{20}(z) = \frac{\beta_0 \omega p_0^2}{2\rho_0 c_0^3} I_0(z) \tag{6.6}$$

with

$$I_0(z) = \frac{e^{-2\alpha_{10}z} - e^{-\alpha_{20}z}}{\alpha_{20} - 2\alpha_{10}} \tag{6.7}$$

In these equations, the subscript 0 is also used for the attenuation. Indeed, the reference medium and the unknown one can have different attenuation values. Then the ratio between the second-harmonics of the reference medium and the unknown medium can be computed with arbitrary sound velocity, density, inhomogeneous attenuation and inhomogeneous nonlinear coefficient:

$$\frac{p_{2i}(z)}{p_{20}(z)} = \frac{(\rho c^3)_0}{(\rho c^3)_i} \frac{e^{-\int_0^z \alpha_{2i}(v)dv} \int_0^z \beta_i(u) e^{\int_0^u (\alpha_{2i}(v) - 2\alpha_{1i}(v))dv} du}{\beta_0 I_0(z)} \tag{6.8}$$

After isolating the integrative part of the nonlinear coefficient of medium i, the derivative is computed to obtain the formulation of the nonlinear coefficient with the comparative method. The extended formulation is:

$$\int_0^z \beta_i(u) e^{\int_0^u (\alpha_{2i}(v) - 2\alpha_{1i}(v))dv} du = \beta_0 \frac{(\rho c^3)_i}{(\rho c^3)_0} \frac{p_{2i}(z)}{p_{20}(z)} I_0(z) e^{\int_0^z \alpha_{2i}(v)dv} \tag{6.9}$$

$$\beta_i(z) e^{\int_0^z (\alpha_{2i}(v) - 2\alpha_{1i}(v))dv} = \beta_0 \frac{(\rho c^3)_i}{(\rho c^3)_0} \frac{d}{dz} \left(\frac{p_{2i}(z)}{p_{20}(z)} I_0(z) e^{\int_0^z \alpha_{2i}(v)dv} \right) \tag{6.10}$$

$$\beta_i(z) = \beta_0 \frac{(\rho c^3)_i}{(\rho c^3)_0} \left[V(z) \frac{p_{2i}}{p_{20}} + W(z) \frac{d}{dz} \left(\frac{p_{2i}}{p_{20}} \right) \right] \tag{6.11}$$

Two terms, V and W, are introduced because of the different attenuations of the two distinct media after the derivation process:

$$\begin{cases} V(z) &= \dfrac{e^{-2\alpha_{10}z}(\alpha_{2i}(z) - 2\alpha_{10}) - e^{-\alpha_{20}z}(\alpha_{2i}(z) - \alpha_{20})}{\alpha_{20} - 2\alpha_{10}} e^{\int_0^z 2\alpha_{1i}(v)dv} \\ W(z) &= I_0(z) e^{\int_0^z 2\alpha_{1i}(v)dv} \end{cases} \tag{6.12}$$

The final formulation (6.11) of the ECM is valid in media with different densities, celerities and attenuations. If the attenuations are considered equal in the two media and homogenous during the propagation (classical experimental approximation), V and W are

now expressed as (the subscript 0 and i have been removed):

$$\begin{cases} V(z) &= 1 \\ W(z) &= \dfrac{1-e^{-(\alpha_2-2\alpha_1)z}}{\alpha_2-2\alpha_1} \end{cases} \tag{6.13}$$

and the nonlinear parameter results in:

$$\beta_i(z) = \beta_0 \frac{(\rho c^3)_i}{(\rho c^3)_0}\left[\frac{p_{2i}}{p_{20}} + \frac{1-e^{-(\alpha_2-2\alpha_1)z}}{\alpha_2-2\alpha_1}\frac{d}{dz}\left(\frac{p_{2i}}{p_{20}}\right)\right] \tag{6.14}$$

6.2.4 Extended SURF method (ESURF)

An extension of the SURF method (ESURF), taking into account the variation of the nonlinear coefficient, is proposed here. Initially, the formulation for the spectral ratio from [Fukukita *et al.* (1996)] was:

$$S_x(z) = \frac{2\omega_l}{B_0^2} \times f_x(z) \times \tau \tag{6.15}$$

with τ the propagation delay time between pump waves with and without distortion. For an inhomogeneous nonlinear coefficient, this delay τ is expressed as:

$$\tau = \frac{p_0}{\rho_0 c_0^3}\int_0^z \beta(u)du \tag{6.16}$$

With equation (6.15) and equation (6.16), the formula of the ESURF can be expressed after derivation by:

$$\int_0^z \beta(u)du = \frac{\rho_0 c_0^3 B_0^2}{2\omega_l p_0} \times \frac{S_x(z)}{f_x(z)} \tag{6.17}$$

$$\beta(z) = \frac{\rho_0 c_0^3 B_0^2}{2\omega_l p_0} \times \frac{d}{dz}\left(\frac{S_x(z)}{f_x(z)}\right) \tag{6.18}$$

From the equation (6.17), if a constant nonlinear parameter is considered, the integration in the left term can be conducted and the same formula as in equation (5.43) is obtained.

6.3 Evaluation of the proposed extensions with fields simulations

6.3.1 Simulation of a simple medium

Chosen simulator

The finite difference simulator of Voormolen has been chosen because of its high-order nonlinear interaction requested for the SURF and ESURF methods. The pressure

evolution transmitted by a linear array is recorded at the different depths. The second-harmonic $p_2(z)$ is then calculated and used in the different extensions. This simulator has also the possibility to consider the diffraction effects of the probe using the Burgers (no diffraction) or the KZK (with diffraction) equation.

Probe and medium characteristics

First, a simple medium with different layers of different nonlinear parameter has been used in simulations to evaluate the different proposed extensions. It is 150 mm long and its physical parameter are described in Table 3.2 (pp. 38). It is composed of three slices of homogeneous media with a linear variation of the B/A parameter at the interface between two media. The first and the third slices have a B/A value of 5, the intermediate slice has a B/A value of 12. The profile of the B/A parameter along the simulated medium is given by the dashed line in Fig. 6.1. The probe parameters used in simulation correspond to the LA533 probe (Appendix A.2). A five-cycle sine at 1 MHz with a gaussian windows and focalized at 70 mm has been used in transmission. No apodization has been used on the active elements.

Simulations results

The resulting evaluations of the nonlinear parameter for the three extended method are summarized in Fig. 6.1, without (left panel) and with (right panel) the consideration of the probe diffraction. For each simulation, the results obtained with the classic solutions (equations (5.14), (5.29) and (5.43)) and the proposed extensions (equation (6.5), (6.14) and (6.18)) are compared. For the three extensions proposed, the results are accurate when the diffraction is neglected. When considering the diffraction, the EDM (Fig. 6.1.b) and the ESURF (Fig. 6.1.f) methods fail while the ECM works nicely in the two first media. This method is able to accurately detect the first significant variation of the nonlinear parameter but not the second one.

Discussion

The different extensions proposed here are valid for plane waves and do not take into account the diffraction of the probe. A specific theoretical background is needed to understand the diffraction effects in nonlinear propagation. Some authors, such as [Law *et al.* (1985)] and [Gong *et al.* (1989)], have proposed formulations to correct this outcome for circular transducers. However, with standard linear array probes, the diffraction pattern is very different because of the numerous elementary transducers of finite size and rectangular geometry. For the extensions proposed here, the formulation does not take into account the diffraction of a linear probe. However, with our objective of implementing this technique for clinical use, these corrections are not usable for a linear array. [Fujii *et al.* (2004)] and [Fukukita *et al.* (1996)] proposed limiting the diffraction effect of the probe by doing the ratio between the second-harmonic obtained in two similar experiments. The

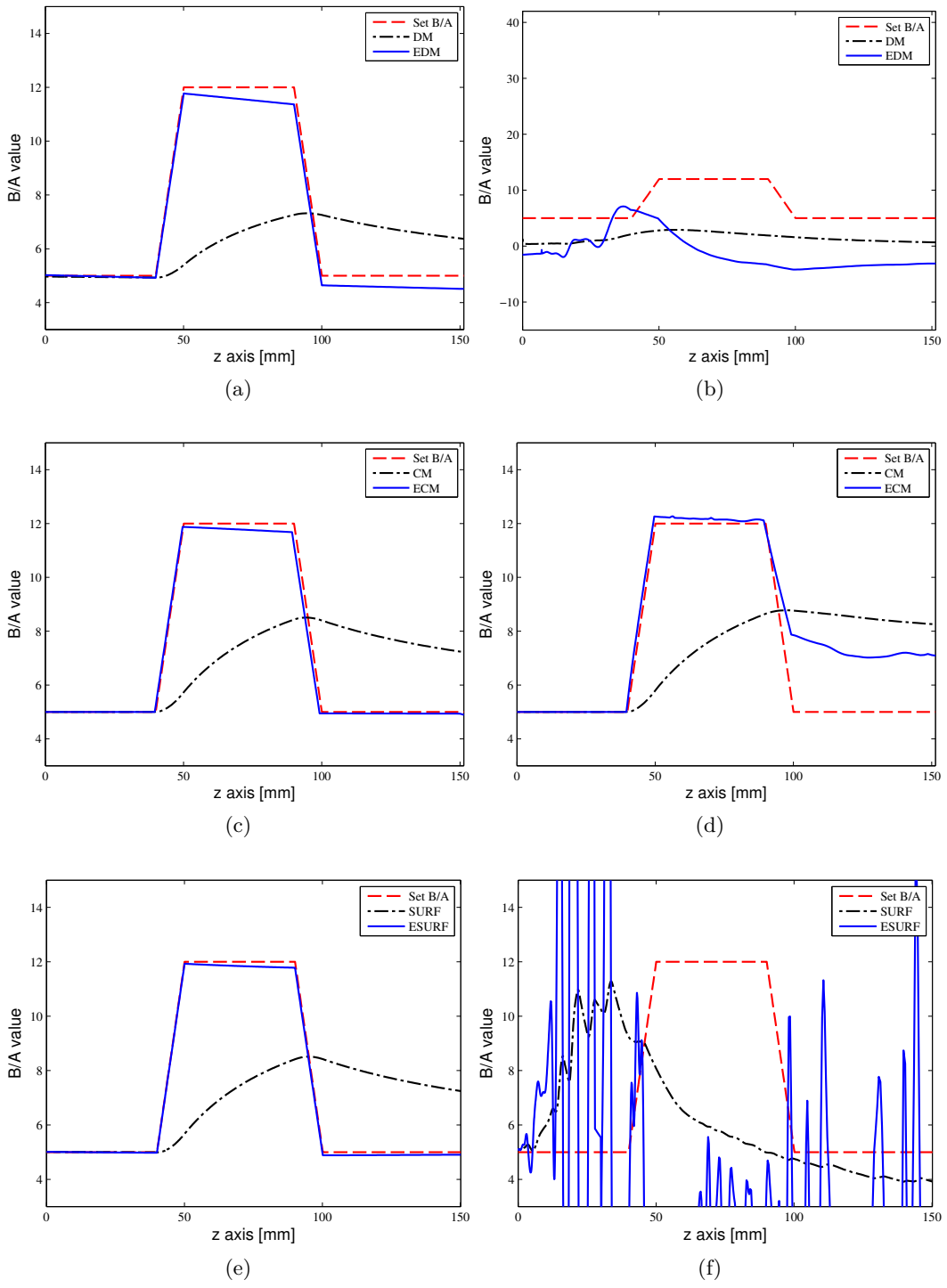

Figure 6.1: Resulting B/A parameters for the different methods. Set B/A is the reference B/A value. The diffraction is neglected in the left column (a, c and e) but not in the right column (b, d and f). All extended approaches provide accurate results when the diffraction of the probe is neglected. When the diffraction is considered, the nonlinear parameter estimation fails, except for the ECM, which gives encouraging results.

results, obtained with the ECM, consolidate this hypothesis and encourage to use the formulation proposed in equation (6.14) with or without the consideration of the diffraction effect.

6.3.2 Simulation of a complex medium

The ECM is the method that presents the best results in the previous section. Because of the facility to implement this technique and the relevance of the first results, we focussed our work on this method. In order to continue to evaluate its performance, an inhomogeneous nonlinear medium has to be simulated.

Chosen simulator

To estimate the ECM on a more complex medium in term of nonlinear parameter has to be used. Indeed, the nonlinear map of the medium can be completely inhomogeneous and not only composed of layers. In order to test the method, 163 GASM simulations were made. Each simulations is based on the 64 active elements of the LA533 probe (A.2). This 64 active elements of the sub-probe are then moved to compute the entire image. For each simulation, the corresponding nonlinear coefficient map in front of the active elements has to be used. This is illustrated in Fig. 6.2 with the display, in front of the nonlinear map, of the sub-probe that transmitted the ultrasound wave. Then, the central line of the produced second-harmonic field is saved in the second-harmonic field image. When the different simulations are done, the second-harmonic field image of the studied medium is obtained.

Probe and medium characteristics

Two different complex nonlinear media have been simulated. The first one consists of an elliptic inclusion of nonlinear parameter 10 in a surrounding medium of nonlinear parameter 5. The second input medium is composed of a background with a B/A value of 5 and an egg-shape inclusion with a B/A value of 9. Inside this egg-shape, two regions with different nonlinear parameter (3 and 7) were disposed. The two images of the nonlinear parameter have been displayed in Fig. 6.2. A four-cycle sine at 3 MHz with a gaussian window focalized at 70 mm has been transmitted in the media. No apodization has been used on the active elements in order to maximize the energy transmitted in the medium. The physical parameters of the medium are the same as in the previous KZK simulations (Table 3.2, p. 38).

Simulation results

The simulation results are displayed in Fig. 6.3 for the first case and in Fig. 6.4 for the second one. In Fig. 6.3.a and Fig. 6.4.a, the two vertical lines delimitate the region of the medium that is used as the reference in the ECM. In this region, the nonlinear

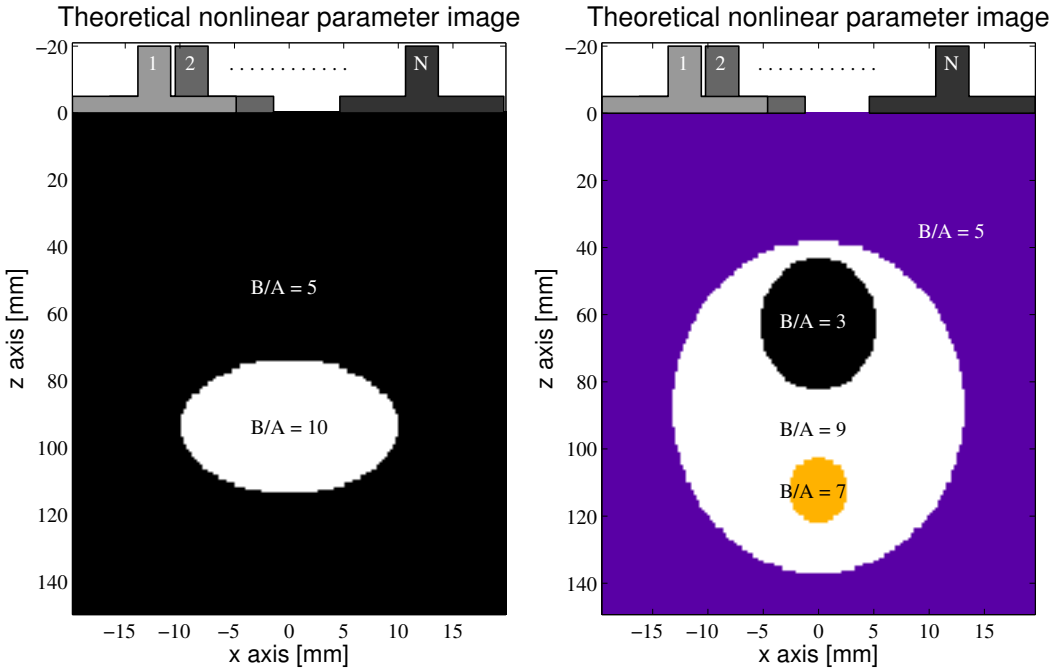

(a) (b)

Figure 6.2: Illustration of the two different nonlinear parameter maps used in simulation. 1, 2, ..., N illustrate the different sub-probe position in order to compute the corresponding nonlinear medium used in GASM simulations.

parameter is constant and the corresponding second-harmonic is used as the $p_{20}(z)$ in the equation (6.5). With this knowledge, the ratio images (p_{2i}/p_{20}) are computed and presented in Fig. 6.3.b and Fig. 6.4.b. The different structures of the nonlinear parameter map (Fig. 6.3.c and Fig. 6.4.c) can be observed in the resulting images. The mean value and the standard deviation of each initial area have been computed and are summarized in Table 6.1.

Discussion

The resulting B/A images are in good accordance with the theoretical value. However, as for the initial simulation using the Voormolen simulator, the ECM has difficulties to follow multiple variations in the nonlinear parameter and its estimation is degraded when the investigated depth increases. This effect can be similarly related to the shadow cone effect although, with shadow cone, no more signal is acquired after a high backscattering region. Here, the signal is still present after the higher part of the nonlinear parameter, but the method fails to compute its correct value. However, the ECM provided very promising results for B/A imaging. In simulation, the attenuation, the celerity and the density have been considered constant. This approximation, although is does not correspond to a clinical exam, is necessary to estimate the B/A parameter in simulated images.

Medium	Set B/A	Mean value of estimated B/A	Standard deviation of estimated B/A
Medium 1	5	5.34	0.76
(Fig. 6.2.a)	10	8.71	0.83
	3	3.41	1.16
Medium 2	5	5.59	1.13
(Fig. 6.2.b)	7	6.54	0.29
	9	8.63	1.20

Table 6.1: Evaluation of the estimated nonlinear parameter on GASM simulations.

6.4 Evaluation of the ECM on simulated RF images

6.4.1 Proposed method

The obtained estimation from the second-harmonic field images shows a good agreement between the theoretical and the measured nonlinear parameter of the medium. However, during clinical exams, the acoustic field is not available and must be computed from the RF images. This possibility is studied in this section.

Chosen simulator

The CREANUIS software, presented in chapter 4, gives the possibility to simulate the nonlinear RF image of an inhomogeneous nonlinear medium. The two previously described nonlinear media are used and the corresponding nonlinear RF images are simulated using CREANUIS. The estimation of the nonlinear parameter is then conducted on resulting nonlinear RF images.

Probe and medium characteristics

The probe and medium characteristics are the same as in the previous GASM simulations. For the RF image reconstruction, no apodization has been used in reception. The number of scatterers used in simulation has been chosen in order to have a fully developed speckle in the fundamental but also in the second-harmonic images. This has been verified with the distribution of the B-mode images and the corresponding Rayleigh distributions.

Methods

The ECM cannot be directly applied on the B-mode image. The ultrasound image is composed of the speckle created by the scatterers inside the medium. This noise has a disastrous effect on the derivative term of the ECM if the method is directly applied.

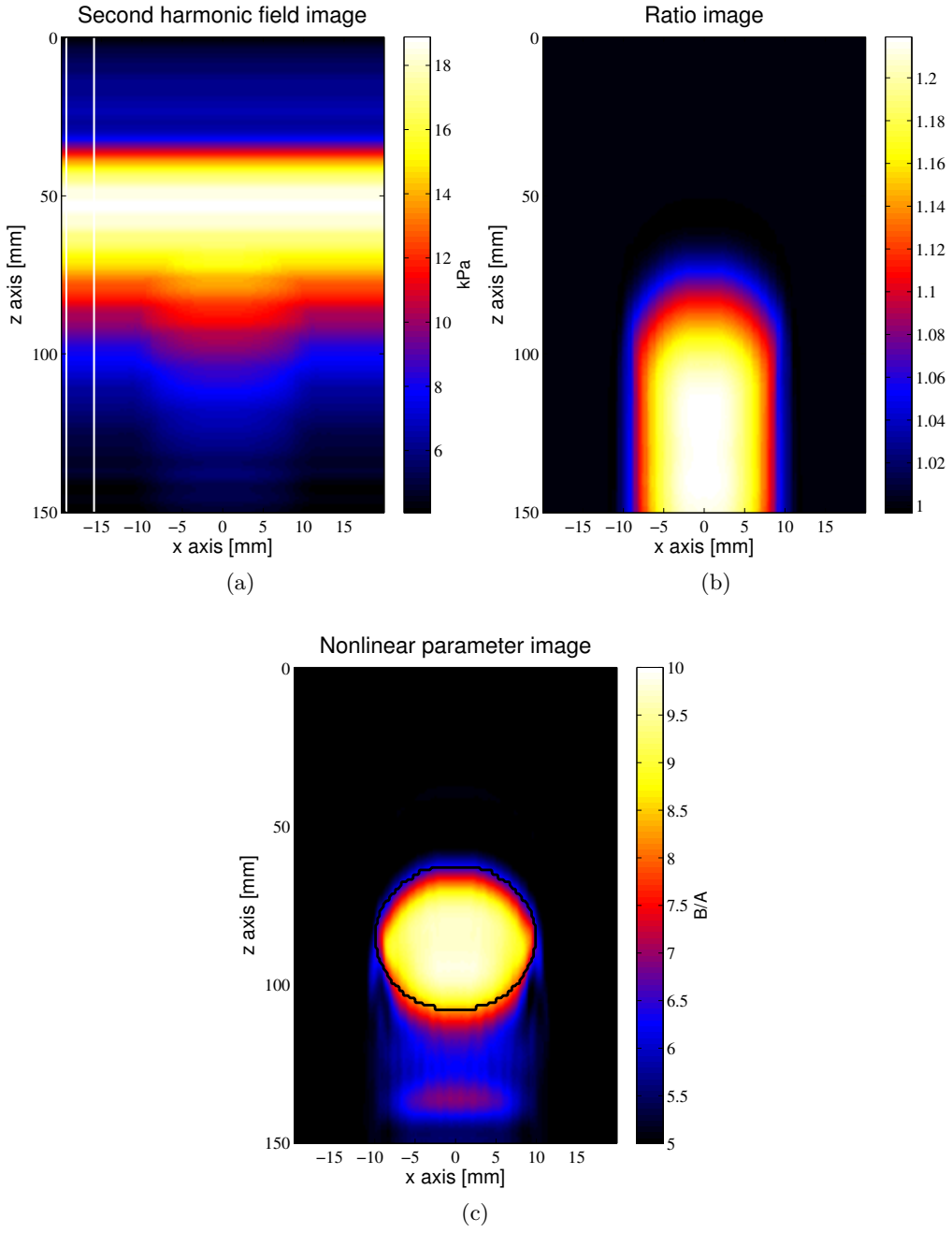

Figure 6.3: Resulting images obtained with the ECM method on the simulated media 1 (Fig. 6.2.a). (a) is the second-harmonic field image produced by GASM with the region between the two vertical lines considered as the reference medium p_{20}, (b) is the ratio image between p_{2i} and p_{20} and (c) is the final B/A images obtained with the ECM. The solid line in (c) outlines the inclusion searched.

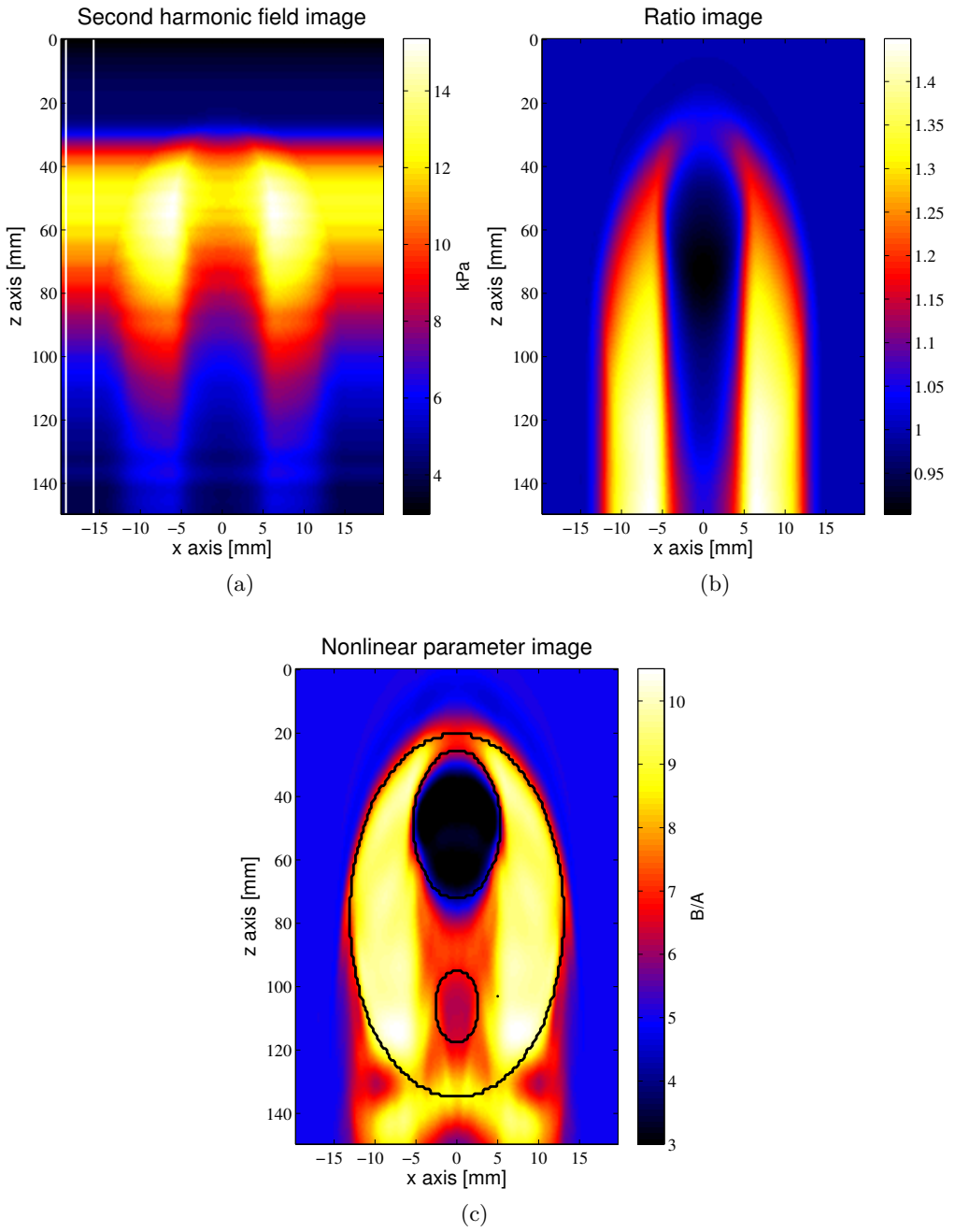

Figure 6.4: Resulting images obtained with the ECM method on the simulated media 2 (Fig. 6.2.b). (a) is the second-harmonic field image produced by GASM with the region between the two vertical lines considered as the reference medium p_{20}, (b) is the ratio image between p_{2i} and p_{20} and (c) is the final B/A images obtained with the ECM. In (a) the region between the two vertical lines is considered as the reference medium. The solid line in (c) outlines the different regions.

However, if from the B-mode image, it is possible to obtain an image similar to the second-harmonic field image, the ECM could be applied and the resulting estimation could be very promising in B/A imaging. The hypothesis made here is to consider that, with a fully developed speckle, the B-mode image is related to its pressure field if the effects of the scatterers are successfully suppressed. In this way, the scatterers' density, even if the medium is inhomogeneous, always produces a fully developed speckle.

Different strategies have been tested to extract, from the RF image, the more similar information corresponding to the second-harmonic pressure image. Indeed, the beamforming in reception creates a speckle that is not identical in the fundamental and second-harmonic field images and which can be seen as high frequency noise. To extract the evolution of the pressure along the propagation axis, different methods have been tested as:

- **Low-pass filtering**: low-pass filtering suppresses the speckle, which is a high-frequency information.
- **Frequency compounding**: by coupling different second-harmonic images, related to the same nonlinear medium, the signal-to-noise (SNR) is increased and the speckle impact is decreased.
- **Short mean filtering**: this filter decreases the impact of the speckle and smooths the speckle noise.
- **Alternating sequential filter**: this filter extracts the background of the image, related to the pressure field.

The first three approaches have been eliminated because they too much depend of the simulation parameters and the results are not stable for the different tested images. The chosen solution is based on an alternating sequential filter (ASF). This ASF has been introduced by [Sternberg (1986)] and [Serra (1988)]. This type of filters allows to progressively decrease the noise of an image and to estimate the initial signal [Couprie and Bertrand (2004)]. From the initial image I, a succession of opening γ_i and closing φ_i are conducted [Serra (1982)] with an increasing structuring element of dimension i. The resulting fundamental I^f_{1b} and second-harmonic I^f_{2b} filtered images after an ASF of dimension n can be mathematically defined as:

$$I^f_{1/2b} = \gamma_n \circ \varphi_n \circ ... \circ \gamma_2 \circ \varphi_2 \circ \gamma_1 \circ \varphi_1(I_{1/2b}) \tag{6.19}$$

where I_{1b} (I_{2b}) is the fundamental (second-harmonic) image. In fact, the ASF can be seen as a multiscale approach where each opening and closing work at a resolution i. With the increase of i, the resolution is progressively decrease but the previous operations are still taken into account. The ASF are suited to extract background information. For examples, [Decencière and Jeulin (2001)] used the ASF to suppress the high frequency noise created on engine cylinder and [Mura *et al.* (2010)] used it to simplify an image.

However, depending on the scatterer's distribution, the filtered image can contain some high or low intensity area. In the design of CREANUIS, the fundamental image did not depend on the nonlinear parameter map used in input. The resulting variation in the filtered fundamental image are related to the scatterer's distribution. These variations, also present in the second-harmonic image, are suppressed by doing a normalization of the second-harmonic image by the fundamental one. The normalization is made pixel by pixel. To ensure the reduction of entire high frequency information, a low pass filtering (lpf) is applied on the normalized image before to obtain the final filtered second-harmonic image I_2^f. This image did no more depend of the scatterer's distribution and can be expressed as:

$$I_2^f = lpf(\frac{I_{2b}^f}{I_{1b}^f}) \tag{6.20}$$

This final second-harmonic image is used to compute the ratio image and then the nonlinear parameter image. In this image, the possible high frequency variations have been removed in order to be able to compute a reasonable derivative term in the ECM. The resolution of the method, because of the smoothing operated by the different filters, has been decreased. The results obtained with such methodology are presented hereafter.

6.4.2 Evaluation of the ECM on homogeneous scattering medium

Medium characteristics

First, the method is estimated on a medium defined with an homogeneous distribution of scatterers. 600 000 scatterers are randomly defined in space (13 scatterers/mm^3) and amplitude. The resulting B-mode images for the fundamental and second-harmonic of the two previously presented nonlinear media are displayed in Fig. 6.5.

Results

The proposed method is used on the previously displayed B-mode images. For the nonlinear medium 1, the resulting images are presented in Fig. 6.6 and in Fig. 6.7 for the nonlinear medium 2.

The resulting images presented improvements and drawbacks compare to initial RF images. Indeed, even if the initial B/A image is not accurately obtained, the resulting images highlight areas that were completely hide in the classical B-mode images for the fundamental and the second-harmonic image (Fig. 6.5). With homogeneous media, the ratio between the two filtered images is not very useful because the second-harmonic directly contains the variation due to the nonlinear parameter but did not change the estimated B/A parameter. A statistical estimation of the nonlinear values measure on the different regions is proposed in the Table 6.2.

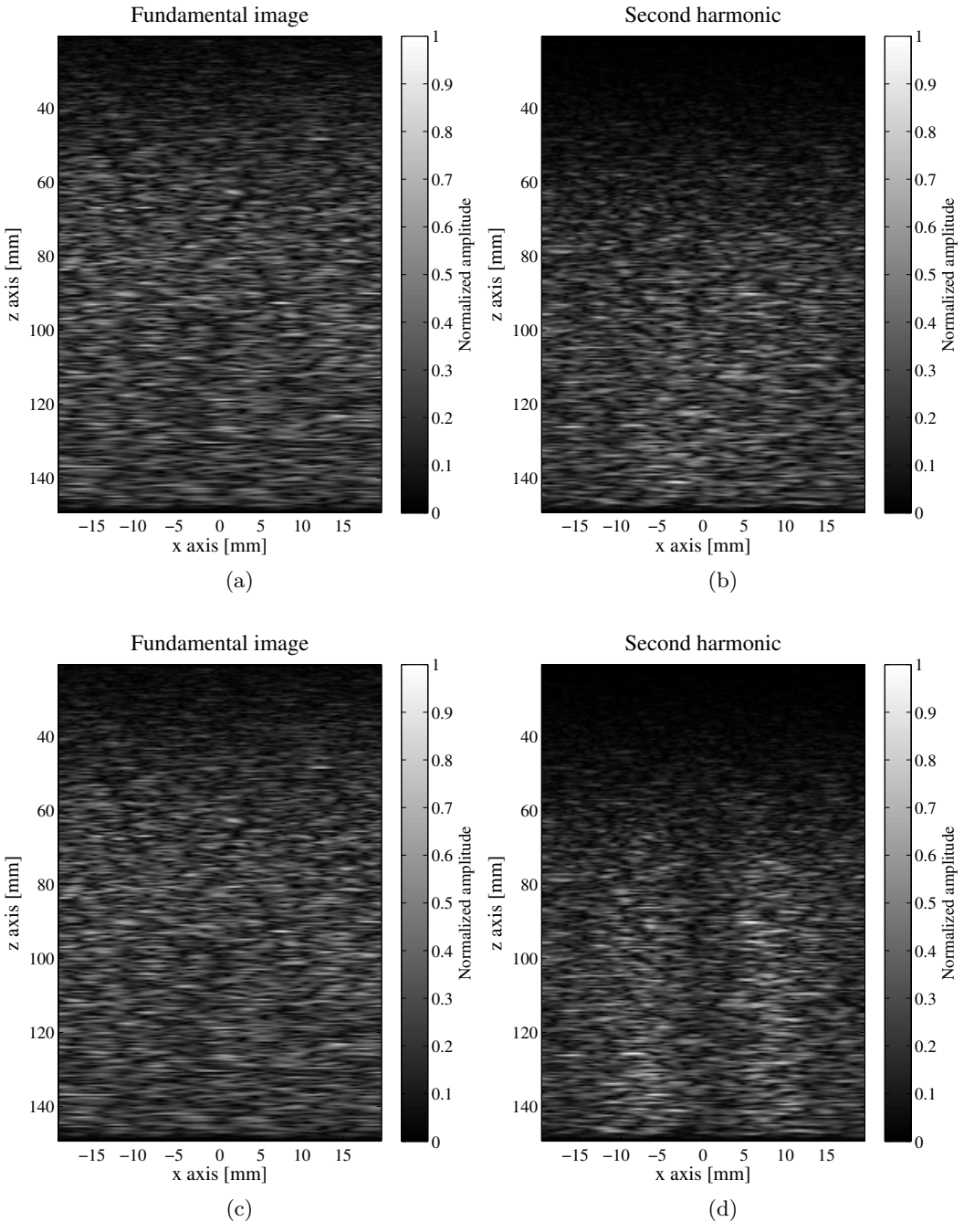

Figure 6.5: Resulting fundamental (a, c) and second-harmonic (b, d) B-mode images obtained on two different nonlinear media using CREANUIS and an homogeneous scatterer's distribution. The images (a) and (b) are obtained with nonlinear medium 1 (Fig. 6.2.a) and the images (c) and (d) are obtained with nonlinear medium 2 (Fig. 6.2.b).

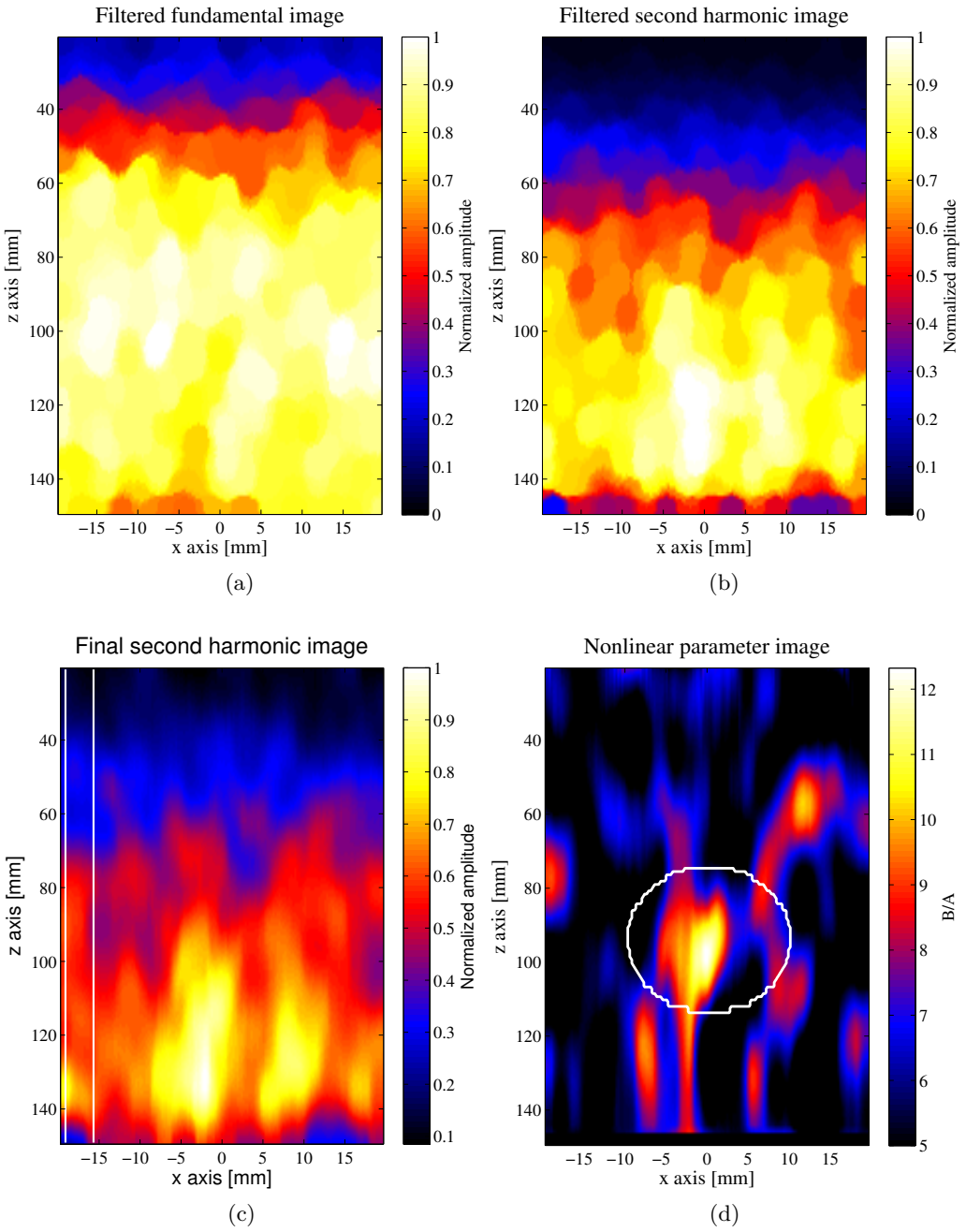

Figure 6.6: Resulting intermediate and final images obtained with the ECM. (a) is the filtered fundamental image, (b) is the second-harmonic filtered image, (c) is the final second-harmonic image (where the scatterer's effects are suppressed) and (d) is the resulting B/A image. In (c) the region between the two vertical lines is considered as the reference medium. The solid line in (d) outlines the inclusion.

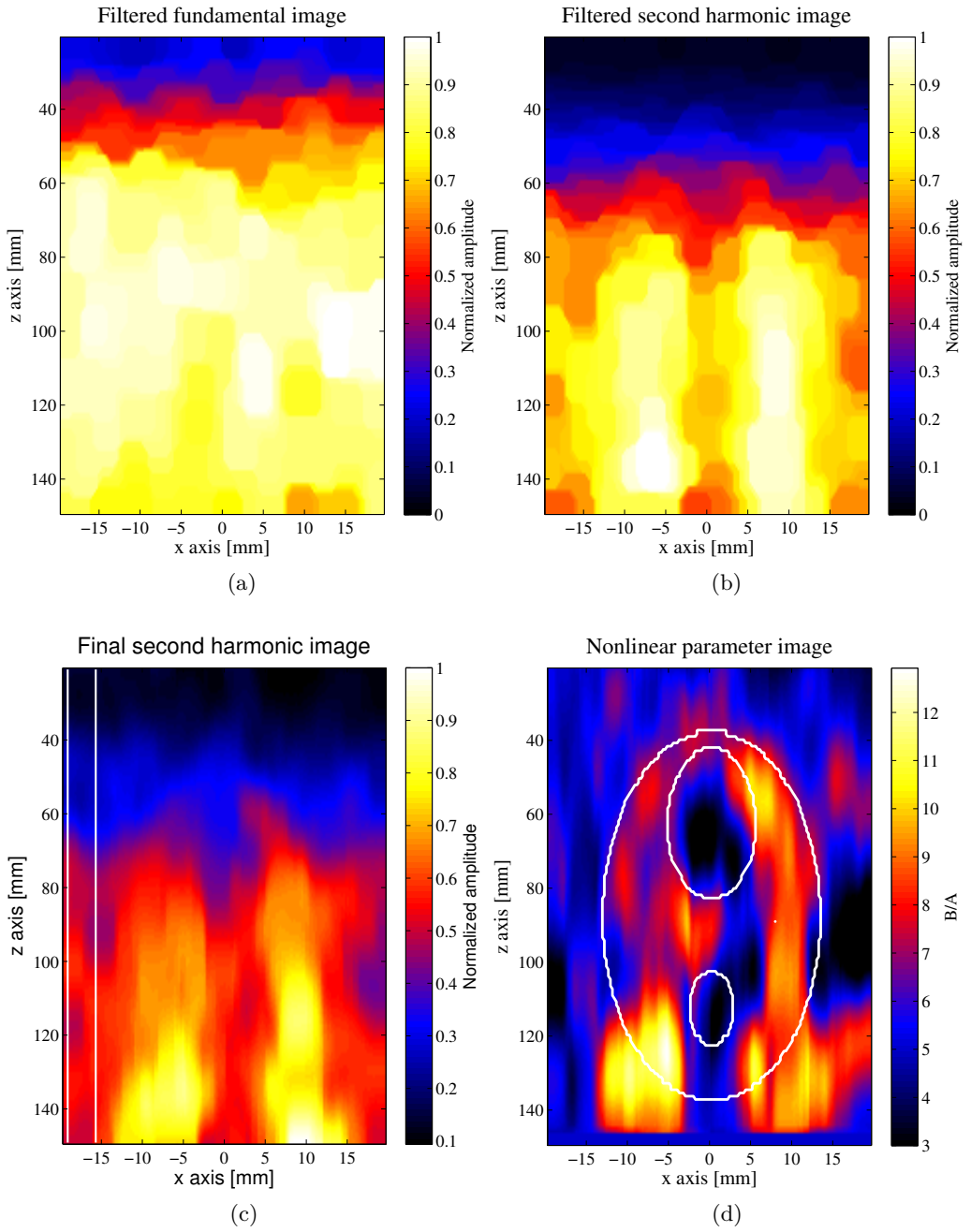

Figure 6.7: Resulting intermediate and final images obtained with the ECM. (a) is the filtered fundamental image, (b) is the second-harmonic filtered image, (c) is the final second-harmonic image (where the scatterer's effects are suppressed) and (d) is the resulting B/A image. In (c) the region between the two vertical lines is considered as the reference medium. The solid line in (d) outlines the different regions.

Medium	Set B/A	Mean value of estimated B/A	Standard deviation of estimated B/A
Medium 1	5	5.48	1.36
(Fig. 6.2.a)	10	7.96	2.01
	3	5.20	1.77
Medium 2	5	5.94	1.84
(Fig. 6.2.b)	7	4.44	1.21
	9	7.33	1.74

Table 6.2: Evaluation of the estimated nonlinear parameter with CREANUIS simulation and homogeneous scattering medium.

6.4.3 Evaluation of the ECM on inhomogeneous scattering medium

Medium characteristics

Now, an inhomogeneous scatterer's distribution is used. Indeed, in addition to the randomly distribute 600 000 scatterers, 300 000 reflectors have been added in the negative x axis to increase the response of this part of the tissue. The amplitude of each scatterer is still randomly chosen. Now, 900 000 scatterers are used in the CREANUIS simulation. It corresponds to a density of 26 scatterers/mm^3 in the negative x-axis and a 13 scatterers/mm^3 for the rest of the space. The resulting B-mode images for the fundamental and second-harmonic image of the two previously presented nonlinear media are displayed in Fig. 6.8. Now, in the left part of the fundamental and second-harmonic images, the signal backscattered by the tissue is higher due to the increase of the scatterer's density. However, the nonlinear parameter has not change.

Results

Before, the estimation of the nonlinear parameter is conducted on previously presented images. For the nonlinear medium 1, the resulting images are presented in Fig. 6.9 and in Fig. 6.10 for the nonlinear medium 2.

Contrary to the homogeneous case, the ratio between the second-harmonic and the fundamental images is crucial to suppress the scatterer's effect in the final second-harmonic image and the resulting B/A images are not very different from the one obtained in the homogeneous case. The proposed method appears to be effective to estimate the nonlinear parameter on arbitrary medium with the use of the fundamental and the second-harmonic images. A statistical estimation of the nonlinear values measure on the different regions is proposed in the Table 6.3.

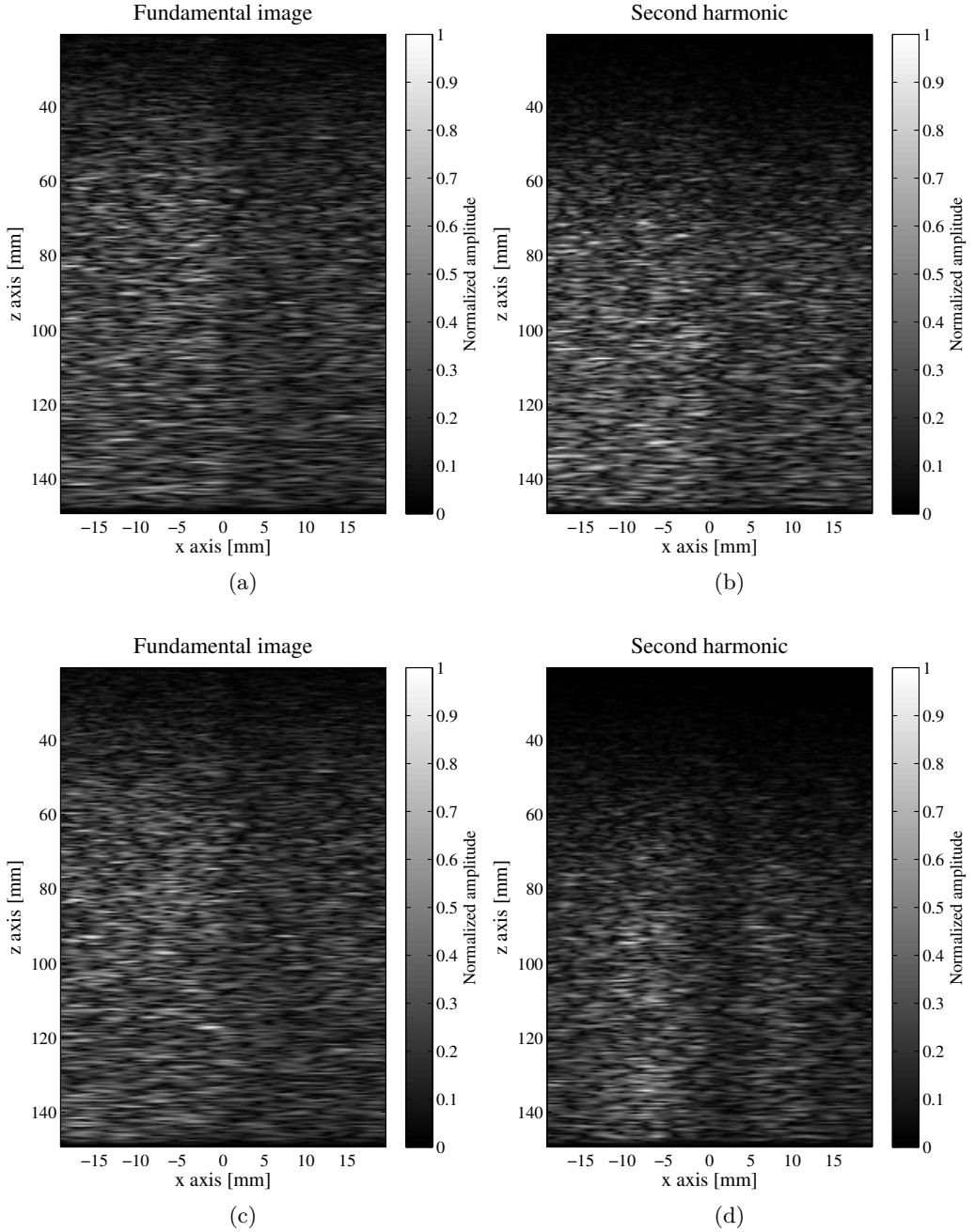

Figure 6.8: Resulting fundamental (a, c) and second-harmonic (b, d) B-mode images obtained on two different nonlinear media using CREANUIS and an inhomogeneous scatterer's distribution. The images (a) and (b) are obtained with nonlinear medium 1 (Fig. 6.2.a) and the images (c) and (d) are obtained with nonlinear medium 2 (Fig. 6.2.b).

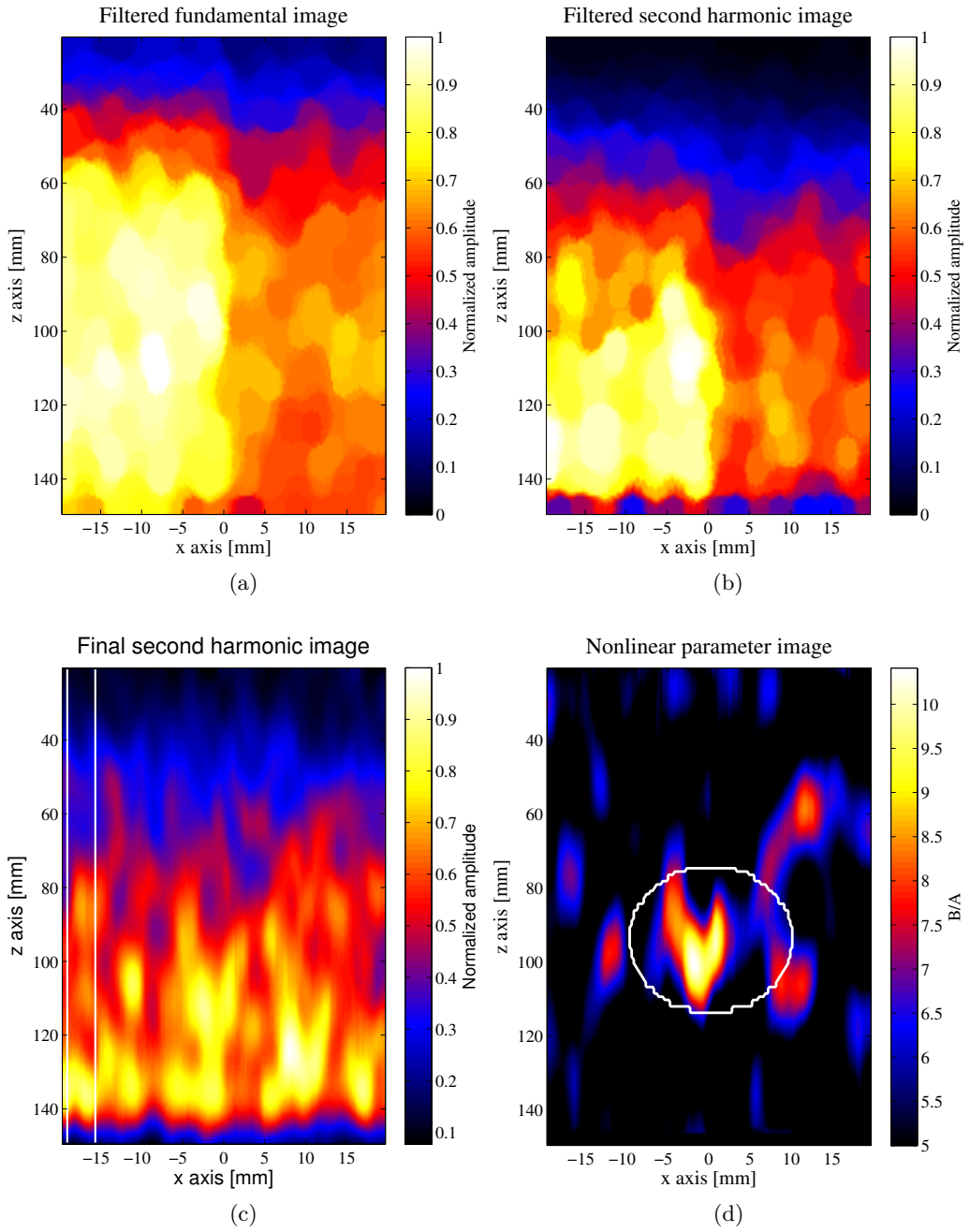

Figure 6.9: Resulting intermediate and final images obtained with the ECM. (a) is the filtered fundamental image, (b) is the second-harmonic filtered image, (c) is the final second-harmonic image (where the scatterer's effects are suppressed) and (d) is the resulting B/A image. In (c) the region between the two vertical lines is considered as the reference medium. The solid line in (d) outlines the inclusion.

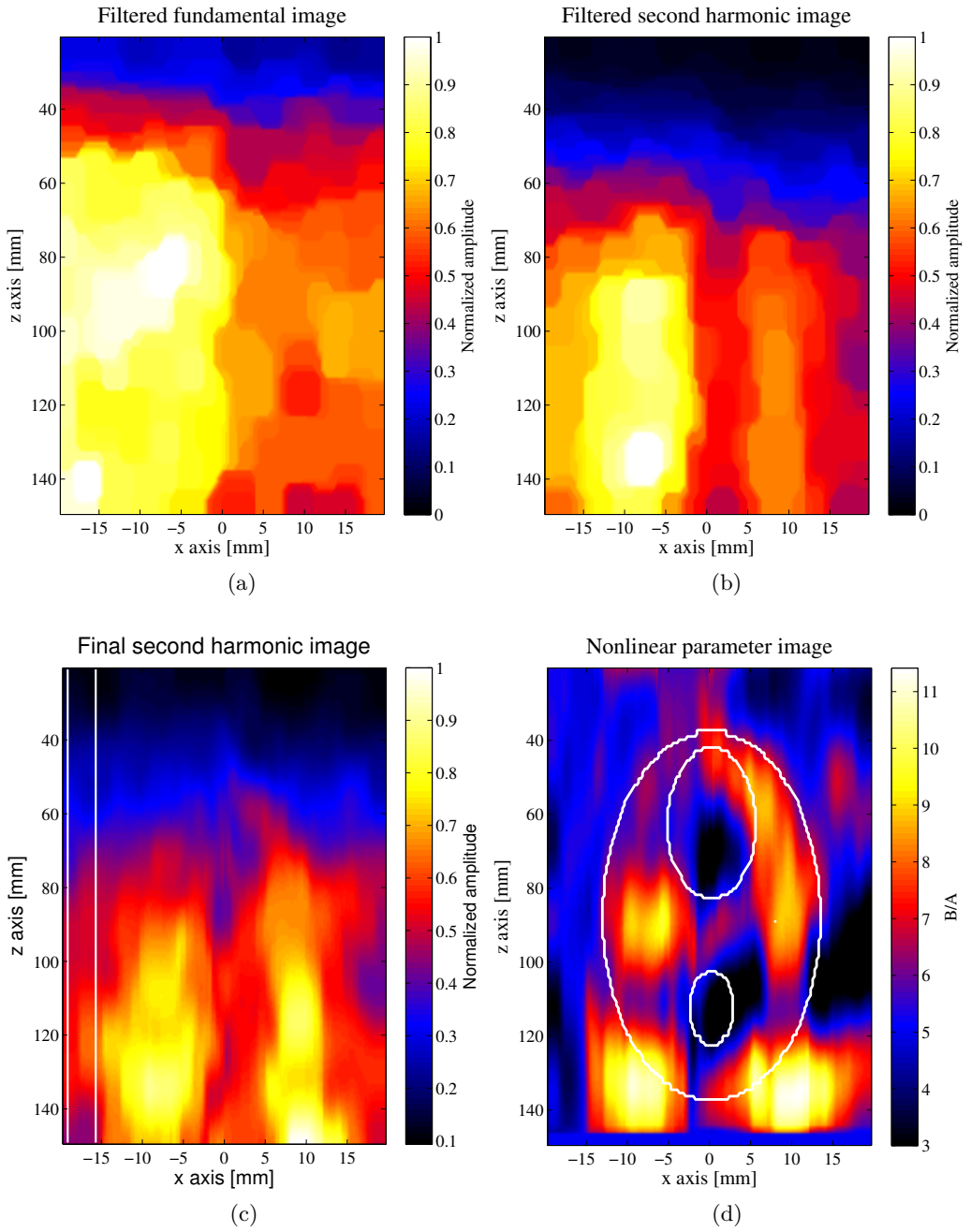

Figure 6.10: Resulting intermediate and final images obtained with the ECM. (a) is the filtered fundamental image, (b) is the second-harmonic filtered image, (c) is the final second-harmonic image (where the scatterer's effects are suppressed) and (d) is the resulting B/A image. In (c) the region between the two vertical lines is considered as the reference medium. The solid line in (d) outlines the different regions.

Medium	Set B/A	Mean value of estimated B/A	Standard deviation of estimated B/A
Medium 1	5	4.68	0.99
(Fig. 6.2.a)	10	6.48	1.44
	3	5.27	1.49
Medium 2	5	5.74	1.87
(Fig. 6.2.b)	7	3.24	1.01
	9	6.69	1.47

Table 6.3: Evaluation of the estimated nonlinear parameter with CREANUIS simulation and inhomogeneous scattering medium.

6.5 Discussion and conclusion

In conclusion, the different proposed extensions work nicely if the diffraction effect of the probe is neglected. With clinical imaging probes, this effect is no more negligeable and only the ECM is able to detect the different nonlinear media. However, the method is not able to follow multiple changes in the nonlinear parameter. Using the GASM simulator, the second-harmonic field images of two complex nonlinear media have been simulated. The ECM is able to detect the different nonlinear regions. However, an effect similar to the shadow cone in ultrasound images has been observed.

With CREANUIS, it is now possible to simulate the RF images of an inhomogeneous nonlinear parameter medium. This tool allows to test the ECM on realistic ultrasound images. To take into account the density and the echogenicity of tissues, a ASF is used before the calculus of the ratio image. With such a methodology, the B/A estimation did no more depend on the simulated medium and the obtained map shows similarity with the initial nonlinear parameter set in simulation. Even if the accuracy of the method is relatively weak, this new imaging technique allows to highlight some nonlinear behavior not visible on the initial second-harmonic image.

The drawback of the ASF is classical in morphological operations. With the used of the ASF, the structuring element is presented in the fundamental and second-harmonic filtering image. On the initial ratio image, it creates a new high frequency noise due to the border of the structuring element. However, this effect is suppressed by the low-pass filter and the obtained ratio images show similarity with the ratio image obtained with the GASM simulations.

Finally, the ECM proposes new type of images and needs to be tested on experimental images in order to validate or not its results. This is conducted in the next chapter.

Chapter 7

Nonlinear parameter imaging in experimental data

This chapter is devoted to the estimation of the nonlinear parameter in biological tissues. Indeed, in the previous chapter, the comparative method has been extended and a complete algorithm has been developed to image the nonlinear parameter. It has been evaluated in simulations and its estimation on experimental phantoms and on *ex-vivo* media are described hereafter. This work has been partly presented in [Varray *et al.* (2011)a].

7.1 Introduction

The ECM is able to image the different nonlinear behavior of a given medium. However, some shadow effects are present in the B/A estimation in the simulated images and this effect degrades the measure and the resulting images obtained in chapter 6 cannot be directly compared to the reference images. However, they exhibit some strong similarities with the reference B/A images. The method appears to be very attractive to produce an original image which is completely different from the initial second-harmonic image and carry a completely new information.

The objective of this chapter is to test the B/A imaging thanks to the ECM on experimental images. However, no calibrated phantoms exist to have a reference for the B/A imaging. The lack of reference makes difficult the estimation of the accuracy and the results of the ECM. However, in medium including contrast agent, the nonlinear parameter has a strong value compared to surrounding medium [Wu and Tong (1998)]. The ECM may

easily detect this region. In this chapter, two types of measurements are conducted. First, the nonlinear parameter of some tissue-mimicking phantom are done. An elastography and agar phantoms are used. Second, the nonlinear parameter imaging is conducted on *ex-vivo* pork's liver when a high intensity focalized ultrasound (HIFU) therapy technique is applied. These different experimental set-ups and measures are described hereafter.

7.2 Phantoms measurements

7.2.1 Materials and methods

Elastography phantom

A commercial phantom (CIRS, Breast Elastography Model 059) has been used. It is composed of several inclusions in a surrounding medium. The acoustic characteristics of these two media are the same (density, celerity and attenuation). Only the Young modulus of each medium is different. The nonlinear coefficient of the two media are not provided by the manufacturer as the echogeneicity. A schematic view of the phantom is proposed in Fig 7.1.a.

Agar phantom

A second phantom has been built. A block of agar gel was made with an empty cylindrical cavity (7 mm of diameter) inside. The initial concentration of agar powder was 5%. Then, Levovist® contrast agent was injected into this cavity. The initial dilution of the contrast agent was 250 mg/ml. Then, 1 ml of the solution was injected in 250 ml of water. A schematic view of the phantom is proposed in Fig 7.1.b.

Acquisition

Experimental RF echo-signals have been acquired with the ULA-OP scanner (Appendix A.1). A total of 192 lines were obtained. The transmitted signal was a 3-cycle sine at 5 MHz focalized at 30 mm. No apodization have been used in transmission. Then, the ECM, as described in chapter 6, has been applied on the resulting RF lines.

7.2.2 Results

The resulting images obtained on the experimental RF echo-signals are proposed in Fig 7.2 for the elastography phantom and in Fig 7.3 for the contrast agent one. Because the nonlinear parameter of each media is unknown, no quantitative results can be given and only qualitative results can be developed. However, the contrast agent must have a high nonlinear parameter compared to the agar phantom [Wu and Tong (1998)]. With the ECM, the inclusion and the cavity of the two different media are highlighted. It can also be observed that the near- and far-fields have been improved by removing the focalization effect thanks to the ratio image. The colorbar proposed in the nonlinear parameter image

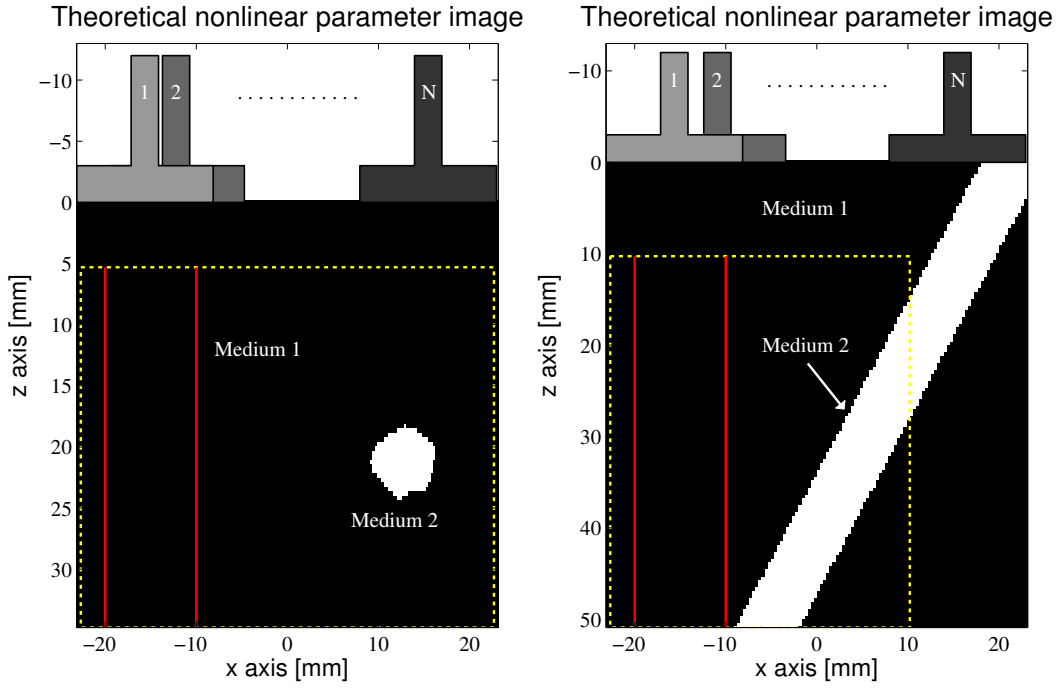

(a) (b)

Figure 7.1: Schematic view of the two used phantom: (a) is the elastography one and (b) is the one with the contrast agent. The region between the two vertical lines (red) is considered as the reference medium for the ECM and the dashed box (yellow) displays the region of interest where the nonlinear coefficient is computed.

(Fig 7.2.c and Fig 7.3.c) was set using the nonlinear parameter of water as reference ($B/A = 5$).

7.2.3 Discussion

In both experimental cases, to create the nonlinear parameter image, the acoustic parameters of the medium (density, speed of sound and attenuation) were considered identical in the two media (the reference medium and the unknown medium). For the elastography phantom, this approximation is correct and no error is added in the nonlinear coefficient image. For the contrast agent image, this assumption is not totally valid. Indeed, the attenuation of the contrast agent is larger than the attenuation of the agar phantom, but the propagation distance inside the contrast agent is very short. The interface between the upper side of the cavity and the agar medium creates known artifacts: bubbles are trapped near the interface and create strong backscattering. These regions should not be considered because the nonlinearity usually did not come from the nonlinear propagation but from the scattering effects. In terms of nonlinearity, the nonlinear parameter of agar is $B/A = 4.96$ [Preobrazhensky *et al.* (2009)] and for Levovist®, [Wu and Tong (1998)] estimated the nonlinear coefficient at $B/A = 132$ for a concentration of 1.2 mg/ml. In our experiment, the concentration of Levovist® was 1 mg/ml. By interpolating these results, the nonlinear parameter B/A of our contrast agent is in the range $[80, 120]$. This estimation is valid when the fundamental frequency is near the resonance frequency of the contrast agent. However, our transmitted frequency was higher than the resonance frequency, so the nonlinear coefficient of the contrast agent may be lower. The attenuation of the contrast agent at fundamental and second-harmonic frequency is in the range 2.2 dB/cm to 8 dB/cm. The attenuation in contrast agent is no more linear with the frequency. This effect provides another underestimation of the nonlinear parameter. Our final estimation of the contrast agent, even if the numerical value did not correspond to the reality, give a first idea of the difference between the phantom and the contrast agent.

7.3 *Ex-vivo* measurements

7.3.1 Materials and methods

A second type of experiments has been conducted on *ex-vivo* pork's liver. The local estimation of nonlinear propagation could be of interest associated to HIFU treatment, because there is no method to accurately estimate the HIFU lesions.

The estimation of the nonlinear parameter is conducted on different degassed pork's liver. The experimental set-up contains the HIFU probe and the imaging probe of an Ultrasonix Sonix RP scanner. The imaging probe is the L14-5W-60 which is a linear array with a central frequency at 6.6 MHz. The experimental set-up is displayed in Fig. 7.4. Because the liver size is limited, the image obtained with the Sonix RP is larger than the

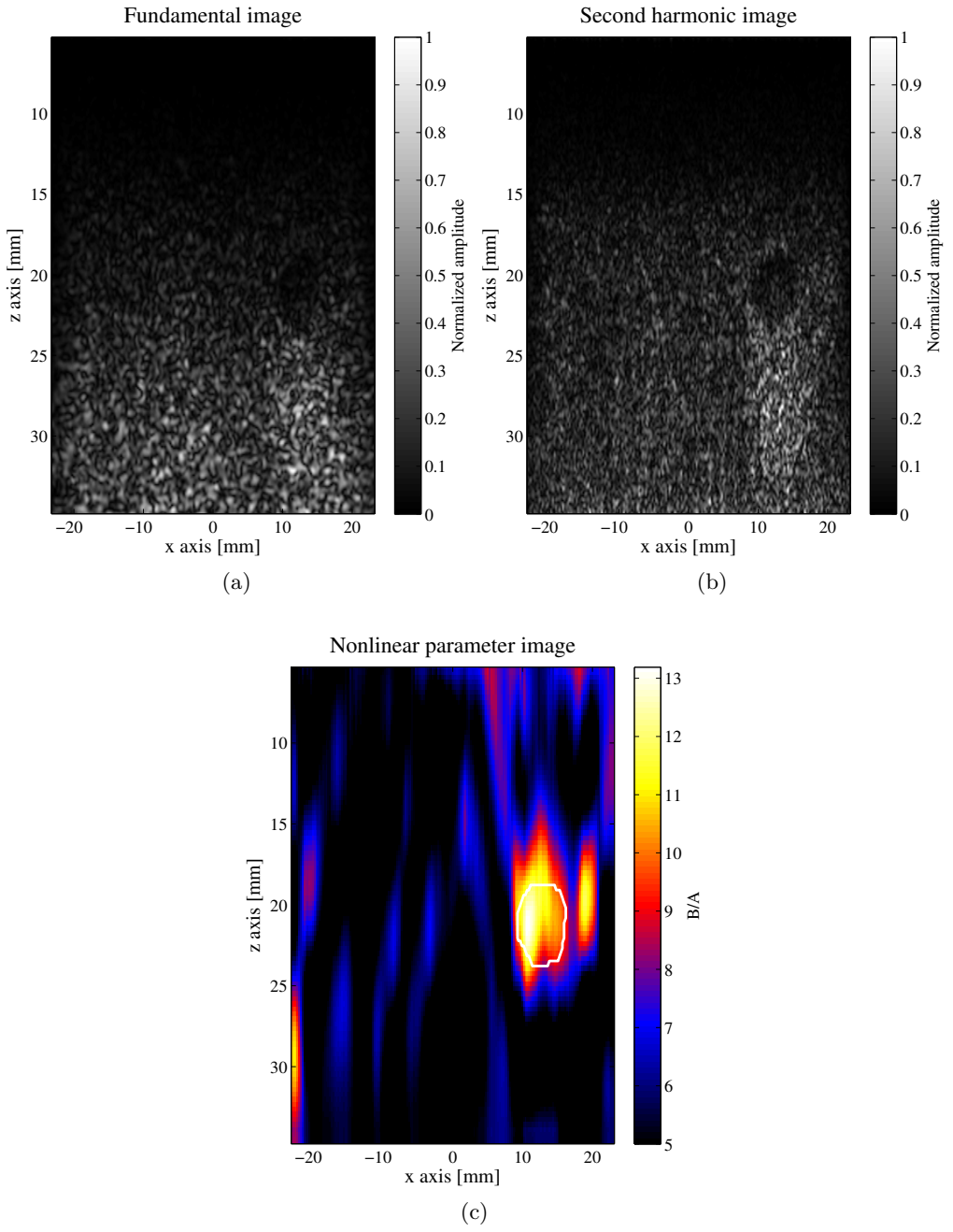

Figure 7.2: Resulting intermediate and final images obtained with the ECM. (a) is the fundamental image, (b) is the second-harmonic image, and (c) is the resulting B/A image. The solid line in (c) outlines the inclusion.

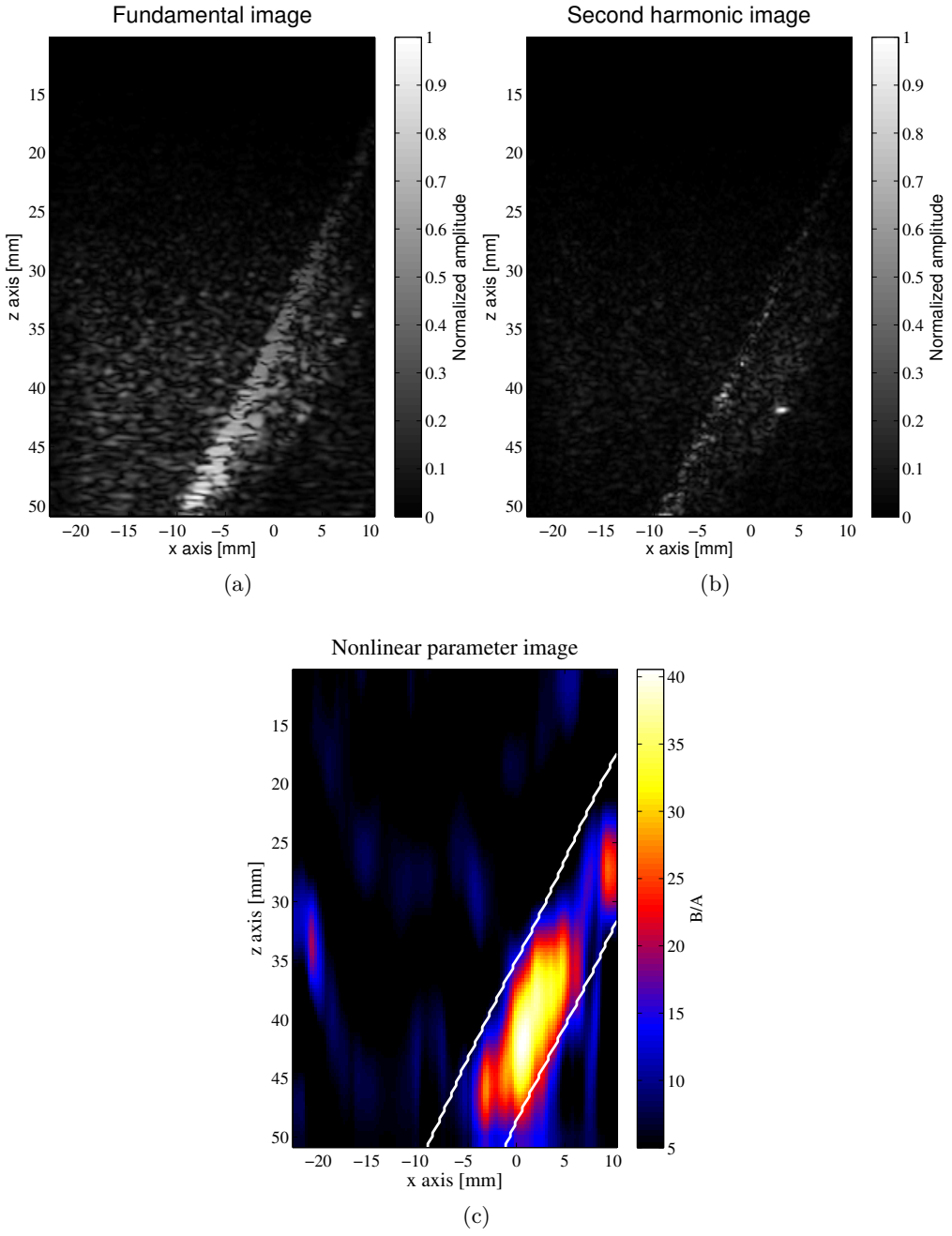

Figure 7.3: Resulting intermediate and final images obtained with the ECM. (a) is the fundamental image, (b) is the second-harmonic image, and (c) is the resulting B/A image. The two lines in (c) delimitate the contrast agent.

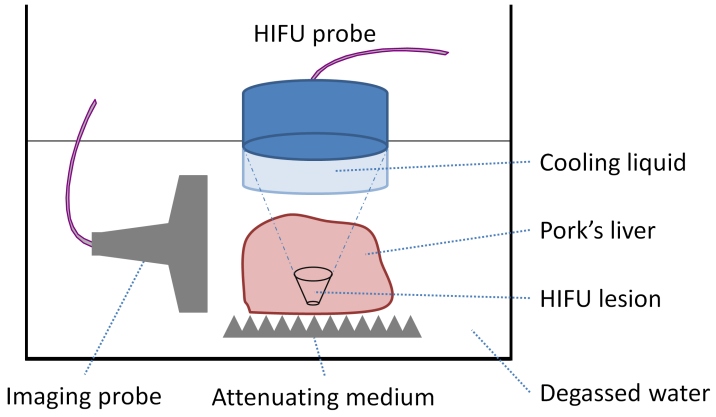

Figure 7.4: Experimental scheme coupling the HIFU probe and the imaging one. The attenuating medium is placed to avoid the propagation of the HIFU in the water tank.

liver dimension. The region of interest, where liver is present, is chosen before to estimate the nonlinear parameter.

The HIFU therapy sequence repeats 40 times a HIFU shoot of 1 second. Between each HIFU shoot, a pause of 100 ms is made. During this interval, the imaging system is able to make about 3 or 4 images in function of the beamforming. Because of the high acoustic level transmitted by the HIFU probe, only one or two images acquired during the pause are readable for processing. Indeed, no synchronization are made between the Sonix RP and the HIFU probe, and the HIFU sequence can stop and/or begin during the acquisition of an image. After the HIFU application, the liver is cut in the imaging plane to compare the acquired images and the lesion obtained. The intensity of the HIFU sequence is adapted in function of the desired lesion and its dimensions.

7.3.2 Results

The estimation of the nonlinear parameter has been computed at three different times:

- Before the HIFU application: this acquisition is considered as the reference compared to the next one.
- During the HIFU application: this acquisition is made after 20 shoots of the HIFU pulse. Practically, it is acquired 22 seconds after the first shoot. This image is used to observe the evolution of the medium.
- After the HIFU application: this acquisition is made after the 40 shoots of HIFU application, when the liver is cold down (around 1 minute after the last HIFU shoot). This image relates the final aspect of the liver.

From the three acquired images, the nonlinear coefficient is estimated on each of them. Because no strong variation is clearly visible between them, the difference between the nonlinear images made during or after the HIFU ablation with the one made before is exploited. The resulting images obtained are presented in Fig. 7.5. In the HIFU lesion, a change in the nonlinear parameter can be observed (Fig. 7.1.d). However, the contour of the treated region is not clear.

7.3.3 Discussion

The ECM imaging brings new information on the acquired images. Indeed, the nonlinear parameter images obtained before and after HIFU ablation show significant differences. The ECM has a good potential for the characterization of HIFU treatments: initial results demonstrate the feasibility of this application. This information, combined with other methods such as elastography, could provide new parametric images that could help to characterize the HIFU lesion. In addition, ECM imaging can be a useful complement to conventional sonograms. Further investigation is required to determine the full potential of the ECM for visualizing and guiding HIFU therapies *in vivo* as well.

7.4 Discussion and conclusion

After its validation in simulation, the ECM has been tested on experimental images. First, two phantoms have been used. A commercial phantom has been first evaluated. Then, an agar phantom containing contrast agents has been used. The evaluation of the nonlinear parameter highlights the two media in the elastography phantom and the contrast agents in the second phantom. Even if no quantitative value can currently be computed with the method, the ECM emphasizes structures that are not visible in the initial fundamental and second-harmonic images.

A second type of measurement has been conducted. In HIFU therapy, the quantification of the lesion is very important to control the treatment given to the patient. The ECM has been applied at different moment of the treatment and the obtained nonlinear maps have been compared to the one made before the treatment. An evolution of the nonlinear parameter has been highlighted in the lesion and the ECM appears to be a new strategy that can provide new tissue characterization information.

The principal drawback of the ECM comes from its resolution. Indeed, with the different filters used in the ECM (ASF and low-pass filter), it is difficult to estimate the resolution of the ECM. The lack of reference phantoms also complicates the evaluation of the method. Because of the derivative term in the ECM, it was necessary to limit the possible variation of the ratio image. However, this limitation curbs the possibility to detect little change in the nonlinear parameter. A compromise has to be found in order to control the ratio image and the resolution of the method.

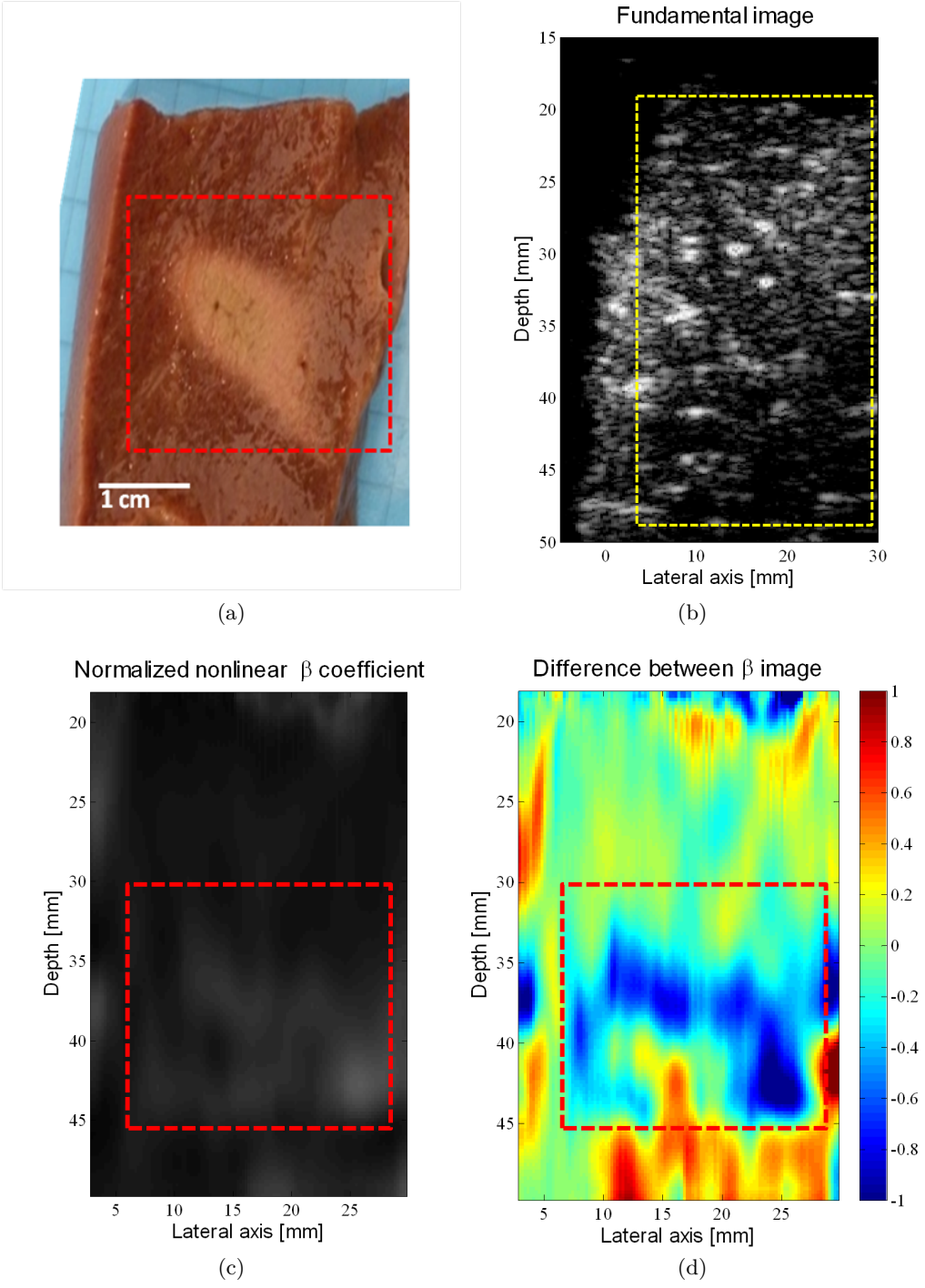

Figure 7.5: Evaluation of the nonlinear parameter in porcine liver. (a) is the histological picture of the liver in the imaging plane, (b) is the B-mode image of the porcine liver, (c) is the B/A image of the liver after HIFU ablation and (d) is the difference image of the nonlinear parameter after and before HIFU ablation. The box in (a) is the region of interest where the nonlinear parameter is computed. The box in (b-d) highlights the region of the HIFU ablation.

Conclusions and perspectives

Conclusions

In the different sections of this thesis, significant improvements of existing techniques have been demonstrated. First, the GASM has been presented. This simulator, based on an angular method and the quasi-linear approximation is faster than classical finite difference KZK simulation. The new mathematical background is valid for inhomogeneous nonlinear parameter media. This consideration, not present in the literature, allows to simulate completely arbitrary nonlinear media with inclusions such as contrast agent or tumoral tissues. The estimation of the accuracy of the GASM has been conducted by comparing the obtained field with the one simulated with FieldII, the Voormolen simulator and an experimental measurements. The difference between them is weak and the GASM can be validly used in several applications. The angular spectrum strategy naturally reduces the computation time by decreasing the number of derivative terms in the propagation equation. However, the proposed mathematical background is particularly suited to GPU programming and the GASM has been implemented on CPUs and GPUs. The total computation time has been strongly reduced, especially using the GPU programming. This simulator opens new opportunities to quickly simulate the nonlinear propagation in arbitrary nonlinear media.

Second, the CREANUIS software has been presented. This software allows to simulate the radio-frequency images that contain fundamental as well as second harmonic information. To simulate these images, two strategies have to be coupled: the nonlinear ultrasound field and the backscattering behavior of the medium. The nonlinear ultrasound field is estimated using the previously presented GASM simulator. Using GASM, the fundamental but also the second harmonic component are computed. Then a similar approach as the one proposed in FieldII [Jensen (1996)] has been used to create the final radio frequency image. Each scatterer backscatters an echo whose amplitude depends on its position, the attenuation, the pressure amplitude, etc. Thanks to the GASM background, arbitrary nonlinear media can be simulated with CREANUIS. The resulting fundamental images obtained with CREANUIS are close to the ones obtained with FieldII, the reference linear radio-frequency images simulator. Moreover, this software opens new opportunities in nonlinear imaging simulation such as the amplitude modulation or pulse inversion [Eckersley

et al. (2005)].

Then, the measure of the nonlinear parameter has been conducted. From the initial set of existing methods of the literature, the ones suitable to the echo mode configuration have been selected and extended to follow the possible inhomogeneity of the nonlinear parameter. The proposed extensions have been validated in simulation with the Voormolen simulator. Three methods can theoretically be used in echo mode configuration to measure the nonlinear parameter. However, these methods are valid with plane waves and only the extended comparative method (ECM) follows the variation of the nonlinear parameter and works with the consideration of the probe's diffraction. The ECM has then be evaluated using the nonlinear pressure field obtained with the GASM simulations and the nonlinear RF image obtained with the CREANUIS software. A modification has been added to take into account the scattering effect of the medium. Then, the ECM has been tested on experimental acquisitions. However, the lack of reference in term of nonlinear measurement and especially in echo mode did not allow to completely validate our proposed ECM. The first results of the B/A imaging on *in-vitro* liver tissue are interesting but more experiments are required.

Perspectives

The work of this thesis opens the following opportunities:

GASM. This simulator is currently valid for only the fundamental and second harmonic. Recent work proposed an extension and GPU implementation for the third harmonic [Varray *et al.* (2011)d]. A more general mathematical background has to be considered including nonlinear propagation of a higher number of harmonics. The calculation of a new component increases the total simulation time because its value is related to the previous computed one.

CREANUIS software. This software is currently valid for linear arrays. However, medical ultrasound is not only based on this type of probe. Extensions have to be proposed to take into account phased arrays or 3D arrays, and other ultrasound imaging opportunities. Currently, only the field propagation with GASM is computed on the graphic card. The radio frequency image reconstruction consists in repeating the same actions for each scatterer. This type of algorithm is particularly suitable for GPU implementation and a whole graphic version of CREANUIS could be implemented to continue decreasing the total simulation time. The diffusion of the software is also made under a CeCILL-B licence (Appendix C).

The B/A imaging. The proposed method leads to interesting results in simulations

and first experimental images are attractive. However, the resolution of such images is currently relatively poor and B/A cannot be used alone as a tissue characterization tool. Coupled with other imaging methods, such as elastography, new parametric images can be obtained and could help radiologists to establish a diagnosis. The proposed method is not only limited to 2D images and the ECM can be envisaged in 3D images.

Implementation of GPU in ultrasound applications. In GASM, the implementation on CPU and GPU allows to strongly decrease the computation time and new strategies of parameter optimization can be envisaged. In a more general way, the GPU programming is very interesting for intensive calculus at a reasonable price. Recent works have been published on the interest of the GPU for different ultrasound applications such as imaging [Chang *et al.* (2009)], 3D or 4D (3D+t) rendering [Elnokrashy *et al.* (2009),Kiss *et al.* (2010)] or intensive calculus such as block matching [Kiss *et al.* (2009)]. The use of GPUs for fast ultrasound simulation is also promising and paves the way for the investigation of new applications. For example, the so far prohibitively long parameter sweep that is needed for optimization purposes becomes possible. Pasovic et al. [Pasovic *et al.* (2010)] have recently discussed the advantages of limiting the level of second harmonics created during nonlinear propagation. In this technique, an optimal limitation can be achieved through a specific probe excitation, provided the amount of second harmonic is compensated for. A fast calculation of the second harmonic component, as it is possible with the GPUs, reveals the possibility of adapting the second harmonic reduction during clinical exams. Indeed, in these cases, the probe or the medium movements limit the resulting reduction. If fast simulations are possible, the optimization of the second harmonic reduction can be conducted concurrently with the exam in order to adapt the reduction in real time. From the hardware point of view, GPU programming is not limited to specific equipment, because each scanner owns its graphic card. All the methods or algorithms would theoretically be exportable to the different equipments.

cMUT array. The use of the capacitive micromachined ultrasonic transducer (CMUT) open new perspectives in nonlinear imaging [Mills and Smith (2003),Mills (2004)]. Indeed, the transmitted bandwidth of such array are upper than 100% and theoretically infinite in reception. With such technology, higher order harmonics can be received and the measure of the B/A or C/A parameter can be more accurate [Liu *et al.* (2007)]. New harmonics methods, as super harmonic imaging [Bouakaz *et al.* (2002)], would also be usable for *in-vivo* applications.

Appendix

Appendix A

Technical specification of different hardware equipments

A.1 ULA-OP

The Ultrasound advanced Open Platform (ULA-OP) is a research scanner develop by the group of Piero Tortoli *et al.* in Firenze [Tortoli *et al.* (2009)]. This scanner has the possibility to transmit and to receive an ultrasound wave with a completely personalized beamforming strategy. The RF or B-mode images can be recorded with the system. The scanner is directly configured and drive on a laptop and its simplicity is very useful for the different applications test in this PhD. An image of the system is presented in Fig. A.1.

A.2 Probe LA533

The LA533 probe has been design by Esaote (Genova, Italy). Its principal characteristics are presented in Table A.2.a and its bandwidth in Fig. A.2.b.

A.3 GPU specification

The technical specification of two GPUs are proposed in the Table A.1.

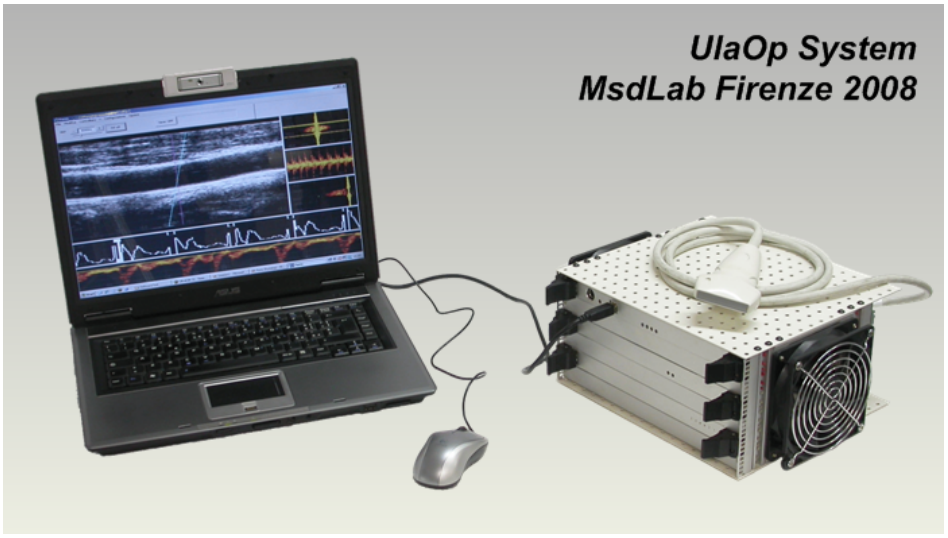

Figure A.1: ULA-OP system developed by the MSD laboratory. The dimension of the system make it easily portable and moveable for different acquisitions.

Parameter	Value
Pitch	245 μm
Kerf	30 μm
Height	6 mm
Elevation focus	23 mm
Active elements (maximum)	64
Total of elements (maximum)	192

(a)

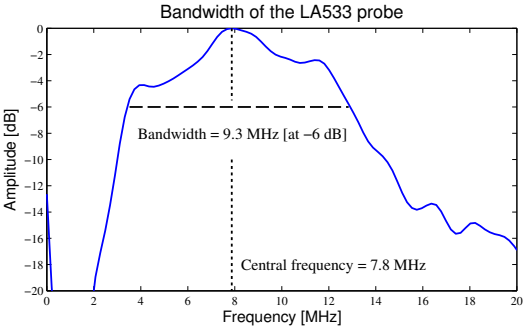

(b)

Figure A.2: Geometric parameter of the LA533 probe (a) and its bandwidth at -6dB (b).

		Machine 1	Machine 2
CPU	Name	Intel Core2 Duo T9400	Intel Xeon E5220
	Speed	2.53 GHz	2.27 GHz
	Memory	3.48 GB	5.9 GB
GPU	Name	Quadro NVS 160M	GTX 285
	Global memory	256 MB	1024 MB
	Number of multi-processors	1	30
	Total of cores	8	240
	CUDA capability	1.1	1.3

Table A.1: Specification of two different CPUs and GPUs of two computers. Machine 1 is a laptop computer and Machine 2 is a desktop one.

Appendix B

Variation of the constant in second-harmonic evaluation

The equation to solve is a classical oscillator system with a constant. Equation (3.21) is given by:

$$\frac{d^2g(z)}{dz^2} + K^2 g(z) = M(z) \tag{B.1}$$

To solve equation (B.1), the variation of the constant technique is needed. First, the two characteristic solutions of (B.1) are:

$$g_{1,2}(z) = e^{\pm iKz} \tag{B.2}$$

To obtain the final solution of (B.1), the constant value of g_1 and g_2 must be computed. To do this, the two functions $\lambda_1(z)$ and $\lambda_2(z)$ have to be calculated with:

$$\lambda_1'(z)g_1(z) + \lambda_2'(z)g_2(z) = 0 \tag{B.3}$$

The system to be solved is:

$$\begin{cases} \lambda_1(z)g_1(z) + \lambda_2(z)g_2(z) = g(z) \\ \lambda_1'(z)g_1(z) + \lambda_2'(z)g_2(z) = 0 \end{cases} \tag{B.4}$$

By deriving the first equation of (B.4) twice using the expression of g_1 and g_2, the system can be further developed:

$$\begin{cases} \lambda_1'(z)g_1(z) + \lambda_2'(z)g_2(z) = 0 \\ \lambda_1'(z)g_1'(z) + \lambda_2'(z)g_2'(z) = M(z) \end{cases} \tag{B.5}$$

Substitution of (B.2) in (B.5) leads to:

$$\begin{cases} \lambda_1'(z) = -\lambda_2'(z)e^{-2iKz} \\ \lambda_1'(z)(iK)e^{iKz} + \lambda_2'(z)(-iK)e^{-iKz} = M(z) \end{cases} \tag{B.6}$$

Then $\lambda_1'(z)$ and $\lambda_2'(z)$ can be extracted:

$$\begin{cases} \lambda_1'(z) = -\dfrac{iM(z)}{2K}e^{-iKz} \\ \lambda_2'(z) = \dfrac{iM(z)}{2K}e^{iKz} \end{cases} \tag{B.7}$$

The final solution of equation (B.1) is given by:

$$g(z) = \left(\int_{z_0}^{z} \lambda_1'(u)du\right) e^{iKz} + \left(\int_{z_0}^{z} \lambda_2'(u)du\right) e^{-iKz} \tag{B.8}$$

Appendix C

CREANUIS: software description

Download link: urlhttp://www.creatis.insa-lyon.fr/site/fr/CREANUIS

C.1 Introduction

C.1.1 General overview

CREANUIS is a tool that simulates nonlinear radio frequency (RF) ultrasound images. It is the combination of two specific tools. The former is a nonlinear ultrasound propagation simulator, that allows to compute the increase of the fundamental and second-harmonic wave [Varray *et al.* (2011)f]. Then, using this field information, a reconstruction algorithm creates the corresponding nonlinear radio frequency (RF) image [Varray *et al.* (2011)b]. The resulting RF image contains the fundamental evolution, but also the second harmonic one. The design of the nonlinear propagation simulator, which is a generalization of an angular spectrum method (GASM), allows to consider media with an inhomogeneous nonlinear coefficient and the simulated field will impact the final RF image simulation. An effort of the computation time has been done on the computation time of the nonlinear field with a version of the software working on GPU (graphic processing unit) [Varray *et al.* (2011)d].

C.1.2 Software description

CREANUIS has been design in C/C++ in order to quickly simulate the nonlinear propagation and the RF images. An interface is proposed in Qt[1], but can also be disabled. In the GASM simulation, the Fourier transform are performed using the FFTW library[2] [Frigo and Johnson (2005)], or the cuFFT library[3], when the GPU programming is used. Some accompanying files are proposed to load the simulated data with Matlab. The

[1] http://qt.nokia.com/products/
[2] http://www.fftw.org/
[3] http://developer.nvidia.com/cuda-downloads

structures of the saved data are detailed hereafter and the image can also be loaded with other programs as soon as an interpreter is designed.

C.2 Installation

C.2.1 Windows

On windows, two files are needed. First, the CREANUIS exe file has to be installed. Then, the vcredist_x86, if not present on the system, has also to be installed. During the installation of CREANUIS, the path of the installation has to be change **(do not used Program Files/ directory)** because last windows operating system forbids to write in this directory. The installation pastes in the output folder the different dll required by CREANUIS, the CREANUIS application, the accompanying Matlab files, and creates three directories (input/, nlrf_file/, pressure_field/).

C.2.2 Linux (Fedora) distribution

On Fedora distribution, the tar.gz file has just to be extracted. Then, the program can directly be used. The same directories as in the Windows installation are created.

C.2.3 Created folder

Three directories are created by the install files and are required in the same root direction. The input folder is used to save some user inputs. All the created nonlinear radio frequency (nlrf) images are saved in the nlrf_file folder. The field, nonlinear coefficient map and setting (if saved) are saved in the pressure_field folder.

C.3 Interface description

The CREANUIS interface is divided in three distinct thumbs coupled to some general settings.

C.3.1 General settings

In the general setting (Fig. C.1) the user can defined the path of the working directory of CREANUIS (G2). By default, this path is set to the directory where the CREANUIS exe file is located, with the addition of the directory pressure_field/a_default. This path can be change using the button G3. In the box G4, the name of the output file can be chose. If the file exists in the nlrf_file directory, it replaces the previous nlrf file. The G5 button launches the simulation. The box G6 corresponds to the debug level wanted. If 0 is chose, just some messages are displayed in the terminal. If 1 is selected, the debug messages corresponding to the RF image reconstruction are displayed. With 2, the messages of the GASM simulation are also displayed. In the G1 menu, the user can save or load settings in the action menu. The help menu displayed a link to the CREANUIS web site and the licence specification. The save/load actions save/load the data in the save_settings.txt file. This file is created/read in the path directory G2.

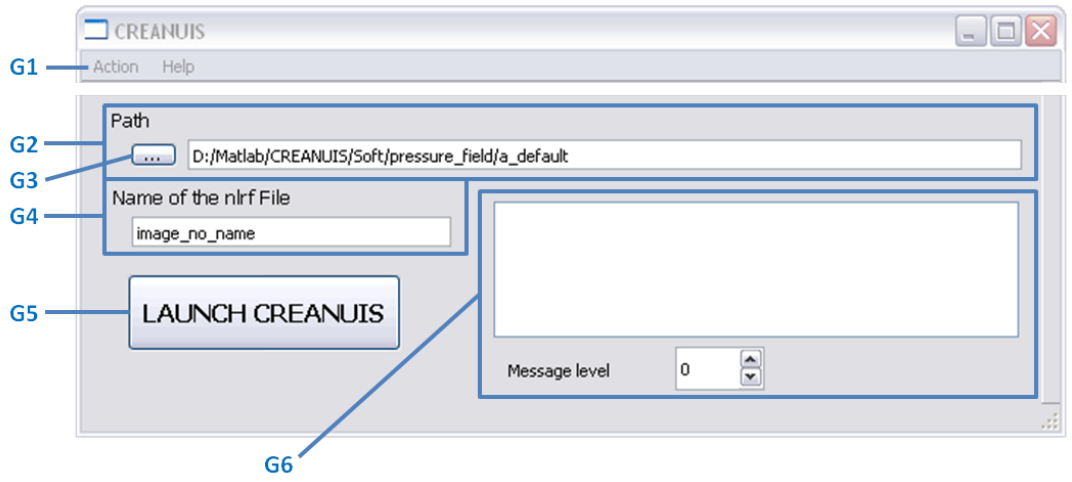

Figure C.1: Illustration of the general settings of the CREANUIS interface.

C.3.2 Probe, space and beamforming strategy

The first part of the interface (Fig. C.2) allows to specify the probe geometry (P), the medium characteristic (M) and the beamforming configuration (B). All these parameters are saved in the save_setting.txt file. In the beamforming, the user can save the pre-beamformed data. If yes, for each RF line, all the elementary receive RF lines on each active elements are saved. This must be done carefully because of the large size of the resulting nonlinear RF data.

Currently, only linear arrays are simulated with CREANUIS. In a future version of CREANUIS, more complex arrays are going to be taken into account. For the attenuation, a frequency dependent law has been chosen because the second harmonic wave is faster attenuated than the fundamental one [Szabo (1978)].

C.3.3 Scatterers and GASM configuration

In this second thumbs (Fig. C.3) the scatterers of the medium (S) and the nonlinear map (NL) are configured.

In the scatterers part (S), the dimensions of the space where the scatterers are placed are defined with the maximum lateral and elevation distance. In the z direction, the minimal and maximal depth to reach is selected. These depths are the one used in the final image creation. The density of reflectors, N, allows to quickly select the number of scatterer per resolution cell. However, in some case, this number is directly the number of scatterers in the medium. For example with the diagonal, vertical or PSF configuration, exactly N scatterers are used in the medium. Moreover, with the grid case, a grid of N x N is design to simulate the medium. The backscattering amplitude follows a normal distribution. The scatterers can also be imported from a file.

Concerning the GASM configuration (NL), the discretisation in the x, y, and t axis are used in the definition of the 3D matrix used in the GASM simulation. The discretization of the z axis defines the different incremental step in the computation of the second harmonic field. Then, the obtained field is interpolated using the interpolation dimension on the z axis. In the right part, some pre-configured situations of nonlinear coefficient map are proposed. The default map is a constant medium with ?=3.5. Then, by clicking on the add button, the user modifies the map using a new ? value. The different checkable boxes

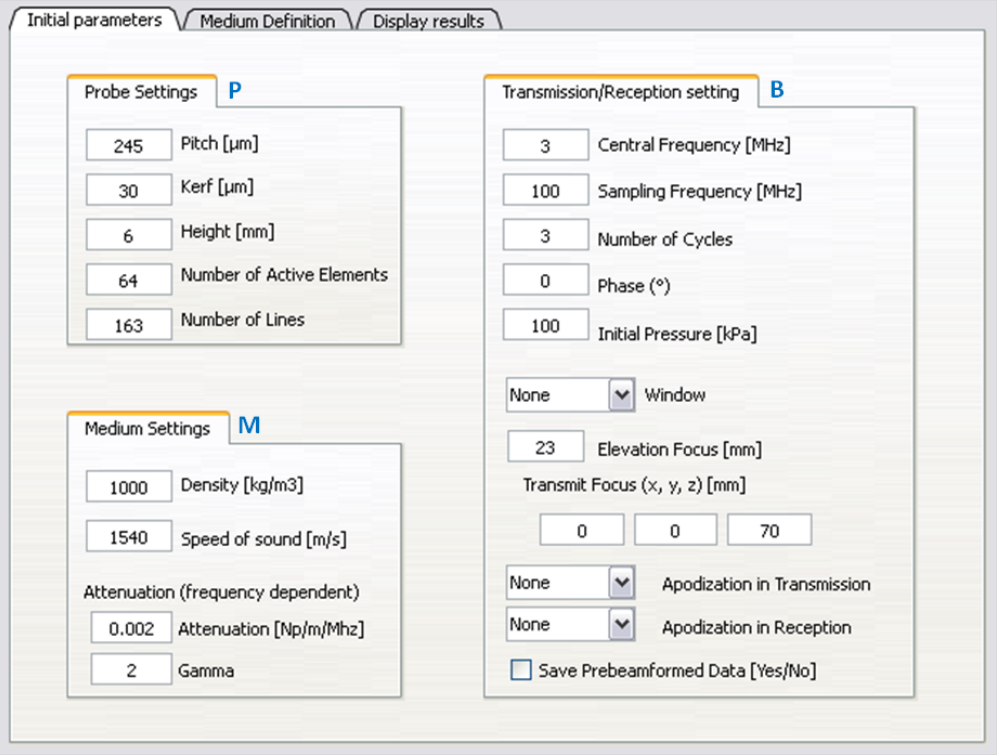

Figure C.2: Illustration of the probe, medium and beamforming setting in the CREANUIS interface.

have different actions:

- Compute one way field: if yes, only do the GASM simulation (no impact of scatterers and image creation). The field is saved with the same output name as the nlrf image, but in the current path.
- Compute GASM: if yes, the GASM simulations are conducted. Otherwise, the saved field in the current folder is loaded. This option is very useful to save computation time when the field has already been simulated.
- Save all the field: if yes, the field compute are saved.
- Use GPU: if yes, the GASM simulations are conducted on the GPU if it is correctly initialized.

Existing nonlinear coefficient map can be imported by the user. The dimension of the imported image has no impact because interpolation is used in the field simulations. However, it has to be considered, during the creation of the map, that the dimension of the map is set by the probe and space parameter. Indeed, the nonlinear map will have a dimension in the lateral dimension [-Nelement Pitch ; Nelement Pitch] and in the axial dimension [0; z_max]. The number of points, that composes this image, has no impact once loaded in CREANUIS.

C.4 Display interface

This last thumb (Fig. C.4) is the display interface. It allows to see the nonlinear coefficient, the pressure field or the nonlinear RF (nlrf) file. The different buttons allow to

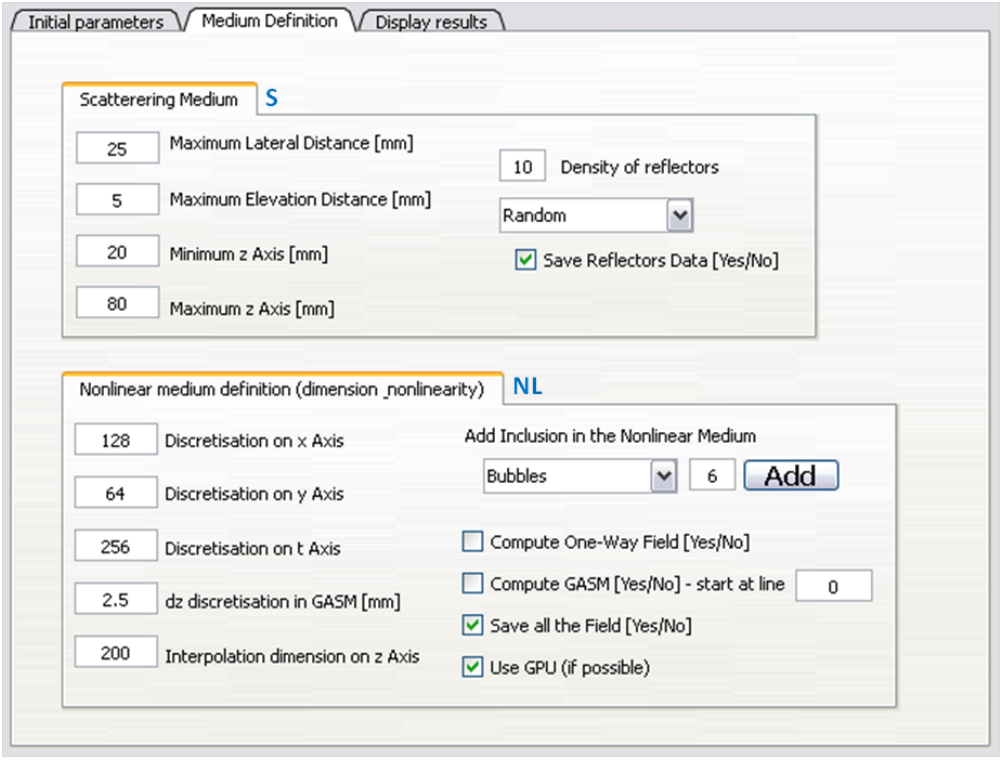

Figure C.3: Illustration of the scatterers definition and the GASM configuration.

select some other file, and to quickly visualize the different results. D1 allows to display the current nonlinear coefficient map, D2 to load an existing pressure field and D3 to load an exiting nlrf image. For the last two, the fundamental/second-harmonic component is displayed in the left/right part of the thumb.

C.5 Data structure

C.5.1 Nlrf files

The nlrf file is the output format of the nonlinear RF image that is computed by CREANUIS. The file is binary file only write with float. A header of 18 float is present. The header is composed (in this order) of: HEADER: Transmitted frequency, sampling frequency, speed of sound, initial pressure, density, pitch, kerf, height, number of elements, number of points on one RF line, third dimension of the RF image (different of 1 if the pre-beamformed data are saved), number of active elements, transmitted focus (z direction), elevation focus, minimal depth, maximal depth, number of transmitted cycle, transmitted phase (in degree).

Then, the other elements correspond to the amplitude of the RF image. The dimension of the radio frequency image is number of element by the number of point on one RF line by the third dimension of the RF image (1 is the beamforming has been done).

C.5.2 Nonlinear coefficient files

The nonlinear coefficient file is a binary file that contains first, two entire N and M, and then NxM float element. To create a nonlinear coefficient file, such configuration has to be used in order to be understood by CREANUIS.

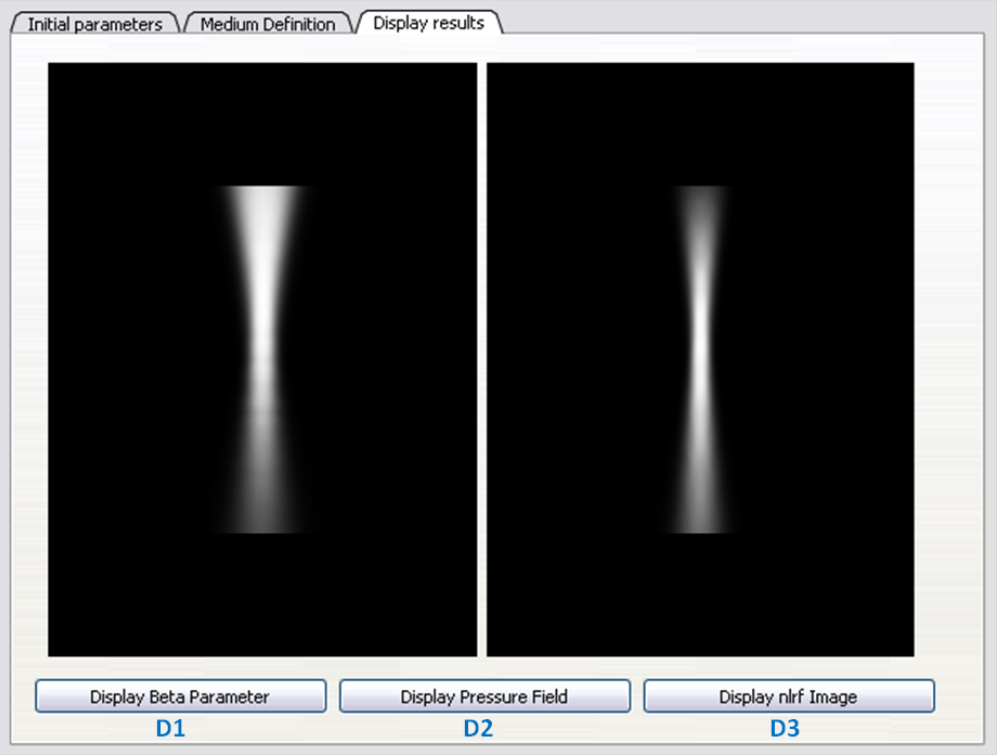

Figure C.4: Illustration of the display thumbs and the possibility to visualize the nonlinear coefficient, the pressure field and the nonlinear image.

C.5.3 Reflectors files

The reflector file is a binary file that contains first, an entire N and then the position and the amplitude of each scatterer (in float). The rest of the file is successively composed of the N x position, the N y position, the N z position and the N amplitude value. To create a reflector file, such configuration has to be used in order to be understood by CREANUIS.

C.6 Utilization of CREANUIS in command line

CREANUIS can be used in command line in order to suppress the graphic interface and then, launch the simulation in a cluster for example. To do this, some arguments have to be added after the CREANUIS launch.

Obligatory arguments

- –path path_name: the user must specify the path where the save_settings.txt file is backup in order to access to the entire parameters need to configure CREANUIS. If the setting file is not placed in path_name directory, an error is return by CREANUIS.
- –scatterers scatterers_file: the user must specify the file where the scatterers position and amplitude is saved. Using CREANUIS in command line did not yet allow to used the classical random, diagonal, grid,... distribution. This file can be generated using the accompanying Matlab file.

Read	Write
read_nonlinear_coefficient_file.m	write_nonlinear_coefficient_file.m
read_scatterers_file.m	write_scatterers_file.m
read_image_rf.m	write_image_rf.m
read_field.m	write_apodization.m

Table C.1: List of the accompanying Matlab files.

Optional arguments

- –nonlinearity nonlinear_coefficient_file: if a specific nonlinear coefficient medium is desired, it has to be generated previously. If the -nonlinearity tag is not present, a nonlinear coefficient medium of ?=3.5 is used in the GASM simulations.
- –debug debug_number: if the output messages are desired in the terminal, a number bigger than 0 has to be selected. The number are the same as the graphic use of CREANUIS. It must not be forgot that the tag do_gasm in the save_setting.txt has to be equal to 1 to do the GASM simulations.

C.7 Accompanying Matlab files

With CREANUIS, several accompanying files are proposed to be able to use the produced results in a Matlab interface. The files are divided in two categories and are summarized in Table C.1:

- Files to read information saved by CREANUIS
- Files to write information that can be read by CREANUIS

The action of each file is detailed in the help header of the Matlab file. If specific apodization, scatterers or nonlinear medium are required, it is recommended to use these files.

C.8 Licence

The CREANUIS software has been placed under the CeCILL-B licence[4]. This licence gives to the user the authorization to use CREANUIS and published work obtained with this software. The only condition is to cite in each work where CREANUIS has been used the following publications:

- F. Varray, A. Ramalli, C. Cachard, P. Tortoli, and O. Basset, "Fundamental and second-harmonic ultrasound field computation of inhomogeneous nonlinear medium with a generalized angular spectrum method", IEEE Transactions on Ultrasonics, Ferroelectrics and Frequency Control, In Press
- F. Varray, C. Cachard, P. Tortoli, and O. Basset, "Nonlinear Radio Frequency Image Simulation for Harmonic Imaging - CREANUIS", IEEE International Ultrasonics Symposium, San Diego, USA, pp. in-press, 2010

[4] http://www.cecill.info/licences/Licence_CeCILL-B_V1-en.html

Appendix D

Standard values of nonlinear parameter

This appendix summarized different values of nonlinear parameter that have been found in the literature. They are sort in three distinct groups: the liquids, the solids and the biological media. The method used are highlighted by:

- TM: thermodynamic method
- DM: direct method
- ISM: insertion substitution method
- SURF: second-order ultrasound field technique
- PW: pump wave method

D.1 Liquid media

Medium	Temperature	B/A	Method	Reference
Water	30°C	5.14	TM	[Davies *et al.* (2000)]
BSA (Bovine Serum Albumin)	30°C	6.68	TM	[Apfel (1986)]
Whole blood	30°C	6.3	TM	[Apfel (1986)]
Dextrose	30°C	6.04	TM	[Apfel (1986)]
Dextrose T150	30°C	5.94	TM	[Apfel (1986)]
Dextrose T2000	30°C	6.2	TM	[Apfel (1986)]
Alcohol	-	8 -10	TM	[Coppens *et al.* (1965), Everbach and Apfel (1995), Banchet and Cheeke (2000), Saito *et al.* (2006)]

Glycerol (4% water)	25°C	8.58 ± 0.34	TM	[Zhu *et al.* (1983)]
Glycerol	25°C	9.4	DM	[Law *et al.* (1985)]
Etylene glycerol	25°C	9.88 ± 0.40	TM	[Zhu *et al.* (1983)]
	26°C	9.9 ± 0.40	ISM	[Gong *et al.* (1989)]
	20°C	9.9	SURF	[Fukukita *et al.* (1996)]

D.2 Solid media

Medium	B/A	Method	Reference
Fused silica	-16.8	PW	[Jacob *et al.* (2003)]
Polystyrene	25.4	PW	[Jacob *et al.* (2003)]
Duraluminum	25.6	PW	[Jacob *et al.* (2003)]
Titanium	12.4	PW	[Jacob *et al.* (2003)]

D.3 Biological media

Medium	Temperature	B/A	Method	Reference
Breast fat	22°C	9.206	TM	[Sehgal *et al.* (1984)]
	30°C	9.909	TM	
	37°C	9.633	TM	
Multiple myeloma	22°C	5.603	TM	[Sehgal *et al.* (1984)]
	30°C	5.796	TM	
	37°C	6.178	TM	
Human liver	30°C	6.54	TM	[Sehgal *et al.* (1985)]
	Normal 30°C	7.6 ± 0.8	DM	[Bjørnø (1986)]
	Congested 30°C	7.2 ± 0.7	DM	[Bjørnø (1986)]
Liver	-	7.3 ± 0.7	DM	[Zhang *et al.* (2001)]
Fat	26°C	10.8	ISM	[Gong *et al.* (1989)]
	-	10.7 ± 0.9	DM	[Zhang *et al.* (2001)]
Fatty liver	-	8.3 ± 0.5	ISM	[Zhang and Gong (1999)]
	-	10.3 ± 0.9	DM	[Zhang *et al.* (2001)]
	-	8.3	ISM	[Gong *et al.* (2004)]
Egg white	-	6.2 ± 0.5	DM	[Zhang *et al.* (2001)]
	27°C	5.2	DM	[Zhang *et al.* (2002)]
Egg yolk	-	8.3 ± 0.7	DM	[Zhang *et al.* (2001)]
	27°C	8.0	DM	[Zhang *et al.* (2002)]
Healthy liver	-	6.8 ± 0.3	ISM	[Zhang and Gong (1999)]
Parasitic hepatitis	-	7.4 ± 0.4	ISM	[Zhang and Gong (1999)]

Fibrinoid hepatitis	-	7.4 ± 0.4	ISM	[Zhang and Gong (1999)]
Necrotic hepatitis	-	7.6 ± 0.4	ISM	[Zhang and Gong (1999)]
Interstitial hepatocirrhosis	-	7.4 ± 0.4	ISM	[Zhang and Gong (1999)]
Parasitic hepatocirrhosis	-	7.8 ± 0.5	ISM	[Zhang and Gong (1999)]
Biliary hepatocirrhosis	-	8.1 ± 0.5	ISM	[Zhang and Gong (1999)]
Hepatonecrosis	-	8.5 ± 0.5	ISM	[Zhang and Gong (1999)]
	-	10.5	ISM	[Gong *et al.* (2004)]
Healthy spleen	-	6.9 ± 0.3	ISM	[Zhang and Gong (1999)]
	Normal 30°C	7.8 ± 0.8	DM	[Bjørnø (1986)]
	Congested 30°C	7.8	DM	[Bjørnø (1986)]
Chronic splentis	-	7.1 ± 0.3	ISM	[Zhang and Gong (1999)]
Healthy kidney	-	7.1 ± 0.3	ISM	[Zhang and Gong (1999)]
Interstitial nephritis	-	7.2 ± 0.3	ISM	[Zhang and Gong (1999)]
Red infarct nephritis	-	7.7 ± 0.4	ISM	[Zhang and Gong (1999)]
Lipoid nephrosis	-	8.0 ± 0.5	ISM	[Zhang and Gong (1999)]
Crescentic nephritis	-	8.1 ± 0.5	ISM	[Zhang and Gong (1999)]
Beef liver	-	6.88	TM	[Law *et al.* (1983)]
	25°C	7.0	TM	[Law *et al.* (1985)]
	25°C	6.8	DM	[Law *et al.* (1985)]
Pig fat	25°C	10.9	TM	[Law *et al.* (1985)]
	25°C	11.3	DM	[Law *et al.* (1985)]
	25°C	10.8	ISM	[Gong *et al.* (1989)]
Cat liver	-	6.7 ± 0.2	DM	[Zhang and Dunn (1987)]
Porcine liver	26°C	7.1	ISM	[Gong *et al.* (1989)]
	27°C	6.9	DM	[Zhang *et al.* (2002)]
	-	6.9	ISM	[Gong *et al.* (2004)]

Personal bibliography

International journal

[Varray *et al.* (2011)a] **F. Varray**, O. Basset, P. Tortoli, and C. Cachard, "Extensions of nonlinear B/A parameter imaging methods for echo mode", IEEE Transactions on Ultrasonics, Ferroelectrics and Frequency Control, vol. 58, no. 6, pp. 1232-1244, 2011.

[Varray *et al.* (2011)f] **F. Varray**, A. Ramalli, C. Cachard, P. Tortoli, and O. Basset, "Fundamental and second-harmonic ultrasound field computation of inhomogeneous nonlinear medium with a generalized angular spectrum method", IEEE Transactions on Ultrasonics, Ferroelectrics and Frequency Control, vol. 58, no. 7, pp. 1366-1376, 2011.

[Varray *et al.* (2011)c] **F. Varray**, C. Cachard, A. Ramalli, P. Tortoli, and O. Basset, "Simulation of ultrasound nonlinear propagation on GPU using a generalized angular spectrum method", EURASIP journal on Image and Video Processing, *accepted*

International conference

[Varray *et al.* (2011)d] **F. Varray**, C. Cachard, P. Tortoli, and O. Basset, "Simulation of (3D+t) nonlinear pressure filed propagation on GPU with the Angular Spectrum Method", IEEE International Ultrasonics Symposium, Orlando, USA, 2011.

[Varray *et al.* (2011)e] **F. Varray**, J. Chenot, O. Basset, P. Tortoli, D. Melodelima and C. Cachard, "Nonlinear parameter measurement to characterize *ex-vivo* pork liver undergoing HIFU ablation: first results", IEEE International Ultrasonics Symposium, Orlando, USA, 2011.

[Lin *et al.* (2011)] F. Lin, **F. Varray**, A. Guibal, C. Cachard and O. Basset, "Experimental Implementation of the Second Harmonic Inversion Imaging on an Open Ultrasonic Scanner", IEEE International Ultrasonics Symposium, Orlando, USA, 2011.

[Varray *et al.* (2010)a] **F. Varray**, C. Cachard, P. Tortoli, and O. Basset, "Nonlinear radio frequency image simulation for harmonic imaging - CREANUIS", IEEE International Ultrasonics Symposium, San Diego, USA, pp. 2179-2182, 2010.

[Varray *et al.* (2009)] **F. Varray**, M. Pasovic, C. Cachard, P. Tortoli, and O. Basset, "Acoustic nonlinearity parameter of tissue on echo mode: review and evaluation of the different approaches for B/A imaging", IEEE International Ultrasonics Symposium, Roma, Italy, pp. 41-44, 2009.

National conference

[Varray *et al.* (2010)b] **F. Varray**, M. Pasovic, C. Cachard, P. Tortoli, and O. Basset, "Imagerie du paramètre de non linéearité par une méthode comparative en échographie médicale faisabilité expérimentale", Congrès Français d'Acoustique, Lyon, France, pp. 63, 2010.

Software development

CREANUIS software: http://www.creatis.insa-lyon.fr/site/fr/CREANUIS

Submitted international journal

[Varray *et al.* (2011)b] **F. Varray**, O. Basset, P. Tortoli, and C. Cachard, "Nonlinear Radio Frequency Image Simulation for Harmonic Imaging Application: CREANUIS", IEEE Transactions on Ultrasonics, Ferroelectrics and Frequency Control, *submitted*

Bibliography

[Aanonsen *et al.* (1984)] Aanonsen, S. I., Barkve, T., Tjotta, J. N. and Tjotta, S. (1984). Distortion and harmonic generation in the nearfield of a finite amplitude sound beam. *The Journal of the Acoustical Society of America*, 75(3):749–768.

[Adler and Hiedemann (1962)] Adler, L. and Hiedemann, E. A. (1962). Determination of the nonlinearity parameter B/A for water and m-xylene. *The Journal of the Acoustical Society of America*, 34(4):410–412.

[Akiyama (2000)] Akiyama, I. (2000). Reflection mode measurement of nonlinearity parameter B/A. *In 15th International Symposium of Nonlinear Acoustics*, volume 524, pages 321–324.

[Alais and Hennion (1976)] Alais, P. and Hennion, P. (1976). Intéraction non linéaire paramétrique de deux modes acoustiques d'ondes planes atténuées inhomogènes. *Acad. Sc. Paris*, 282(17):385–287.

[Alais and Hennion (1979)] Alais, P. and Hennion, P. (1979). Etude par une méthode de fourier de l'interaction non linéaire de deux rayonnements acoustiques dans un milieu absorbant. Cas particulier de l'émission paramétrique. *Acta Acustica*, 43(1):1–11.

[Anderson (2000)] Anderson, M. E. (2000). A 2d nonlinear wave propagation solver written in open-source matlab code. *In IEEE Ultrasonics Symposium*, volume 2, pages 1351–1354.

[Angelsen (2000)a] Angelsen, B. (2000a). *Ultrasound Imaging*, volume 2. Emantec.

[Angelsen (2000)b] Angelsen, B. (2000b). *Ultrasound Imaging*, volume 1. Emantec.

[Apfel (1983)] Apfel, R. E. (1983). The effective nonlinearity parameter for immiscible liquid mixtures. *The Journal of the Acoustical Society of America*, 74(6):1866–1868.

[Apfel (1986)] Apfel, R. E. (1986). Prediction of tissue composition from ultrasonic measurements and mixture rules. *The Journal of the Acoustical Society of America*, 79(1):148–152.

[Averkiou *et al.* (1997)] Averkiou, M., Roundhill, D. and Powers, J. (1997). A new imaging technique based on the nonlinear properties of tissues. *In IEEE Ultrasonics Symposium*, volume 2, pages 1561–1566.

[Baker *et al.* (1995)] Baker, A. C., Berg, A. M., Sahin, A. and Tjotta, J. N. (1995). The nonlinear pressure field of plane, rectangular apertures: Experimental and theoretical results. *The Journal of the Acoustical Society of America*, 97(6):3510–3517.

[Bamber and Dickinson (1980)] Bamber, J. C. and Dickinson, R. J. (1980). Ultrasonic b-scanning: a computer simulation. *Physics in Medicine & Biology*, 25(3):463.

[Banchet and Cheeke (2000)] Banchet, J. and Cheeke, J. D. N. (2000). Measurement of the acoustic nonlinearity parameter B/A in solvents: Dependence on chain length and sound velocity. *The Journal of the Acoustical Society of America*, 108(6):2754–2758.

[Barrière and Royer (2001)] Barrière, C. and Royer, D. (2001). Diffraction effects in the parametric interaction of acoustic waves: application to measurements of the nonlinearity parameter B/A in liquids. *IEEE Transactions on Ultrasonics, Ferroelectrics and Frequency Control*, 48(6):1706–1715.

[Belgroune *et al.* (2002)] Belgroune, D., de Belleval, J. F. and Djelouah, H. (2002). Modelling of the ultrasonic field by the angular spectrum method in presence of interface. *Ultrasonics*, 40(1-8):297–302.

[Bereza *et al.* (2008)] Bereza, S., Burov, V. and Evtukhov, S. (2008). Model experiments on acoustic tomography of the nonlinear parameter. *Acoustical Physics*, 54(4):449–459.

[Bernard *et al.* (2006)] Bernard, O., D'hooge, J. and Friboulet, D. (2006). Statistics of the radio-frequency signal based on k distribution with application to echocardiography. *IEEE Transactions on Ultrasonics, Ferroelectrics and Frequency Control*, 53(9):1689–1694.

[Bernard *et al.* (2007)] Bernard, O., Touil, B., D'hooge, J. and Friboulet, D. (2007). Statistical modeling of the radio-frequency signal for partially and fully developed speckle based on a generalized gaussian model with application to echocardiography. *IEEE Transactions on Ultrasonics, Ferroelectrics and Frequency Control*, 54(10):2189–2194.

[Berntsen (1990)] Berntsen, J. (1990). Numerical calculations of finite amplitude sound beams. *In 12th International Symposium of Nonlinear Acoustics*.

[Beyer (1960)] Beyer, R. T. (1960). Parameter of nonlinearity in fluids. *The Journal of the Acoustical Society of America*, 32(6):719–721.

[Beyer (1974)] Beyer, R. T. (1974). *Nonlinear Acoustics*. Naval Ship Systems Command.

[Bjørnø (1986)] Bjørnø, L. (1986). Characterization of biological media by means of their non-linearity. *Ultrasonics*, 24(5):254–259.

[Bjørnø (2002)] Bjørnø, L. (2002). Forty years of nonlinear ultrasound. *Ultrasonics*, 40(1-8):11–17.

[Blackstock (1964)] Blackstock, D. T. (1964). Thermoviscous attenuation of plane, periodic, finite-amplitude sound waves. *The Journal of the Acoustical Society of America*, 36(3):534–542.

[Bleeker *et al.* (1990)] Bleeker, H. J., Shung, K. K. and Barnhart, J. L. (1990). Ultrasonic characterization of albunex[sup r], a new contrast agent. *The Journal of the Acoustical Society of America*, 87(4):1792–1797.

[Bou Matar *et al.* (2002)] Bou Matar, O., Dos Santos, S., Vila, M. and Vander Meulen, F. (2002). Acoustic nonlinear parameter measurement in solid with a contact phase modulation method. *In IEEE Ultrasonics Symposium*, volume 1, pages 881–884.

[Bouakaz and de Jong (2007)] Bouakaz, A. and de Jong, N. (2007). Wfumb safety symposium on echo-contrast agents: Nature and types of ultrasound contrast agents. *Ultrasound in Medicine & Biology*, 33(2):187 – 196.

[Bouakaz *et al.* (2002)] Bouakaz, A., Frigstad, S., Ten Cate, F. J. and de Jong, N. (2002). Super harmonic imaging: a new imaging technique for improved contrast detection. *Ultrasound in Medicine & Biology*, 28(1):59–68.

[Brysev *et al.* (2004)] Brysev, A., Krutyansky, L., Pernod, P. and Preobrazhensky, V. (2004). Nonlinear ultrasonic phase-conjugate beams and their application in ultrasonic imaging. *Acoustical Physics*, 50:623–640. 10.1134/1.1825091.

[Burov *et al.* (1994)] Burov, V., Gurinovich, I., Rudenko, O. and Tagunov, E. (1994). Reconstruction of the spatial distribution of the nonlinearity parameter and sound velocity in acoustic nonlinear tomography. *Acoustical Physics*, 40(6):816–823.

[Cai *et al.* (1992)] Cai, A., Sun, J. and Wade, G. (1992). Imaging the acoustic nonlinear parameter with diffraction tomography. *IEEE Transactions on Ultrasonics, Ferroelectrics and Frequency Control*, 39(6):708–715.

[Cain (1985)] Cain, C. (1985). Ultrasonic reflection mode imaging of the nonlinear parameter B/A: A theoretical basis. *In IEEE Ultrasonics Symposium*, pages 887–890.

[Cain (1986)] Cain, C. A. (1986). Ultrasonic reflection mode imaging of the nonlinear parameter B/A. I: A theoretical basis. *The Journal of the Acoustical Society of America*, 80(1):28–32.

[Cain and Houshmand (1989)] Cain, C. A. and Houshmand, H. (1989). Ultrasonic reflection mode imaging of the nonlinear parameter B/A. II: Signal processing. *The Journal of the Acoustical Society of America*, 86(1):28–34.

[Cain *et al.* (1986)] Cain, C. A., Nishiyama, H. and Katakura, K. (1986). On ultrasonic methods for measurement of the nonlinear parameter B/A in fluid-like media. *The Journal of the Acoustical Society of America*, 80(2):685–688.

[Calmon *et al.* (2006)] Calmon, P., Mahaut, S., Chatillon, S. and Raillon, R. (2006). CIVA: An expertise platform for simulation and processing ndt data. *Ultrasonics*, 44(1):975 – 979.

[Chang *et al.* (2009)] Chang, L.-W., Hsu, K.-H. and Li, P.-C. (2009). Gpu-based color doppler ultrasound processing. *In IEEE Ultrasonics Symposium*, pages 1836–1839.

[Chavrier *et al.* (2006)] Chavrier, F., Lafon, C., Birer, A., Barriere, C., Jacob, X. and Cathignol, D. (2006). Determination of the nonlinear parameter by propagating and modeling finite amplitude plane waves. *The Journal of the Acoustical Society of America*, 119(5):2639–2644.

[Christopher and Parker (1991)a] Christopher, P. T. and Parker, K. J. (1991a). New approaches to nonlinear diffractive field propagation. *The Journal of the Acoustical Society of America*, 90(1):488–499.

[Christopher and Parker (1991)b] Christopher, P. T. and Parker, K. J. (1991b). New approaches to the linear propagation of acoustic fields. *The Journal of the Acoustical Society of America*, 90(1):507–521.

[Cleveland *et al.* (1996)] Cleveland, R. O., Hamilton, M. F. and Blackstock, D. T. (1996). Time-domain modeling of finite-amplitude sound in relaxing fluids. *The Journal of the Acoustical Society of America*, 99(6):3312–3318.

[Coppens *et al.* (1965)] Coppens, A. B., Beyer, R. T., Seiden, M. B., Donohue, J., Guepin, F., Hodson, R. H. and Townsend, C. (1965). Parameter of nonlinearity in fluids. ii. *The Journal of the Acoustical Society of America*, 38(5):797–804.

[Couprie and Bertrand (2004)] Couprie, M. and Bertrand, G. (2004). Topology preserving alternating sequential filter for smoothing 2d and 3d objects. *Journal of Electronic Imaging*, 13(4):720–730.

[Davies *et al.* (2000)] Davies, J. R., Tapson, J. and Mortimer, B. J. (2000). A novel phase locked cavity resonator for B/A measurements in fluids. *Ultrasonics*, 38(1-8):284–291.

[Decencière and Jeulin (2001)] Decencière, E. and Jeulin, D. (2001). Morphological decomposition of the surface topography of an internal combustion engine cylinder to characterize wear. *Wear*, 249(5-6):482 – 488.

[Demi *et al.* (2010)a] Demi, L., Verweij, M. D., De Jong, N. and Van Dongen, K. (2010a). Modeling nonlinear acoustic wave fields in media with inhomogeneity in the attenuation and in the nonlinearity. *In IEEE Ultrasonics Symposium*.

[Demi *et al.* (2010)b] Demi, L., Verweij, M. D., De Jong, N. and Van Dongen, K. (2010b). Modeling nonlinear medical ultrasoun via a linearized constrast source method. *In IEEE Ultrasonics Symposium*.

[Ding (2000)] Ding, D. (2000). A simplified algorithm for the second-order sound fields. *The Journal of the Acoustical Society of America*, 108(6):2759–2764.

[Ding (2004)] Ding, D. (2004). A simplified algorithm for second-order sound beams with arbitrary source distribution and geometry (l). *The Journal of the Acoustical Society of America*, 115(1):35–37.

[Ding and Huang (2007)] Ding, D. and Huang, J.-h. (2007). Second-harmonic generation of limited diffraction beams. *Journal of Optics A: Pure and Applied Optics*, 9(12):1131.

[Dong *et al.* (1999)] Dong, F., Madsen, E. L., MacDonald, M. C. and Zagzebski, J. A. (1999). Nonlinearity parameter for tissue-mimicking materials. *Ultrasound in Medicine & Biology*, 25(5):831–838.

[Du and Breazeale (1985)] Du, G. and Breazeale, M. A. (1985). The ultrasonic field of a gaussian transducer. *The Journal of the Acoustical Society of America*, 78(6):2083–2086.

[Du *et al.* (2010)] Du, Y., Jensen, H. and Jensen, J. (2010). Simulation of second harmonic ultrasound fields. *In IEEE Ultrasonics Symposium*.

[Du and Jensen (2008)] Du, Y. and Jensen, J. (2008). Feasibility of non-linear simulation for field ii using an angular spectrum approach. *In IEEE Ultrasonics Symposium*, pages 1314–1317.

[Dunn *et al.* (1981)] Dunn, F., Law, W. and Frizzell, L. (1981). Nonlinear ultrasonic wave propagation in biological materials. *In IEEE Ultrasonics Symposium*, pages 527–532.

[Dursun *et al.* (2005)] Dursun, S., Varslot, T., Johansen, T., Angelsen, B. and Torp, H. (2005). Fast 3d simulation of 2nd harmonic ultrasound field from arbitrary transducer geometries. *In IEEE Ultrasonics Symposium*, pages 1964–1967.

[Eckersley *et al.* (2005)] Eckersley, R. J., Chin, C. T. and Burns, P. N. (2005). Optimising phase and amplitude modulation schemes for imaging microbubble contrast agents at low acoustic power. *Ultrasound in Medicine & Biology*, 31(2):213–9.

[Elnokrashy *et al.* (2009)] Elnokrashy, A., Elmalky, A., Hosny, T., Ellah, M., Megawer, A., Elsebai, A., Youssef, A.-B. and Kadah, Y. (2009). Gpu-based reconstruction and display for 4d ultrasound data. *In IEEE Ultrasonics Symposium*, pages 189–192.

[Errabolu *et al.* (1988)] Errabolu, R. L., Sehgal, C. M., Bahn, R. C. and Greenleaf, J. F. (1988). Measurement of ultrasonic nonlinear parameter in excised fat tissues. *Ultrasound in Medicine & Biology*, 14(2):137–146.

[Escoffre *et al.* (2010)] Escoffre, J., Kaddur, K., Rols, M. and Bouakaz, A. (2010). In vitro gene transfer by electrosonoporation. *Ultrasound in Medicine & Biology*, 36(10): 1746 – 1755.

[Everbach and Apfel (1995)] Everbach, E. C. and Apfel, R. E. (1995). An interferometric technique for *B/A* measurement. *The Journal of the Acoustical Society of America*, 98(6):3428–3438.

[Fatemi and Greenleaf (1996)] Fatemi, M. and Greenleaf, J. F. (1996). Real-time assessment of the parameter of nonlinearity in tissue using "nonlinear shadowing". *Ultrasound in Medicine & Biology*, 22(9):1215–1228.

[Fatemi and Greenleaf (1998)] Fatemi, M. and Greenleaf, J. F. (1998). Ultrasound-stimulated vibro-acoustic spectrography. *Science*, 280(5360):82–85.

[Fenlon (1972)] Fenlon, F. H. (1972). An extension of the bessel-fubini series for a multiple-frequency CW acoustic source of finite amplitude. *The Journal of the Acoustical Society of America*, 51(1B):284–289.

[Ferrara *et al.* (2007)] Ferrara, K., Pollard, R. and Borden, M. (2007). Ultrasound microbubble contrast agents: Fundamentals and application to gene and drug delivery. *Annual Review of Biomedical Engineering*, 9(1):415–447.

[Franceschini *et al.* (2007)] Franceschini, E., Yu, F., Fenech, M. and Cloutier, G. (2007). Evaluation of the structure factor size estimator (sfse) with simulated ultrasonic backscattered signals from blood. *In IEEE Ultrasonics Symposium*, pages 2503–2506.

[Freedman (1960)] Freedman, A. (1960). Sound field of a rectangular piston. *The Journal of the Acoustical Society of America*, 32(2):197–209.

[Frigo and Johnson (2005)] Frigo, M. and Johnson, S. G. (2005). The design and implementation of fftw3. *Proceedings of the IEEE*, 93(2):216–231.

[Frijlink *et al.* (2008)] Frijlink, M., Kaupang, H., Varslot, T. and Måsøy, S. (2008). Abersim: A simulation program for 3d nonlinear acoustic wave propagation for arbitrary pulses and arbitrary transducer geometries. *In IEEE Ultrasonics Symposium*, pages 1282 – 1285.

[Fubini (1935)] Fubini, G. (1935). Anomalie nella propagazione di onde acutiche di grande ampiezza. *Alta Freq.*, 4:530.

[Fujii *et al.* (2004)] Fujii, Y., Taniguchi, N., Akiyama, I., Tsao, J.-W. and Itoh, K. (2004). A new system for in vivo assessment of the degree of nonlinear generation using the second harmonic component in echo signals. *Ultrasound in Medicine & Biology*, 30(11):1511–1516.

[Fukukita *et al.* (1996)] Fukukita, H., Ueno, S.-i. and Yano, T. (1996). Ultrasound pulse reflection mode measurement of nonlinearity parameter B/A and attenuation coefficient. *The Journal of the Acoustical Society of America*, 99(5):2775–2782.

[Gilliam and Acton (2007)] Gilliam, A. and Acton, S. (2007). Echocardiographic simulation for validation of automated segmentation methods. *In Proceedingss of the IEEE International Conference on Image Processing*, pages 529–532.

[Gong *et al.* (1984)] Gong, X., Feng, R., Zhu, C. and Shi, T. (1984). Ultrasonic investigation of the nonlinearity parameter B/A in biological media. *The Journal of the Acoustical Society of America*, 76(3):949–950.

[Gong *et al.* (2004)] Gong, X., Zhang, D., Liu, J., Wang, H., Yan, Y. and Xu, X. (2004). Study of acoustic nonlinearity parameter imaging methods in reflection mode for biological tissues. *The Journal of the Acoustical Society of America*, 116(3):1819–1825.

[Gong *et al.* (1989)] Gong, X., Zhu, Z.-m., Shi, T. and Huang, J.-h. (1989). Determination of the acoustic nonlinearity parameter in biological media using fais and itd methods. *The Journal of the Acoustical Society of America*, 86(1):1–5.

[Goursolle *et al.* (2008)] Goursolle, T., Dos Santos, S., Bou Matar, O. and Call'e, S. (2008). Non-linear based time reversal acoustic applied to crack detection: Simulations and experiments. *International Journal of Non-Linear Mechanics*, 43(3):170–177.

[Hamilton and Blackstock (1988)] Hamilton, M. F. and Blackstock, D. T. (1988). On the coefficient of nonlinearity beta in nonlinear acoustics. *The Journal of the Acoustical Society of America*, 83(1):74–77.

[Hamilton and Blackstock (1997)] Hamilton, M. F. and Blackstock, D. T. (1997). *Nonlinear acoustics*. Academic Press.

[Harris *et al.* (2007)] Harris, G., Liu, Y., Maruvada, S. and Gammell, P. (2007). Finite amplitude method for measurement of nonlinearity parameter B/A using plane-wave tone bursts. *In IEEE Ultrasonics Symposium*, pages 2072–2074.

[Holm (2001)] Holm, S. (2001). Ultrasim - a toolbox for ultrasound field simulation. *In Nordic Matalb Conference*.

[Houshmand *et al.* (1988)] Houshmand, H., McGough, R., Ebbini, E., Lee, H. and Cain, C. (1988). Ultrasonic transmission mode imaging of the nonlinear parameter B/A: A simulation study. *In IEEE Ultrasonics Symposium*.

[Huijssen and Verweij (2010)] Huijssen, J. and Verweij, M. D. (2010). An iterative method for the computation of nonlinear, wide-angle, pulsed acoustic fields of medical diagnostic transducers. *The Journal of the Acoustical Society of America*, 127(1):33–44.

[Ichida *et al.* (1984)] Ichida, N., Sato, T., Miwa, H. and Murakami, K. (1984). Real-time nonlinear parameter tomography using impulsive pumping waves. *IEEE Transactions on Sonics and Ultrasonics*, 31(6):635–641.

[Ingenito and Williams (1971)] Ingenito, F. and Williams, J. A. O. (1971). Calculation of second-harmonic generation in a piston beam. *The Journal of the Acoustical Society of America*, 49(1B):319–328.

[Jacob *et al.* (2003)] Jacob, X., Barrière, C. and Royer, D. (2003). Acoustic nonlinearity parameter measurements in solids using the collinear mixing of elastic waves. *Applied Physics Letters*, 82(6):886–888.

[Jensen and Nikolov (2000)] Jensen, J. and Nikolov, I. (2000). Fast simulation of ultrasound images. *In IEEE Ultrasonics Symposium*, volume 2, pages 1721 –1724.

[Jensen (1996)] Jensen, J. A. (1996). Field: A program for simulating ultrasound systems. *In 10th Nordic-Baltic Conference on Biomedical Imaging Published in Medical & Biological Engineering & Computing*, volume 34, pages 351–353.

[Jensen and Munk (1997)] Jensen, J. A. and Munk, P. (1997). Computer phantoms for simulating ultrasound b-mode and cfm images. *In 23rd Acoustical Imaging Symposium.*

[Jensen and Svendsen (1992)] Jensen, J. A. and Svendsen, N. B. (1992). Calculation of pressure fields from arbitrarily shaped, apodized, and excited ultrasound transducers. *IEEE Transactions on Ultrasonics, Ferroelectrics and Frequency Control*, 39(2):262–267.

[Jiang and Hall (2007)] Jiang, J. and Hall, T. J. (2007). A parallelizable real-time motion tracking algorithm with applications to ultrasonic strain imaging. *Physics in Medicine & Biology*, 52(13):3773.

[Kamakura *et al.* (1992)] Kamakura, T., Tani, M., Kumamoto, Y. and Ueda, K. (1992). Harmonic generation in finite amplitude sound beams from a rectangular aperture source. *The Journal of the Acoustical Society of America*, 91(6):3144–3151.

[Kashkooli *et al.* (1987)] Kashkooli, H. A., Dolan, Jr., P. J. and Smith, C. W. (1987). Measurement of the acoustic nonlinearity parameter in water, methanol, liquid nitrogen, and liquid helium-ii by two different methods: A comparison. *The Journal of the Acoustical Society of America*, 82(6):2086–2089.

[Kaya *et al.* (2006)] Kaya, O. A., Sahin, A. and Kaleci, D. (2006). Pressure field of rectangular transducers at finite amplitude in three dimensions. *Ultrasound in Medicine & Biology*, 32(2):271–280.

[Khelladi *et al.* (2009)] Khelladi, H., Plantier, F., Daridon, J. L. and Djelouah, H. (2009). Measurement under high pressure of the nonlinearity parameter B/A in glycerol at various temperatures. *Ultrasonics*, 49(8):668–675.

[Kim *et al.* (1990)] Kim, D., Greenleaf, J. F. and Sehgal, C. M. (1990). Ultrasonic imaging of the nonlinear parameter B/A: Simulation studies to evaluate phase and frequency modulation methods. *Ultrasound in Medicine & Biology*, 16(2):175–181.

[Kiss *et al.* (2009)] Kiss, G., Nielsen, E., Orderud, F. and Torp, H. (2009). Performance optimization of block matching in 3d echocardiography. *In IEEE Ultrasonics Symposium*, pages 1403–1406.

[Kiss *et al.* (2010)] Kiss, G., Steen, E., Asen, J. P. and Torp, H. (2010). Gpu volume rendering in 3d echocardiography: real-time pre-processing and ray-casting. *In IEEE Ultrasonics Symposium*.

[Kourtiche *et al.* (2001)] Kourtiche, D., Alliès, L., Chitnalah, A. and Nadi, M. (2001). Harmonic propagation of finite amplitude sound beams: comparative method in pulse echo measurement of nonlinear B/A parameter. *Measurement Science and Technology*, 12(11):1990–1995.

[Krutyansky *et al.* (2007)] Krutyansky, L., Preobrazhensky, V., Pernod, P. and Bou Matar, O. (2007). Nonlinear imaging of isoechogenic phantoms using phase conjugation of the second acoustic harmonic. *Physics of Wave Phenomena*, 15:186–190. 10.3103/S1541308X07030053.

[Kuznetsov (1970)] Kuznetsov, V. (1970). Equation of nonlinear acoustics. *Sov. Phys. Acoustics*, 16:749–768.

[Labat *et al.* (2000)] Labat, V., Remenieras, J. P., Bou Matar, O., Ouahabi, A. and Patat, F. (2000). Harmonic propagation of finite amplitude sound beams: experimental determination of the nonlinearity parameter B/A. *Ultrasonics*, 38(1-8):292–296.

[Landsberger and Hamilton (2001)] Landsberger, B. J. and Hamilton, M. F. (2001). Second-harmonic generation in sound beams reflected from, and transmitted through, immersed elastic solids. *The Journal of the Acoustical Society of America*, 109(2):488–500.

[Law *et al.* (1981)] Law, W. K., Frizzell, L. A. and Dunn, F. (1981). Ultrasonic determination of the nonlinearity parameter B/A for biological media. *The Journal of the Acoustical Society of America*, 69(4):1210–1212.

[Law *et al.* (1983)] Law, W. K., Frizzell, L. A. and Dunn, F. (1983). Comparison of thermodynamic and finite amplitude methods of B/A measurement in biological materials. *The Journal of the Acoustical Society of America*, 74(4):1295–1297.

[Law *et al.* (1985)] Law, W. K., Frizzell, L. A. and Dunn, F. (1985). Determination of the nonlinearity parameter B/A of biological media. *Ultrasound in Medicine & Biology*, 11(2):307–318.

[Lee *et al.* (2007)] Lee, W.-N., Ingrassia, C., Fung-Kee-Fung, S., Costa, K., Holmes, J. and Konofagou, E. (2007). Theoretical quality assessment of myocardial elastography with in vivo validation. *IEEE Transactions on Ultrasonics, Ferroelectrics and Frequency Control*, 54(11):2233–2245.

[Lee and Hamilton (1995)] Lee, Y.-S. and Hamilton, M. F. (1995). Time-domain modeling of pulsed finite-amplitude sound beams. *The Journal of the Acoustical Society of America*, 97(2):906–917.

[Lin *et al.* (2011)] Lin, F., Varray, F., Guibal, A., Cachard, C. and Basset, O. (2011). Experimental implementation of the second harmonic inversion imaging on an open ultrasonic scanner. *In IEEE Ultrasonics Symposium*.

[Liu and Nikoonahad (1989)] Liu, D. and Nikoonahad, M. (1989). Pulse-echo *B/A* measurement using variable amplitude excitation. *In IEEE Ultrasonics Symposium*, volume 2, pages 1047 –1051.

[Liu *et al.* (2007)] Liu, X., Li, J., Gong, X., Zhu, Z. and Zhang, D. (2007). Theoretical and experimental study of the third-order nonlinearity parameter c/a for biological media. *Physica D: Nonlinear Phenomena*, 228(2):172–178.

[Lu (1997)] Lu, J. Y. (1997). Designing limited diffraction beams. *IEEE Transactions on Ultrasonics, Ferroelectrics and Frequency Control*, 44(1):181–193.

[Lucas and Muir (1983)] Lucas, B. G. and Muir, T. G. (1983). Field of a finite-amplitude focusing source. *The Journal of the Acoustical Society of America*, 74(5):1522–1528.

[Ma *et al.* (2005)] Ma, Q., Ma, Y., Gong, X. and Zhang, D. (2005). Improvement of tissue harmonic imaging using the pulse-inversion technique. *Ultrasound in Medicine & Biology*, 31(7):889–894.

[Marion *et al.* (2009)] Marion, A., Porée, J. and Vray, D. (2009). CREASIMUS: a fast simulator of ultrasound image sequence using 3d tissue motion. *In IEEE International Ultrasonics Symposium*, pages 2308–2311, Roma, Italy.

[Marion and Vray (2009)] Marion, A. and Vray, D. (2009). Toward a real-time simulation of ultrasound image sequences based on a 3d set of moving scatterers. *2009*, 56(10):2167–2179.

[Meunier and Bertrand (1995)a] Meunier, J. and Bertrand, M. (1995a). Echographic image mean gray level changes with tissue dynamics: a system-based model study. *IEEE Transactions on Biomedical Engineering*, 42(4):403 –410.

[Meunier and Bertrand (1995)b] Meunier, J. and Bertrand, M. (1995b). Ultrasonic texture motion analysis: theory and simulation. *IEEE Transactions on Biomedical Engineering*, 14(2):293 –300.

[Mills (2004)] Mills, D. (2004). Medical imaging with capacitive micromachined ultrasound transducer (cmut) arrays. *In IEEE Ultrasonics Symposium*, volume 1, pages 384–390 Vol.1.

[Mills and Smith (2003)] Mills, D. and Smith, L. (2003). Real-time in-vivo imaging with capacitive micromachined ultrasound transducer (cmut) linear arrays. *In IEEE Ultrasonics Symposium*, volume 1, pages 568–571 Vol.1.

[Mura *et al.* (2010)] Mura, M. D., Benediktsson, J. A. and Bruzzone, L. (2010). Alternating sequential filters with morphological attribute operators for the analysis of remote sensing images. *In Proc SPIE (Image and Signal Processing for Remote Sensing XVI)*, volume 7830.

[Nakagawa *et al.* (1986)] Nakagawa, Y., Hou, W., Cai, A., Arnold, N. and Wade, G. (1986). Nonlinear parameter imaging with finite-amplitude sound waves. *In IEEE Ultrasonics Symposium*, pages 901–904.

[Nakagawa *et al.* (1984)] Nakagawa, Y., Nakagawa, M., Yoneyama, M. and Kikuchi, M. (1984). Nonlinear parameter imaging computed tomography by parametric acoustic array. *In IEEE Ultrasonics Symposium*, pages 673–676.

[Nikoonahad and Liu (1990)] Nikoonahad, M. and Liu, D. (1990). Pulse-echo single frequency acoustic nonlinearity parameter (b /a) measurement. *IEEE Transactions on Ultrasonics, Ferroelectrics and Frequency Control*, 37(3):128–134.

[Novell *et al.* (2009)] Novell, A., Legros, M., Felix, N. and Bouakaz, A. (2009). Exploitation of capacitive micromachined transducers for nonlinear ultrasound imaging. *IEEE Transactions on Ultrasonics, Ferroelectrics and Frequency Control*, 56(12):2733 –2743.

[Nowicki *et al.* (2007)] Nowicki, A., Wojcik, J. and Secomski, W. (2007). Harmonic imaging using multitone nonlinear coding. *Ultrasound in Medicine & Biology*, 33(7): 1112–22.

[Pasovic *et al.* (2011)] Pasovic, M., Danilouchkine, M., Faez, T., van Neer, P. L. M. J., Cachard, C., van der Steen, A. F. W., Basset, O. and de Jong, N. (2011). Second harmonic inversion for ultrasound contrast harmonic imaging. *Physics in Medicine and Biology*, 56(11):3163–3180.

[Pasovic *et al.* (2010)] Pasovic, M., Danilouchkine, M., Matte, G., van der Steen, A. F. W., Basset, O., de Jong, N. and Cachard, C. (2010). Broadband reduction of the second harmonic distortion during nonlinear ultrasound wave propagation. *Ultrasound in Medicine & Biology*, 36(10):1568–1580.

[Pasovic *et al.* (2009)] Pasovic, M., Danilouchkine, M., Van Neer, P., Basset, O., Cachard, C., Van der Steen, A. and De Jong, N. (2009). Angular spectrum method for the estimation of the lateral profile of the ultrasound pressure field in the super harmonic band. *In IEEE Ultrasonics Symposium*.

[Pasovic *et al.* (2007)] Pasovic, M., Matte, G., Van der Steen, A., Basset, O., de Jong, N. and Cachard, C. (2007). Preliminary investigation of nonlinear dual frequency mixing technique for the estimation of the nonlinear paramter *B/A*. *In IEEE EMBC*, pages 2179–2182.

[Pinton *et al.* (2009)] Pinton, G., Dahl, J., Rosenzweig, S. and Trahey, G. (2009). A heterogeneous nonlinear attenuating full-wave model of ultrasound. *IEEE Transactions on Ultrasonics, Ferroelectrics and Frequency Control*, 56(3):474 –488.

[Pinton *et al.* (2011)] Pinton, G. F., Trahey, G. E. and Dahl, J. J. (2011). Sources of image degradation in fundamental and harmonic ultrasound imaging using nonlinear, full-wave simulations. *IEEE Transactions on Ultrasonics, Ferroelectrics and Frequency Control*, 58(4):754–765.

[Piwakowski and Sbai (1999)] Piwakowski, B. and Sbai, K. (1999). A new approach to calculate the field radiated from arbitrarily structured transducer arrays. *IEEE Transactions on Ultrasonics, Ferroelectrics and Frequency Control*, 46(2):422 –440.

[Plantier *et al.* (2002)] Plantier, F., Daridon, J. and Lagourette, B. (2002). Nonlinear parameter (*B/A*) measurements in methanol, 1-butanol and 1-octanol for different pressures and temperatures. *Journal of Physics D: Applied Physics*, 35(10):1063–1067.

[Preobrazhensky *et al.* (2008)] Preobrazhensky, S., Preobrazhensky, V., Pernod, P. and Bou Matar, O. (2008). Testing for inhomogeneity of the nonlinear parameter in an acoustic medium by ultrasonic phase conjugation. *Acoustical Physics*, 54:15–19. 10.1134/S106377100801003X.

[Preobrazhensky *et al.* (2009)] Preobrazhensky, V., Pernod, P., Pyl'Nov, Y., Krutyansky, L., Smagin, N. and Preobrazhensky, S. (2009). Nonlinear acoustic imaging of isoechogenic objects and flows using ultrasound wave phase conjugation. *Acta Acustica*, 95(1):36–45.

[Sahin and Baker (1994)] Sahin, A. and Baker, A. C. (1994). Ultrasonic pressure fields due to rectangular apertures. *The Journal of the Acoustical Society of America*, 96(1): 552–556.

[Saito (1993)] Saito, S. (1993). Measurement of the acoustic nonlinearity parameter in liquid media using focused ultrasound. *The Journal of the Acoustical Society of America*, 93(1):162–172.

[Saito *et al.* (2006)] Saito, S., Kim, J.-H. and Nakamura, K. (2006). Automatic measurement of the nonlinearity parameter B/A in liquid media. *Ultrasonics*, 44(1):1429–1433.

[Sato *et al.* (1986)] Sato, T., Yamakoshi, Y. and Nakamura, T. (1986). Nonlinear tissue imaging. *In IEEE Ultrasonics Symposium*, pages 889–900.

[Schafer *et al.* (1987)] Schafer, M. E., Lewin, P. A. and Reid, J. M. (1987). Propagation through inhomogeneous media using the angular spectrum method. *In IEEE Ultrasonics Symposium*, pages 943–946.

[Scheller *et al.* (2003)] Scheller, B., Speck, U., Romeike, B., Schmitt, A., Sovak, M., BÃűhm, M. and Stoll, H.-P. (2003). Contrast media as carriers for local drug delivery. *European Heart Journal*, 24(15):1462–1467.

[Sehgal *et al.* (1985)] Sehgal, C., Porter, B. and Greenleaf, J. (1985). Relationship between acoustic nonlinearity and the bound and the unbound states of water. *In IEEE Ultrasonics Symposium*, pages 883–886.

[Sehgal *et al.* (1984)] Sehgal, C. M., Bahn, R. C. and Greenleaf, J. F. (1984). Measurement of the acoustic nonlinearity parameter B/A in human tissues by a thermodynamic method. *The Journal of the Acoustical Society of America*, 76(4):1023–1029.

[Sehgal *et al.* (1986)] Sehgal, C. M., Porter, B. R. and Greenleaf, J. F. (1986). Ultrasonic nonlinear parameters and sound speed of alcohol–water mixtures. *The Journal of the Acoustical Society of America*, 79(2):566–570.

[Serra (1982)] Serra, J. (1982). *Image Analysis and Mathematical Morphology*. Elsevier Academic Press.

[Serra (1988)] Serra, J. (1988). *Image Analysis and Mathematical Morphology - Vol II: Theoretical Advances*. Elsevier Academic Press.

[Simpson and Burns (1997)] Simpson, D. and Burns, P. (1997). Pulse inversion doppler: a new method for detecting nonlinear echoes from microbubble contrast agents. *In IEEE Ultrasonics Symposium*, volume 2.

[Simpson *et al.* (1999)] Simpson, D., Chin, C. T. and Burns, P. (1999). Pulse inversion doppler: a new method for detecting nonlinear echoes from microbubble contrast agents. *IEEE Transactions on Ultrasonics, Ferroelectrics and Frequency Control*, 46(2):372 – 382.

[Srinivasan *et al.* (2003)] Srinivasan, S., Righetti, R. and Ophir, J. (2003). Trade-offs between the axial resolution and the signal-to-noise ratio in elastography. *Ultrasound in Medicine & Biology*, 29(6):847 – 866.

[Stepanishen (1971)a] Stepanishen, P. R. (1971a). The time-dependent force and radiation impedance on a piston in a rigid infinite planar baffle. *The Journal of the Acoustical Society of America*, 49(3B):841–849.

[Stepanishen (1971)b] Stepanishen, P. R. (1971b). Transient radiation from pistons in an infinite planar baffle. *The Journal of the Acoustical Society of America*, 49(5B):1629–1638.

[Sternberg (1986)] Sternberg, S. R. (1986). Grayscale morphology. *Computer Vision, Graphics, and Image Processing*, 35(3):333 – 355.

[Szabo (1978)] Szabo, T. L. (1978). Generalized fourier transform diffraction theory for parabolically anisotropic media. *The Journal of the Acoustical Society of America*, 63(1):28–34.

[Thuras *et al.* (1935)] Thuras, A. L., Jenkins, R. T. and O'Neil, H. T. (1935). Extraneous frequencies generated in air carrying intense sound waves. *The Journal of the Acoustical Society of America*, 6(3):173–180.

[Tortoli *et al.* (2009)] Tortoli, P., Bassi, L., Boni, E., Dallai, A., Guidi, F. and Ricci, S. (2009). Ula-op: an advanced open platform for ultrasound research. *IEEE Transactions on Ultrasonics, Ferroelectrics and Frequency Control*, 56(10):2207–2216.

[Treeby and Cox (2010)] Treeby, B. E. and Cox, B. T. (2010). Modeling power law absorption and dispersion for acoustic propagation using the fractional laplacian. *The Journal of the Acoustical Society of America*, 127(5):2741–2748.

[Tupholme (1969)] Tupholme, G. E. (1969). Generation of acoustic pulses by baffled plane pistons. *Mathematika*, 16(02):209–224.

[Ueno *et al.* (1990)] Ueno, S., Hashimoto, M., Fukukita, H. and Yano, T. (1990). Ultrasound thermometry in hyperthermia. *In IEEE Ultrasonics Symposium*, volume 3, pages 1645–1652.

[van Wijk and Thijssen (2002)] van Wijk, M. C. and Thijssen, J. M. (2002). Performance testing of medical ultrasound equipment: fundamental vs. harmonic mode. *Ultrasonics*, 40(1-8):585–591.

[Vander Meulen *et al.* (2004)] Vander Meulen, F., Fortineau, J., Haumesser, L., Santos, S. and Matar, O. (2004). Linear and nonlinear acoustic parameters measurements in plates with various moisture contents. *In IEEE Ultrasonics Symposium*, volume 3, pages 2330–2333.

[Vander Meulen and Haumesser (2008)] Vander Meulen, F. and Haumesser, L. (2008). Evaluation of B/A nonlinear parameter using an acoustic self-calibrated pulse-echo method. *Applied Physics Letters*, 92(21):214106:1–3.

[Varray *et al.* (2011)a] Varray, F., Basset, O., Tortoli, P. and Cachard, C. (2011a). Extensions of nonlinear B/A parameter imaging methods for echo mode. *IEEE Transactions on Ultrasonics, Ferroelectrics and Frequency Control*, 56(6):1232–1244.

[Varray *et al.* (2011)b] Varray, F., Basset, O., Tortoli, P. and Cachard, C. (2011b). Nonlinear radio frequency image simulation for harmonic imaging application: Creanuis. *IEEE Transactions on Ultrasonics, Ferroelectrics and Frequency Control*. submitted.

[Varray *et al.* (2011)c] Varray, F., Cachard, C., Ramalli, A., Tortoli, P. and Basset, O. (2011c). Simulation of ultrasound nonlinear propagation on gpu using a generalized angular spectrum method. *EURASIP journal on Image and Video Processing*. accepted.

[Varray *et al.* (2010)a] Varray, F., Cachard, C., Tortoli, P. and Basset, O. (2010a). Nonlinear radio frequency image simulation for harmonic imaging: Creanuis. *In IEEE Ultrasonics Symposium*, pages 2179–2182.

[Varray *et al.* (2011)d] Varray, F., Cachard, C., Tortoli, P. and Basset, O. (2011d). 4d simulation of nonlinear pressure field propagation on gpu with the angular spectrum method. *In IEEE Ultrasonics Symposium*.

[Varray *et al.* (2011)e] Varray, F., Chenot, J., Basset, O., Tortoli, P., Melodelima, D. and Cachard, C. (2011e). Nonlinear parameter measurement to characterize *ex-vivo* pork liver undergoing hifu ablation: first results. *In IEEE Ultrasonics Symposium*.

[Varray *et al.* (2009)] Varray, F., Pasovic, M., Cachard, C., Tortoli, P. and Basset, O. (2009). Acoustic nonlinearity parameter of tissue on echo mode: review and evaluation of the different approaches for *B/A* imaging. *In IEEE Ultrasonics Symposium*, pages 41–44.

[Varray *et al.* (2010)b] Varray, F., Pasovic, M., Cachard, C., Tortoli, P. and Basset, O. (2010b). Imagerie du paramètre de non linéearité par une méthode comparative en échographie médicale faisabilité expérimentale. *In Congrès Français d'Acoustique*, page 63.

[Varray *et al.* (2011)f] Varray, F., Ramalli, A., Cachard, C., Tortoli, P. and Basset, O. (2011f). Fundamental and second-harmonic ultrasound field computation of inhomogeneous nonlinear medium with a generalized angular spectrum method. *IEEE Transactions on Ultrasonics, Ferroelectrics and Frequency Control*, 58(7):1366–1376.

[Varslot and Måsøy (2006)] Varslot, T. and Måsøy, S.-E. (2006). Forward propagation of acoustic pressure pulses in 3d soft biological tissue. *Modeling, Identification and Control*, 27(3):181–200.

[Varslot and Taraldsen (2005)] Varslot, T. and Taraldsen, G. (2005). Computer simulation of forward wave propagation in soft tissue. *IEEE Transactions on Ultrasonics, Ferroelectrics and Frequency Control*, 52(9):1473–82.

[Vecchio and Lewin (1994)] Vecchio, C. J. and Lewin, P. A. (1994). Finite amplitude acoustic propagation modeling using the extended angular spectrum method. *The Journal of the Acoustical Society of America*, 95(5):2399–2408.

[Vecchio *et al.* (1994)] Vecchio, C. J., Schafer, M. E. and Lewin, P. A. (1994). Prediction of ultrasonic field propagation through layered media using the extended angular spectrum method. *Ultrasound in Medicine & Biology*, 20(7):611–622.

[Verweij and Huijssen (2009)] Verweij, M. D. and Huijssen, J. (2009). A filtered convolution method for the computation of acoustic wave fields in very large spatiotemporal domains. *The Journal of the Acoustical Society of America*, 125(4):1868–1878.

[Vila *et al.* (2004)] Vila, M., Vander Meulen, F., Dos Santos, S., Haumesser, L. and Bou Matar, O. (2004). Contact phase modulation method for acoustic nonlinear parameter measurement in solid. *Ultrasonics*, 42(1-9):1061 – 1065. Proceedings of Ultrasonics International 2003.

[Voormolen (2007)] Voormolen, M. M. (2007). *Three Dimensional Harmonic Echocardiography*. Thèse de doctorat, Erasmus University Rotterdam.

[Wagner *et al.* (1983)] Wagner, R., Smith, S., Sandrik, J. and Lopez, H. (1983). Statistics of speckle in ultrasound b-scans. *IEEE Transactions on Sonics and Ultrasonics*, 30(3):156–163.

[Wallace *et al.* (2007)] Wallace, K. D., Lloyd, C. W., Holland, M. R. and Miller, J. G. (2007). Finite amplitude measurements of the nonlinear parameter *B/A* for liquid mixtures spanning a range relevant to tissue harmonic mode. *Ultrasound in Medicine & Biology*, 33(4):620–629.

[Wells (2006)] Wells, P. N. T. (2006). Ultrasound imaging. *Physics in Medicine and Biology*, 51(13):R83–R98.

[Westervelt (1963)] Westervelt, P. J. (1963). Parametric acoustic array. *The Journal of the Acoustical Society of America*, 35(4):535–537.

[Williams *et al.* (2006)] Williams, R., Cherin, E., Lam, T. Y. J., Tavakkoli, J., Zemp, R. J. and Foster, F. S. (2006). Nonlinear ultrasound propagation through layered liquid and tissue-equivalent media: computational and experimental results at high frequency. *Physics in Medicine & Biology*, 51(22):5809–5824.

[Wójcik (1998)] Wójcik, J. (1998). Conservation of energy and absorption in acoustic fields for linear and nonlinear propagation. *The Journal of the Acoustical Society of America*, 104(5):2654–2663.

[Wójcik *et al.* (2008)] Wójcik, J., Kujawska, T., Nowicki, A. and Lewin, P. A. (2008). Fast prediction of pulsed nonlinear acoustic fields from clinically relevant sources using time-averaged wave envelope approach: comparison of numerical simulations and experimental results. *Ultrasonics*, 48(8):707–15.

[Wójcik *et al.* (2006)] Wójcik, J., Nowicki, A., Lewin, P. A., Bloomfield, P. E., Kujawska, T. and Filipczynski, L. (2006). Wave envelopes method for description of nonlinear acoustic wave propagation. *Ultrasonics*, 44(3):310–329.

[Wu and Tong (1998)] Wu, J. and Tong, J. (1998). Measurements of the nonlinearity parameter *B/A* of contrast agents. *Ultrasound in Medicine & Biology*, 24(1):153–159.

[Xu *et al.* (2003)] Xu, X. C., Mao, F., Gong, X. F. and Zhang, D. (2003). Theoretical calculation and experimental study on the third-order nonlinearity parameter c/a for organic liquids and biological fluids. *The Journal of the Acoustical Society of America*, 113(3):1743–1748.

[Yan and Hamilton (2006)] Yan, X. and Hamilton, M. F. (2006). Angular spectrum decomposition analysis of second harmonic ultrasound propagation and its relation to tissue harmonic imaging workshop. *In 4th International Workshop on Ultrasonic and Advances Methods for Nondestructive Testing and Material Characterization*, pages 11–23.

[Yang and Cleveland (2005)] Yang, X. and Cleveland, R. O. (2005). Time domain simulation of nonlinear acoustic beams generated by rectangular pistons with application to harmonic imaging. *The Journal of the Acoustical Society of America*, 117(1):113–123.

[Yoshizumi *et al.* (1987)] Yoshizumi, K., Sato, T. and Ichida, N. (1987). A physico-chemical evaluation of the nonlinear parameter B/A for media predominantly composed of water. *The Journal of the Acoustical Society of America*, 82(1):302–305.

[Yu *et al.* (2006)] Yu, W., Yan, P., Sinusas, A. J., Thiele, K. and Duncan, J. S. (2006). Towards pointwise motion tracking in echocardiographic image sequences - comparing the reliability of different features for speckle tracking. *Medical image analysis*, 10(4): 495–508.

[Zabolotskaya and Khokhlov (1969)] Zabolotskaya, E. and Khokhlov, R. (1969). Quasi-plane waves in the nonlinear acoustics of confined beams. *Sov. Phys. Acoustics*, 15:35–40.

[Zemp *et al.* (2003)] Zemp, R. J., Tavakkoli, J. and Cobbold, R. S. C. (2003). Modeling of nonlinear ultrasound propagation in tissue from array transducers. *The Journal of the Acoustical Society of America*, 113(1):139–152.

[Zeng and McGough (2008)] Zeng, X. and McGough, R. J. (2008). Evaluation of the angular spectrum approach for simulations of near-field pressures. *The Journal of the Acoustical Society of America*, 123(1):68–76.

[Zhang and Gong (1999)] Zhang, D. and Gong, X. (1999). Experimental investigation of the acoustic nonlinearity parameter tomography for excised pathological biological tissues. *Ultrasound in Medicine & Biology*, 25(4):593–599.

[Zhang and Gong (2006)] Zhang, D. and Gong, X. (2006). Acoustic nonlinear imaging and its application in tissue characterization. *In 4th International Workshop on Ultrasonic and Advanced Methods for Nondestructive Testing and Material Characterization.*

[Zhang *et al.* (2001)] Zhang, D., Gong, X. and Chen, X. (2001). Experimental imaging of the acoustic nonlinearity parameter B/A for biological tissues via a parametric array. *Ultrasound in Medicine & Biology*, 27(10):1359–1365.

[Zhang *et al.* (2000)] Zhang, D., Gong, X., Liu, J.-h., Shao, L.-z., Li, X.-r. and Zhang, Q.-l. (2000). The experimental investigation of ultrasonic properties for a sonicated contrast agent and its application in biomedicine. *Ultrasound in Medicine & Biology*, 26(2):347–351.

[Zhang *et al.* (1996)] Zhang, D., Gong, X. and Ye, S. (1996). Acoustic nonlinearity parameter tomography for biological specimens via measurements of the second harmonics. *The Journal of the Acoustical Society of America*, 99(4):2397–2402.

[Zhang *et al.* (2002)] Zhang, D., Gong, X. and Zhang, B. (2002). Second harmonic sound field after insertion of a biological tissue sample (l). *The Journal of the Acoustical Society of America*, 111(1):45–48.

[Zhang and Dunn (1987)] Zhang, J. and Dunn, F. (1987). In vivo B/A determination in a mammalian organ. *The Journal of the Acoustical Society of America*, 81(5):1635–1637.

[Zhang *et al.* (1991)] Zhang, J., Kuhlenschmidt, M. S. and Dunn, F. (1991). Influences of structural factors of biological media on the acoustic nonlinearity parameter B/A. *The Journal of the Acoustical Society of America*, 89(1):80–91.

[Zhu *et al.* (1983)] Zhu, Z., Roos, M. S., Cobb, W. N. and Jensen, K. (1983). Determination of the acoustic nonlinearity parameter B/A from phase measurements. *The Journal of the Acoustical Society of America*, 74(5):1518–1521.

[Ziomek (1995)] Ziomek, L. J. (1995). *Fundamental of Acoustic Field Theory and Space-Time Signal Processing*. CRC.

TITRE EN FRANCAIS

Simulation non linéaire en ultrasons. Application à l'imagerie du paramètre de non linéarité des tissus en mode écho.

RESUME EN FRANCAIS

L'imagerie ultrasonore harmonique, qui repose sur la non linéarité du milieu de propagation, est une technique d'imagerie clinique qui améliore la résolution des images. La mesure ultrasonore du paramètre local de non linéarité d'un milieu est une voie de recherche qui amènerait de nouvelles perspectives dans le domaine de la caractérisation des tissus. Cependant, l'accès à cette information se heurte à deux écueils : d'une part il n'existe pas actuellement de méthode de mesure de ce paramètre à partir du mode écho classique et d'autre part, les outils de simulation prenant en compte la non-linéarité du milieu sont peu développés.

Une méthode de spectre angulaire a donc été proposée afin de calculer le champ de pression dans des milieux de non linéarité inhomogène. Ce champ de pression est ensuite utilisé pour engendrer des images échographiques contenant l'information harmonique. Cette méthode spectrale a été portée sur GPU afin d'accélérer le calcul et a été intégrée dans un logiciel libre : CREANUIS.

Dans un deuxième temps, une extension d'une méthode comparative (ECM) a été proposée pour prendre en compte des milieux de non linéarité non homogène, fonctionnant en mode écho. Grâce aux outils de simulation développés, différentes configurations ont été utilisées pour la mise au point de l'ECM qui a ensuite été validée à partir d'objets tests et in vitro sur foies d'animaux. Même si la méthode de mesure présente une résolution relativement faible, les images obtenues démontrent le potentiel de l'imagerie du paramètre de non linéarité des tissus.

TITRE EN ANGLAIS

Simulation in nonlinear ultrasound. Application to nonlinear parameter imaging in echo mode configuration.

RESUME EN ANGLAIS

Harmonic imaging, based on the propagated medium nonlinearity, is a clinical imaging technique which increases the resolution of ultrasound images. The ultrasound measure of the local nonlinear parameter brings new perspectives in term tissues characterization. However, access to this information suffers from two strong points: from one hand, there is no current measurement method of this parameter in echo mode configuration and on the other hand, the simulation tools taking into account the nonlinearity are not many developed.

An angular spectrum method has been proposed to compute the nonlinear pressure field with inhomogeneous nonlinear parameter. This pressure field is then used to generate ultrasound images containing the harmonic component. This spectral approach has been implemented on a GPU in order to accelerate the computation and package in a free software made available to the scientific community under the name CREANUIS.

In a second time, a extension of a comparative method (ECM) has been proposed to take into account media with inhomogeneous nonlinearity, working an echo mode configuration. Thanks the developed simulation tools, different configurations have been used to parameterize and to evaluate the ECM which has then be validated on test objects and *in vitro* animal's livers. Even if the measure presents a relatively weak resolution, the obtained images demonstrated a high potential in the nonlinear parameter imaging of tissues.

MOTS-CLES

Ultrasound, nonlinear propagation simulation, nonlinear image simulation, nonlinear parameter coefficient, CREANUIS, GASM

INTITULE ET ADRESSE DE L'U.F.R. OU DU LABORATOIRE

Université de Lyon, CREATIS ; CNRS UMR5220 ; Inserm U1044 ; INSA-Lyon ; Université Lyon 1, 7 Av. Jean Capelle, 69621 VILLLEURBANNE, France.
Microelectronics Systems Design Laboratory, Università di Firenze, Italy